

Localization of Principal Eigenvector in Complex Networks

Ph.D. Thesis

By

PRIODYUTI PRADHAN



DEPARTMENT OF PHYSICS
INDIAN INSTITUTE OF TECHNOLOGY INDORE
OCTOBER 2019

Localization of Principal Eigenvector in Complex Networks

A THESIS

*Submitted in partial fulfillment of the
requirements for the award of the degree*

of
DOCTOR OF PHILOSOPHY

by

PRIODYUTI PRADHAN



DEPARTMENT OF PHYSICS
INDIAN INSTITUTE OF TECHNOLOGY INDORE
OCTOBER 2019



INDIAN INSTITUTE OF TECHNOLOGY INDORE

CANDIDATE'S DECLARATION

I hereby certify that the work which is being presented in the thesis entitled "Localization of Principal Eigenvector in Complex Networks" in the partial fulfillment of the requirements for the award of the degree of DOCTOR OF PHILOSOPHY and submitted in the DEPARTMENT OF PHYSICS, Indian Institute of Technology Indore, is an authentic record of my own work carried out during the time period from December 2015 to September 2019 under the supervision of Prof. Sarika Jalan, Professor, Indian Institute of Technology Indore, India.

The matter presented in this thesis has not been submitted by me for the award of any other degree of this or any other institute.

Priodyuti Pradhan 01/10/2019

Signature of the student with date
PRIODYUTI PRADHAN

This is to certify that the above statement made by the candidate is correct to the best of my/our knowledge.

Signature of Thesis Supervisor with date

Prof. SARIKA JALAN

Sarika Jalan

01/10/2019

PRIODYUTI PRADHAN has successfully given his/her Ph.D. Oral Examination held on 21.01.2021

Sarika Jalan
Signature of Chairperson (OEB)

Date: 21-01-2021

Swadesh Sahoo
Signature of External Examiner

Date: 21-01-2021

Sarika Jalan
Signature(s) of Thesis Supervisor(s)

Date: 21.01.2021

Sarika Jalan
Signature of PSPC Member #1

Date: 21-01-2021

Swadesh Sahoo
Signature of PSPC Member #2

Date: 21-01-2021

Sarika Jalan
Signature of Convener, DPGC

Date: 21-01-2021

Sarika Jalan
Signature of Head of Discipline

Date: 21-01-2021

This Thesis is

Dedicated

to

My Friends and Family

Acknowledgements

With the grace of God and with the help of numerous individuals and organizations, I was able to complete this dissertation successfully. And from the bottom of my heart, I am pleased to thank them. I offer my sincere gratitude to my supervisor Prof. Sarika Jalan, for guiding and supporting me through this thesis journey. She motivated me by posing challenging tasks throughout my time at the Indian Institute of Technology (IIT) Indore. You have helped me to become more confident as a student and as a professional, more than you know.

My sincere regards to the PSPC committee members, Dr. Manavendra Maheto, for providing vital pieces of advice on eigenvalue crossing phenomena and Dr. Swadesh Kumar Sahoo for monitoring and giving constructive suggestions to improve my research work. I am also thankful to the Director, IIT Indore, DPGC convener, Head (Department of Physics), Dean of Academic Affairs (DOAA), all the faculty and staff members of the Department of Physics, IIT Indore (Mr. Ujwal Kulkarni, Mr. Vedprakash Thakur, Mr. Nitin Upadhyay, Mr. Prasant Gupta, Mr. Tanmay Harsh Vaishnav), for their timely help and support. I am always thankful to the staff members of the Academic Office, Accounts Section, R&D Section (Mr. Rahul Geed, Mr. Sunny Namdev), IT Section, Central Library, Medical Team, Hostel Team (Ram Bhaia, Santosh Bhaia, Mr. Digant), IIT Indore whose constant support ascertained smooth functioning of my research work. I would especially like to thank Mr. Tapeshe Parihar for putting his efforts to complete the complex and time consuming official formalities related to the Ph.D. thesis. Also, I would like to acknowledge the Indian Government funding agencies – DST and MHRD for providing me research fellowships and CSIR for Direct senior research fellowship during my Ph.D. program. Further, my thanks go to SERB committee members for selecting and providing the international travel grant to attend the workshop at a beautiful place in École de Physique des Houches, France.

The Ph.D. was a long and bumpy road filled with countless nights stay awake, and I would never find my way out without the wonderful community that resides over the globe. Several personal and email communications made this dissertation more

informative and accurate. First and foremost, I would like to thank Jayendra Bhattacharya (BITS Pilani), M. V. Ivanchenko (Lobachevsky State University), Shashi C. L. Srivastava (Variable Energy Cyclotron Centre, Kolkata) for spending a long time with me to provide many suggestions. I thank A. V. Goltsev (University of Aveiro) for assisting me to understand the analytical calculation on disease spreading and PEV localization, Manlio De Domenico (Universitat Rovira i Virgili) for helping with multilayer network datasets and interpretation, Travis Martin (Software Engineer at Google in the Research & Machine Intelligence division) and M. E. J. Newman (University of Michigan) for useful discussions on the eigenvector localization and centrality measures and Michael C. Grant (CVX Research, Stanford University) for useful discussion on the optimization problem over StackExchange. I would also like to say thanks to Yan-Bin Jia (Iowa State University) for clearing doubts on the roots of the cubic equation, Zdzislaw Burda (AGH University of Science and Technology) for suggesting the usage of maximal entropy random walk in PEV localization setup, and Baruch Barzel (Bar-Ilan University) for suggesting an exciting problem of tuning eigenvectors localization and construct power-law degree distributed networks. I am indebted to Beresford N. Parlett (University of California, Berkeley) for spending his precious time and carefully assisting me to find bounds on the eigenvalues gap and validate our results. My thanks go to all the anonymous persons whose online sources (codes, subject materials) greatly helped me to clear my doubts and proceed with the research work. Mainly, I would like to thank the Khan Academy and MIT OpenCourseWare members for preparing the comprehensive subject materials and making them freely available for all. Finally, I am thankful to all the journal reviewers to critically review the manuscript and provide constructive suggestions to make the content of the thesis more correct.

I am feeling very much blessed, and from the bottom of my heart, I would like to say thanks to all the research scholars at Complex Systems Lab, Dr. Aradhana Singh, Dr. Sanjiv K. Diwedi, Dr. Camellia Sarkar, Dr. Aparna Rai, Dr. Ajaydeep Kachhvah, Dr. Alok Yadav, Dr. Pramod Shinde, Dr. Saptarshi Ghosh, Anil, Guruji (Rahul), Ankit, Vasundhara, Tanu, Sanket for their love, care, support, and

guidance which made my time in IIT Indore so sweet and memorable. Furthermore, I am grateful to the past members of Complex Systems Lab – Sudeep, Parth, Madhoolika, Loïc, Naveen, Pramodini, Neeraj, Ayesha, Bibhabasu, Rishav, Sagar, Angeliya, Shiddhant, Saket, Drashti, and Shraddha for being sources of inspiration. My heartfelt thanks go to all the persons in the IIT Indore mess hall who provide their invaluable services to prepare delicious food, to serve them, and even to clean our plates after having food every day. I really do not know them, but their indirect contribution during my Ph.D. is significant, and I am always grateful to them.

With the aid of generous people, I have effortlessly crossed several steep staircases to reach the final stage of writing the Ph.D. thesis, and I am always grateful to them for making my dream come true. Especially my sincere gratitude goes to Prof. Gautam Mahapatra, Prof. R. Subramanian, Madhusudan Da, Sukanta Da, Dr. Shivakumar Jolad, Prof. Anirban Dasgupta, Dr. Souradyuti Paul, Dr. Bireswar Das, Sushanta Jethu, Boro Dadu, Sudipta Sir, Swapan Kaku, all of my school teachers and Mejo Pici – whose hands I hold to start my academic tour.

I am lucky to have some fantastic friends, my roommate Sudhir – a source of inspiration, Madhurima, Manojit, Anupama, Dhananjay, Gyanswrup, Munesh, Rajdeep, and Manoj, who have always lent a helping hand whenever I needed. Mainly, Amit and Harish, who physically live far away yet mentally reside closer to my heart to motivate me in all the circumstances. Even though I cannot mention all the people's names, I am very much grateful for their generous support throughout my long academic journey.

I owe an incalculable debt to the most important people in my life, my family! My loving and warmhearted mother, inspiring father, affectionate brothers, caring sisters and sister-in-law, adorable nephew, and beloved uncle-aunties. Though my grandparents are not with me at present to cherish this wonderful moment, but their blessings always showers upon me. Without them, I would not be able to embark upon this journey. Finally, I thank almighty God for sending all these wonderful people into my life. Thank you!!!

Priodyuti Pradhan

Synopsis

Introduction

Networks provide a simple framework to understand and predict the properties of complex real-world systems by modeling them in terms of interacting units [28]. This framework is successful in explaining various mechanisms behind the emergence of collective behaviors of systems arising due to the local interaction patterns of their components. Much of the current effort has given to understand the relationship between structure as well as the dynamics of a complex system. As structure always affects the functionality of a system. The eigenvector corresponding to the largest eigenvalue of the adjacency matrix, referred to as the principal eigenvector (PEV), provides information about both the structural and dynamical behavior of the underlying systems [9]. For various linear dynamical processes on networks, for instance, epidemic spreading, population dynamics of Ribonucleic acid (RNA) neutral networks, rumor spreading, brain network dynamical models the steady-state vector has been shown to be approximated using the PEV of the adjacency matrix [9]. Hence, analyzing the behavior of PEV can help us to understand how an individual entity is infected or how information spreads in a network in the steady-state. Particularly, the localization behavior of PEV has been helpful in gaining insight into the propagation or restriction of information in the underlying systems. For instance, analyzing localization behavior of PEV have been shown to provide insight into the criticality in brain network dynamics and disease spreading near epidemic threshold in networks [4, 11]. Localization of PEV refers to a state where a few components of the vector take very high values while the rest of the components take small values independent of the network size. In other words, localization of PEV in networks says few nodes contribute more to the dynamical process, and the rest of the others have very less contribution in steady-state. Similarly, PEV is said to be delocalized when all the entries in PEV receive almost the same weight

independent of the network size. Therefore, for a delocalized PEV, all the nodes have the same amount of contribution to a corresponding dynamical system.

The topic of eigenvector localization is worthy of investigation and arise sufficient interest to the researchers working on network theory and statistical physics [20]. Mainly, emergence or absence of eigenvector localization in networks is of broad importance ranging from spreading dynamics to the numerical computation [20]. Discovering and analyzing network properties leading to increase or decrease the localization of PEV of adjacency matrix can help in understanding the behavior of a linear dynamical process in steady-state and which we have studied in the current thesis.

There have been several investigations attempting to relate one or more structural properties of a network with the localization behavior of PEV of adjacency matrices. Goltsev et al. reported that PEV localization of scale-free networks exists only for the power-law exponent being greater than a critical value [4]. On the contrary, Pastor-Satorras et al. have shown that the PEVs of all the power-law degree distributed networks are localized to some extent, with the existence of two types of localization based on the degree of the nodes [23]. Network properties such as the presence of hubs, the existence of a dense subgraph, and a power-law degree distribution are a few factors known to make a PEV more localized [24]. However, in this thesis, we show that the presence of these features in a network does not guarantee a highly localized PEV of the corresponding adjacency matrix.

In another work, Martin et al. demonstrated that under certain circumstances, PEV might undergo a localization transition leading to a failure of eigenvector centrality (EC) measure [24]. The presence of certain structural features, such as the existence of high degree nodes in a network is recognized to induce the localization transition of PEV. These studies concentrated on finding constraints for a localized PEV and its impact on the EC measures based on random graph model having one high degree node. However, it is not clear the impact of delocalization of PEV state on the EC measure. Using the developed model, we have shown that along with the localization transition, presence of delocalization transition in PEV also causes

problems to the EC measure.

Arruda et al. extended the PEV localization concepts for multilayer networks (MNs) and identified that PEV localization behaviors for MNs could be different from the monolayer networks [73]. Specifically, in the monolayer networks, localization can happen on a few nodes [4] whereas, in MNs, a layer can be localized [73]. These investigations shed light on the properties of the monolayer networks and their relations with the PEV. However, it remains unclear what specific structural features the MNs should have so that they make the corresponding PEV localized. Additionally, how the network structure of an individual layer affects or regulates the PEV localization of the entire MN? Specifically, the question which we address here using the optimization technique is that what structural properties an individual layer should possess so that they correspond to a highly localized PEV of the entire MN.

We attempt to make the concept clear, more straightforward from different dimensions rather than only from the physical science perspective. We perform a rigorous numerical simulation to understand the emergence of structural and spectral properties due to PEV localization in networks as well as perform mathematical analysis to support our findings as it requires. During the study, we use several fundamental ideas from physical science, numerical linear algebra, and recent network theory to present the results in the current thesis.

Objectives

- To understand structural and spectral properties of networks which may help in spreading or restricting information in networks captured by PEV localization.
- To develop a learning framework to make network having localized PEV state in monolayer and multilayer networks.
- To uncover essential network properties leads to a highly localized PEV.

- To understand the failure of EC measure in networks

Background

A finite graph or network can be represented as $\mathcal{G} = (V, E)$ where $V = \{v_1, v_2, \dots, v_n\}$ is the set of nodes and $E = \{e_1, e_2, \dots, e_m\}$ is the set of interactions (edges) among them. Here, we consider undirected, unweighted, and connected networks. Additionally, the present work restricts to simple networks, i.e., the network without multiple connections and self-loop. Hence, the corresponding adjacency matrix can be denoted as $\mathbf{A} \in \mathbb{R}^{n \times n}$ and represented easily as

$$a_{ij} = \begin{cases} 1 & \text{if nodes } i \text{ and } j \text{ are connected} \\ 0 & \text{Otherwise} \end{cases}$$

We denote $|V| = n$ as the number of nodes and $|E| = m$ being the number of edges of \mathcal{G} . We refer $E^c = \{e_1^c, e_2^c, \dots, e_{(n(n-1)/2)-m}^c\}$ as the set of edges which are not present in \mathcal{G} . The number of edges to a particular node is referred as its degree denoted as $k_i = \sum_{j=1}^n a_{ij}$. The average degree of the network is denoted by $\langle k \rangle = \frac{1}{n} \sum_{i=1}^n k_i$. We refer the maximum degree node or hub node of \mathcal{G} as $d = \max_{1 \leq i \leq n} k_i$.

Here, \mathbf{A} is a real symmetric matrix, hence, it has a set of orthonormal eigenvectors

$$\{\mathbf{x}_1, \mathbf{x}_2, \dots, \mathbf{x}_i, \dots, \mathbf{x}_n\} \text{ where } \mathbf{x}_i = ((x_i)_1, (x_i)_2, \dots, (x_i)_n)^T \quad (1)$$

and corresponding real eigenvalues are denoted as $\{\lambda_1, \lambda_2, \dots, \lambda_i, \dots, \lambda_n\}$. Further, \mathbf{A} is a non-negative ($a_{ij} \geq 0$) and irreducible matrix (connected network) and it follows from the Perron-Frobenius theorem [26] that there exists a positive and distinct eigenvalue λ_1 . The eigenvector corresponding to λ_1 is a unique positive eigenvector (\mathbf{x}_1) referred as the principal eigenvector.

We use the inverse participation ratio (IPR) to measure the extent of the PEV localization [4, 24]. This measure had been introduced to quantify the participation

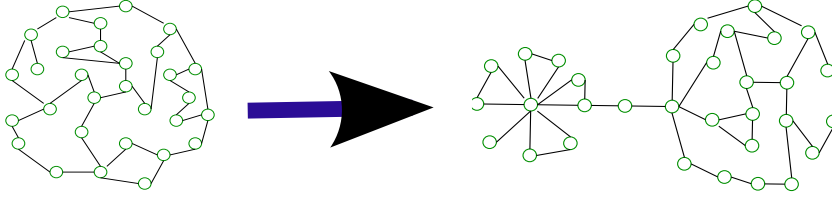


Figure 1: Schematic diagram of an initial (left) and an optimized (right) network structure.

of atoms in a normal mode of vibration and is similar to the fourth moments in statistics [60]. We calculate the IPR value ($Y_{\mathbf{x}_i}$) of an orthonormal eigenvector corresponding to distinct (nondegenerate) eigenvalue of \mathbf{A} as follows:

$$Y_{\mathbf{x}_i} = \sum_{j=1}^n (x_i)_j^4 \quad (2)$$

where $(x_i)_j$ is the j^{th} component of \mathbf{x}_i . A delocalized eigenvector ($\mathbf{x}_i = (\frac{1}{\sqrt{n}}, \frac{1}{\sqrt{n}}, \dots, \frac{1}{\sqrt{n}})^T$) has $Y_{\mathbf{x}_i} = \frac{1}{n}$, whereas the most localized eigenvector ($\mathbf{x}_i = (1, 0, \dots, 0)^T$) yields an IPR value equal to $Y_{\mathbf{x}_i} = 1$. These are two extreme cases for the eigenvector localization. In general, for a network, eigenvector is said to be localized if $Y_{\mathbf{x}_i} = \mathcal{O}(1)$ and delocalized if $Y_{\mathbf{x}_i} \rightarrow 0$ as $n \rightarrow \infty$ [4].

It is known that for any connected regular graph (every node having the same degree), $\mathbf{x}_1 = (\frac{1}{\sqrt{n}}, \frac{1}{\sqrt{n}}, \dots, \frac{1}{\sqrt{n}})^T$ (Theorem 6 [26]) and thus, $Y_{\mathbf{x}_1} = \frac{1}{n}$. Hence, a sparse as well as a dense regular network both will have a delocalized PEV. Next, if we consider a graph where each node is isolated without having any interaction with any one and having a self-loop, adjacency matrix will be nothing but an identity matrix and for which we can choose $\mathbf{x}_1 = (1, 0, \dots, 0)^T$ leading to $Y_{\mathbf{x}_1} = 1$. However, to get a unique positive PEV (i.e. $(x_1)_i > 0, \forall i$), we consider connected networks in our study. Hence, IPR value of the PEV should be in the range $1/n \leq Y_{\mathbf{x}_1} < 1$ for $n \geq 2$. However, to test whether the PEV is localized or not for IPR being in the range $1/n < Y_{\mathbf{x}_1} < 1$, we adopt the procedure proposed for the detection of the Anderson localization [60] and which was recently used to measure the PEV localization in complex networks [23, 24]. According to this procedure, one should calculate the IPR value of PEV for different network sizes. If $Y_{\mathbf{x}_1}$ tends to have a

constant value as $n \rightarrow \infty$, PEV is localized, otherwise it is delocalized [23]. Hence, finding a network structure having delocalized PEV is easier, and it becomes challenging to find a network structure having highly localized PEV.

Summary of the work done

Numerical schemes for the construction of PEV localized networks

This chapter addresses challenges that given an input connected graph \mathcal{G} with n nodes, m edges, and a function $\zeta : \mathbb{R}^n \rightarrow \mathbb{R}$, we want to compute the maximum possible value of $\zeta(\mathbf{x}_1)$ over all the simple, connected, undirected, and unweighted graphs \mathcal{G} where $\zeta = Y_{\mathbf{x}_1} = \sum_{i=1}^n (x_1)_i^4$. We formulate the problem through an optimization technique as follows.

Starting from an initial connected random network having delocalized PEV, we use an edge rewiring approach based on a Monte Carlo algorithm to obtain the optimized network in an iterative manner. For a single edge rewiring process, we choose an edge $e_i \in E$ uniformly at random from \mathcal{G} and remove it. At the same time, we introduce an edge in the network from E^c , which preserves the total number of edges during the network evolution. The new network and the corresponding adjacency matrix are denoted as \mathcal{G}' and \mathbf{A}' , respectively. The eigenvalues and eigenvectors of \mathbf{A}' are indicated as $\{\lambda'_1, \lambda'_2, \dots, \lambda'_n\}$ and $\{\mathbf{x}'_1, \mathbf{x}'_2, \dots, \mathbf{x}'_n\}$, respectively. It is important to remark that during the network evolution, there is a possibility that an edge rewiring makes the network disconnected. We only approve those rewiring steps which yield a connected graph. We calculate the IPR value of PEV from \mathbf{A} and \mathbf{A}' . If $Y_{\mathbf{x}'_1} > Y_{\mathbf{x}_1}$, \mathbf{A} is replaced with \mathbf{A}' . Therefore, in each time step, we get a network which has the PEV more localized than the previous network. We repeat the above steps until we obtain the maximum IPR value corresponding to the optimized network and denote as \mathcal{G}_{opt} .

We find that \mathcal{G}_{opt} has a particular structure consisting of two subgraph components connected via a single node (Fig. 1). We also show that optimized structure is independent of the initial network structure. We analyze structural as well as spectral

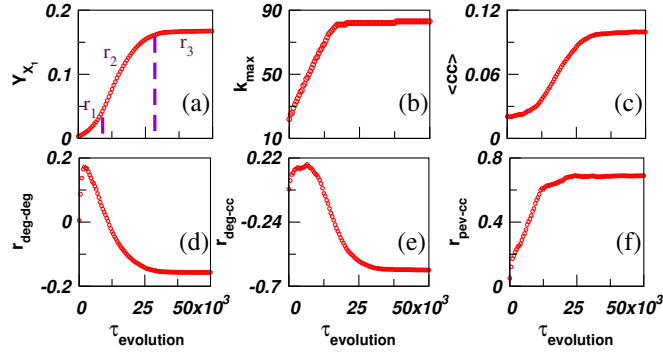


Figure 2: We iterate the rewiring process for 600,000 times and store the network after each 100^{th} steps. Changes of various network properties (a) IPR value of PEV (b) maximum degree (c) average clustering coefficient (d) degree-degree correlation (e) correlation between degree vector and clustering coefficient vector and (f) correlation between PEV and clustering coefficient vector during the evolution ($\tau_{evolution}$). Network size is $n = 500$, and $\langle k \rangle = 10$.

properties during the network evolution and reveals that PEV localization is not a consequence of a single network property, and preferably requires co-existence of various distinct structural as well as spectral features (Fig. 2). Furthermore, we identify a set of edges in \mathcal{G}_{opt} , rewiring any one of them leads to a complete delocalization of PEV (Fig. 3). This sensitivity of PEV at the most localized state turns out to be related to the behavior of the largest (λ_1) and the second-largest (λ_2) eigenvalue of the network. Exactly when the network becomes most localized, the λ_2 of the adjacency matrix become very close to λ_1 . Furthermore, we identify an evolution regime where networks are as localized as the optimized one, but, are robust to single edge rewiring. To conclude, our study provides a deeper insight into the PEV localization on synthetic as well as on empirical networks. Though, the prime concern of our analysis to have insights into the network structure and PEV localization, using susceptible-infected-susceptible (SIS) epidemic spreading model, we verify that in the optimal and the intermediate stages spreading of disease is much slower near the epidemic threshold than the initial random structure.

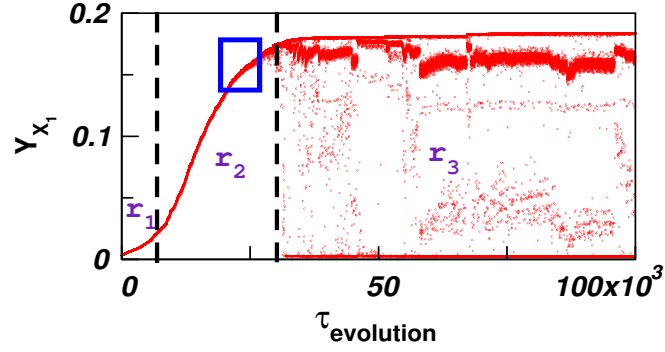


Figure 3: IPR as a function of edge-rewiring. The networks with large IPR value in r_3 region consists of few edge-rewiring, which leads to a sudden drop in the IPR value. Rewiring of the first 1,00,000 edges is depicted. The marked square indicates the regime where the networks attain IPR values which are very close to the optimized network. However, in this regime rewiring an edge does not have a significant impact on the IPR values.

Analytical construction of PEV localized networks

We demonstrate that single edge rewiring in the optimized network leading to delocalization of PEV is accompanied with the eigenvalue crossing phenomenon is an essence of the sensitivity behavior of PEV localization (Fig. 4). Taking a clue from this eigenvalue crossing phenomenon, we find a relationship between the largest eigenvalues ($\lambda_1^{c_1} > \lambda_1^{c_2}$) of the individual subgraph (C_1 and C_2) of the optimized network structure. Using the eigenvalue relation, we construct a cubic equation which provides network parameters required for a direct construction of wheel random regular PEV localized networks. Analysis of the discriminant of this cubic equation reveals another important result that for a wheel random regular (WRR) network, one can achieve a localized PEV in two different ways either by connecting a sparse random regular subgraph with a small wheel subgraph or connecting by a dense random regular subgraph with a large wheel subgraph structure. Further, we also validate that the result obtains from the wheel random regular PEV localized networks are in good agreement with that of the optimized structure. Finally, we substantiate the eigenvalue crossing phenomenon by using the RNA neutral network population dynamical model.

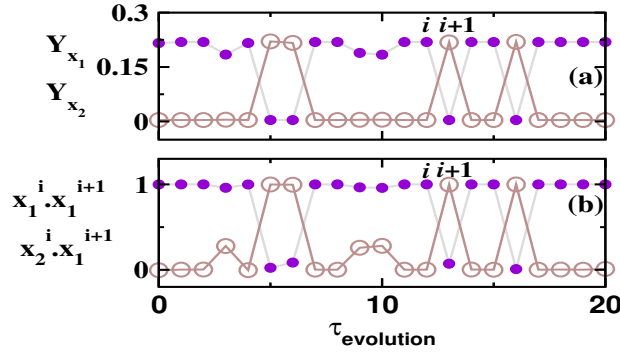


Figure 4: (a) Flipping behavior of IPR values of the largest (●) and second-largest (○) eigenvectors. (b) Detection of eigenvalue crossing through dot products $(\mathbf{x}_1^i)^T \mathbf{x}_1^{i+1}$ (●) and $(\mathbf{x}_2^i)^T \mathbf{x}_1^{i+1}$ (○) during the random edge rewiring process in optimized network structure. Here, $n = 500$ and $\langle k \rangle = 10$.

Impact of PEV localization on eigenvector centrality measure

This chapter explores the problems associated with the eigenvector centrality (EC) measure. The EC measure has been very popular due to its ability in measuring the importance of the nodes based on not only the number of interactions they acquire but also particular structural positions they have in the networks. Despite the considerable success of EC in ranking the nodes of a network [24], using WRR model, we show that along with the occurrence of localization state, the occurrence of delocalization of PEV can also affect weights assignment to the higher degree nodes based on EC, thereby creating difficulties in accessing relative importance of the nodes causing the failure of EC. While it is obvious that random regular networks have delocalized PEV as all the nodes carry the same information in the network, investigations of the WRR model reveal that graphs consisting of heterogeneous degrees can also have delocalized PEVs. Besides, we extend the WRR model network for star-random regular, friendship-random regular and scalefree-random regular models and investigate the localization-delocalization transition of PEV and impact on the EC measure. Our investigation while providing fundamental insight to the relation between PEV localization and centrality of nodes in networks, suggests that for the networks having delocalized PEVs, it is better to use degree centrality measure to rank the nodes.

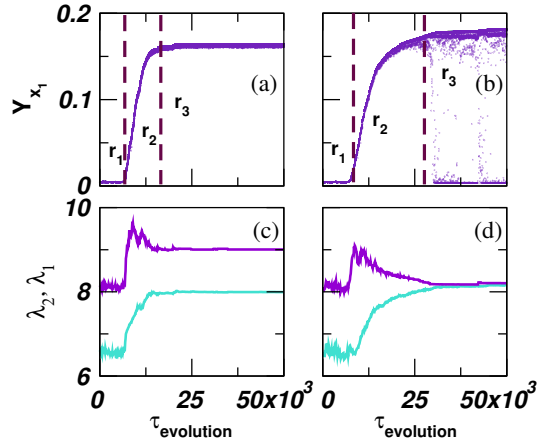


Figure 5: Changes in the IPR values (Y_{x_1}) with the evolution. (a) Single-layer rewiring protocol does not show IPR drops in the saturation region. (b) Both-layers rewiring protocol shows drops in the IPR value in the saturation region. (c) The behavior of the largest two eigenvalues of the single-layer and (d) both-layer rewiring protocols. Here, $N = 400$, $\langle k \rangle = 7$, and $\langle k_1 \rangle = \langle k_2 \rangle$.

Extension to the multilayer networks

The traditional monolayer network framework offers only a limited representation of a complex system having different layers of interactions. Recent years have witnessed the emergence of the multilayer network (MN) framework, which provides more accurate insights into the behaviors of complex systems possessing multiple types of relations among the same units. Previous three chapters were focused on the investigation of PEV localization on single (mono) layer networks. In this chapter, we explore the impact of the optimized edge rewiring for the PEV localization in multilayer networks.

Starting with a multilayer network corresponding to a delocalized PEV, we rewire the network edges using an optimization technique such that PEV of the rewired multilayer network becomes more localized. The framework allows us to scrutinize the structural and spectral properties of the networks at various localization points during the rewiring process. For two layers MN, the optimization process can be implemented considering two different edge rewiring protocols; (1) by rewiring edges in both-layers or (2) by rewiring edges in only one layer. Our investigations reveal that for both the rewiring protocols, the highly localized PEV of the MN for a

given network size possesses specific structural properties, such as the presence of a hub node, high clustering coefficient, and low degree-degree correlation. However, the rewiring protocols lead to a noticeable and essential difference in the spectral properties of the optimized MN structure. For the both-layers rewiring protocol, the PEV is sensitive to a single edge rewiring in the optimized MN structure as also observed in the monolayer networks. However, interestingly, we get rid of this sensitivity of PEV for the single-layer rewiring protocol (Fig. 5). Further, we show that by rewiring a single-layer, one can tune the contribution of the node weights of the other layer to the PEV of the entire MN. We present our results for two layers, three layers, and four layers MNs. Finally, analysis of multilayer networks constructed using real-world social and biological data show that the localization properties of these real-world multilayer networks are in good agreement with the simulation results for the model multilayer network. The study is relevant to applications that require understanding the propagation of perturbation in multilayer networks.

Conclusion and future scope

This thesis develops an optimized edge rewiring based network evolution framework to find network structure having highly localized PEV. Our approach provides a comprehensive way to investigate not only the properties of the optimized network structure but also the structure of the intermediate networks. Analyzing structural and spectral properties of the optimized network reveals that to achieve highly localized PEV, network structure should have (1) two subgraphs, (2) one of them having hub node, (3) another has an almost regular structure and (4) a relationship between the largest eigenvalues of the subgraph components. Based on the observed network properties, we provide a recipe for direct construction of PEV localized network by combining wheel and random regular network. Further, we use wheel random regular network to understand the failure of EC measure due to localization and delocalization transition in PEV. Finally, we extend the optimized edge rewiring process for multilayer networks and reveal that for multilayer networks, single-layer rewiring is enough to get the structure of a highly localized network.

It may not always be feasible to rewire a real-world network to such an extent as to get a desired PEV localization behavior. However, the results and approach here will be more useful in constructing an artificial network with the desired localization behavior. Our study provides a more in-depth insight into PEV localization in synthetic as well as on empirical networks.

The present thesis focuses on undirected and unweighted networks; the approach can be extended to obtain a comprehensive picture of PEV localization in directed networks. Furthermore, this dissertation is restricted to the PEV of adjacency matrices; however, it will be interesting to study the consequences of localization of other lower-order eigenvectors in emerging network properties. The current thesis provides a platform to capture the behavior of PEV, which is related to the steady-state of linear dynamics. It would be a great interest to study the eigenvector localization of Laplacian, Jacobian and Hessian matrices which are closely associated with the non-linear dynamics and Anderson localization.

Keywords : Network Science, complex networks, eigenvector localization, optimization, network evolution, Complex Systems.

LIST OF PUBLICATIONS

Publications from thesis

1. **Priodyuti Pradhan** and Sarika Jalan (2020) *From Spectra to Localized Networks: A Reverse Engineering Approach*, IEEE Transactions on Network Science and Engineering 7(4), 3008 (DOI: 10.1109/TNSE.2020.3008999).
2. **Priodyuti Pradhan**, Angeliya C. U. and Sarika Jalan (2020) *Principal eigenvector localization and centrality in networks: revisited*, Physica A: Statistical Mechanics and its Applications 554, 124169 (DOI: 10.1016/j.physa.2020.124169).
3. Sarika Jalan and **Priodyuti Pradhan** (2018) *Localization of multilayer networks by the optimized single-layer rewiring*, Phys. Rev. E **97**, 042314 (DOI: 10.1103/PhysRevE.97.042314).
4. **Priodyuti Pradhan**, Alok Yadav, Sanjiv K. Dwivedi and Sarika Jalan (2017) *Optimized evolution of networks for principal eigenvector localization*, Phys. Rev. E **96**, 022312 (DOI: 10.1103/PhysRevE.96.022312).

Other publications

5. Sarika Jalan and **Priodyuti Pradhan** (2020) *Wheel graph strategy for principal eigenvector localization of networks*, Europhysics Letter 129(4) (DOI: 10.1209/0295-5075/129/46002/meta).
6. Aparna Rai, **Priodyuti Pradhan**, Jyothi Nagraj, K. Lohitesh, Rajdeep Chowdhury and Sarika Jalan (2017) *Understanding cancer complexome using networks, spectral graph theory and multilayer framework*, Sci. Rep. **7**, 41676 (DOI: 10.1038/srep41676).

Table of Contents

1	Introduction	1
1.1	Overview	1
1.2	Networks and basic definitions	3
1.2.1	Spectral properties	4
1.2.2	Model Networks	5
1.3	Multilayer networks:	7
1.3.1	Eigenvectors in networks	8
1.3.2	Eigenvector localization in networks	9
1.3.3	Inverse Participation Ratio	11
1.4	Motivation behind this thesis	12
1.5	Thesis Overview	14
2	Numerical schemes for the construction of PEV localized networks	17
2.1	Introduction	17
2.2	Background	19
2.3	Methods	20
2.4	Results	22
2.4.1	Network evolution	22
2.4.2	Analyzing network properties during network evolution	23
2.4.3	Revealing Optimized network structure	25
2.4.4	Impact of initial network structure and size on evolution	26
2.4.5	Sensitivity of PEV in r_3 region	27
2.5	Disease spreading in localized networks	30
2.6	Conclusion	31
3	Analytical construction of PEV localized networks	35
3.1	Introduction	35

3.2	Background	37
3.3	Results	38
3.3.1	Analysis of eigenvectors angles: signature of eigenvalue crossing	38
3.3.2	Analytical construction of localized network using wheel and random regular graph	43
3.4	Localization behavior on linear-dynamical system	47
3.5	Conclusion	51
3.6	Appendix: Discriminant analysis	51
4	Impact of PEV localization on Eigenvector centrality measure	57
4.1	Introduction	57
4.2	Background	59
4.3	Results and Discussion	61
4.3.1	Localization transition in Random Graph Model	61
4.3.2	Wheel-Random-Regular Model	63
4.3.3	Localization transition in other graph models	69
4.3.4	Delocalization transition in other graph models	70
4.4	Failure of EC measure	71
4.5	Conclusion	72
4.6	Appendix: Wheel-Random-Regular model	73
5	Extension to the multilayer networks	77
5.1	Introduction	77
5.2	Background	79
5.3	Methods	81
5.4	Results and Discussion	82
5.4.1	Localization of model multilayer network	83
5.4.2	Layer rewiring based on simulated annealing	85
5.4.3	Network properties during network evolution	86
5.4.4	Revealing optimized multilayer structure and sensitivity in PEV	88
5.4.5	Impact of layer rewiring	91
5.4.6	Localization in real-world multilayer networks	92
5.5	Conclusion	95
6	Conclusion and future scope	97
6.1	Conclusion	97

6.2	Future scope	101
6.3	Basic definitions	104
6.4	Results related to eigenvalues	104
6.5	Non-degenerate test of close eigenvalues	105
6.6	Details of optimization process	106
6.6.1	Monte Carlo based algorithm	108
6.6.2	Simulated annealing based algorithm	109
6.7	Structural properties during network evolution	111
6.8	Behavior of all IPR values	113
6.9	Eigenvalues behavior of real-world networks	114

Bibliography **118**

List of Figures

1	Schematic diagram of an initial (left) and an optimized (right) network structure.	viii
2	We iterate the rewiring process for 600,000 times and store the network after each 100 th steps. Changes of various network properties (a) IPR value of PEV (b) maximum degree (c) average clustering coefficient (d) degree-degree correlation (e) correlation between degree vector and clustering coefficient vector and (f) correlation between PEV and clustering coefficient vector during the evolution ($\tau_{evolution}$). Network size is $n = 500$, and $\langle k \rangle = 10$	x
3	IPR as a function of edge-rewiring. The networks with large IPR value in r_3 region consists of few edge-rewiring, which leads to a sudden drop in the IPR value. Rewiring of the first 1,00,000 edges is depicted. The marked square indicates the regime where the networks attain IPR values which are very close to the optimized network. However, in this regime rewiring an edge does not have a significant impact on the IPR values.	xi
4	(a) Flipping behavior of IPR values of the largest (\bullet) and second-largest (\circ) eigenvectors. (b) Detection of eigenvalue crossing through dot products $(\mathbf{x}_1^i)^T \mathbf{x}_1^{i+1}$ (\bullet) and $(\mathbf{x}_2^i)^T \mathbf{x}_1^{i+1}$ (\circ) during the random edge rewiring process in optimized network structure. Here, $n = 500$ and $\langle k \rangle = 10$	xii
5	Changes in the IPR values (Y_{x_1}) with the evolution. (a) Single-layer rewiring protocol does not show IPR drops in the saturation region. (b) Both-layers rewiring protocol shows drops in the IPR value in the saturation region. (c) The behavior of the largest two eigenvalues of the single-layer and (d) both-layer rewiring protocols. Here, $N = 400$, $\langle k \rangle = 7$, and $\langle k_1 \rangle = \langle k_2 \rangle$	xiii

1.1	Schematic diagram of (a) cycle (b) star (c) friendship (d) wheel and (e) regular graphs.	5
1.2	Schematic diagram of a multilayer network having two layers. Here, intra-layer edge set are denoted by E_1 , E_2 and inter-layer edge set as E_{12} respectively.	7
2.1	Network size is $n = 500$, $\langle k \rangle = 10$ and we iterate the rewiring process for 600,000 times and store the network after each 100^{th} steps. Changes of various network properties (a) IPR value of PEV (b) maximum degree (c) average clustering coefficient (d) degree-degree correlation (e) correlation between degree vector and clustering coefficient vector and (f) correlation between PEV and clustering coefficient vector during the evolution ($\tau_{evolution}$).	22
2.2	ER network as an initial network. Degree distribution of the (a) initial (b) intermediate and (c) optimized network. PEV entry distribution of the (d) initial (e) intermediate and (f) optimized network.	23
2.3	Schematic diagram representing the (a) initial and the (b) optimized networks.	25
2.4	Change in IPR value as a function of network evolution ($\tau_{evolution}$). (a) SF networks with $n = 500$ and $\langle k \rangle = 10$ (b) <i>C. elegans</i> frontal network with $n = 131$ and $\langle k \rangle = 11$ (c) <i>C. elegans</i> neural network with $n = 297$ and $\langle k \rangle = 14$. We consider crude approximations that edges are undirected and unweighted for <i>C. elegans</i> networks.	26
2.5	(a) Evolution ($\tau_{evolution}$) of IPR values for different network size. As network size increases, it takes more evolution time for a network to reach the optimized state. (b) IPR value of the initial ER and the final optimized networks as a function of n	27
2.6	IPR as a function of edge-rewiring. The networks with large IPR value in r_3 region consists of few edge-rewiring, which leads to a sudden drop in the IPR value. Rewiring of the first 1,00,000 edges is depicted. The marked square indicates the regime where the networks attain IPR values which are very close to the optimized network. However, in this regime rewiring an edge does not have a significant impact on the IPR values.	28
2.7	Behavior of λ_1 (\circ) and λ_2 (\bullet) during the network evolution ($\tau_{evolution}$). Initial network as (a) ER random network (b) SF network (c) <i>C. elegans</i> neural network.	29

2.8	Spreading process of SIS model on the initial ER random network ($\lambda_1^{init} \approx 11.34$, $Y_{x_1}^{init} \approx 0.0007$), an intermediate network ($\lambda_1^{imdt} \approx 11.14$, $Y_{x_1}^{imdt} \approx 0.21$) and an optimized network ($\lambda_1^{opt} \approx 10.77$, $Y_{x_1}^{opt} \approx 0.22$) and the <i>C. elegans</i> neural network ($\lambda_1^{init} \approx 24.36$, $Y_{x_1}^{init} \approx 0.019$ and $\lambda_1^{opt} \approx 17.18$, $Y_{x_1}^{opt} \approx 0.1$) have been depicted. ER network has $n = 2000$ nodes with $\langle k \rangle = 10$	31
3.1	Schematic diagram of (a) initial network and (b) the optimized network structure having two components evolved through the network evolution process discussed in chapter 2, section 2.3.	36
3.2	(a) Flipping behavior of IPR values of the largest (\bullet) and second largest (\circ) eigenvectors. (b) Detection of eigenvalue crossing through dot products $(x_1^i)^T x_1^{i+1}$ (\bullet) and $(x_2^i)^T x_1^{i+1}$ (\circ) in the r_3 region during the network evolution. Network parameters are same as in Fig. 3.	38
3.3	Largest two eigenvectors entries in (a) & (c) optimized network where the entry corresponding to the hub node is marked with circle, (b) & (d) after a single edge rewiring of the optimized network which is connected to the hub node. Network parameters are same as in Fig. 3.2. Due to Perron-Frobenius theorem, PEV entries are all positive, however second-largest eigenvector entries are both positive and negative. Hence, to observe the pattern of the eigenvectors entries, we take square of each entries.	39
3.4	Separation of range of m value based on the behavior of the discriminant value (Δ) of the cubic equation (in Eq. 3.11) for a particular value of n . For sparse network $\Delta < 0$ and $\Delta \geq 0$ as network becomes dense. Here, $\sigma = (1 - \frac{\epsilon}{3})$, $p = \frac{\epsilon^3 + 9\epsilon^2 + 36\epsilon}{27}$, $q = \frac{\epsilon^2 + 6\epsilon + 6}{9}$ and we consider $n \geq 49$	45
3.5	A method to direct construction of PEV localized network through the solution of a cubic equation. Given the input parameters (number of nodes (n), connections (m) and $\epsilon \ll 1$) to the coefficients of the cubic equation provide the roots (average degree κ), from which we calculate the size of wheel (\mathcal{W}) and random regular (\mathcal{R}) networks (Eqs. (3.6) and (3.9)). Finally, connecting \mathcal{W} and \mathcal{R} yields the PEV localized network.	47

- 3.6 We portray the evolution of steady-state vector of the RNA neutral network model population dynamical model on WRR model network. Starting from a uniform state vector, we perform the power iteration method to reach the steady-state vector. Due to the localized PEV in WRR model, the hub node contributes more to the dynamical process, and the rest of them have very less contribution. Here, $n = 500$, $\mu = 0.5$, $f = 2.6$, $L = 18$. For the wheel random regular combined network $\lambda_1^W > \lambda_1^R$ and $Y_{x_1} = 0.22$. We perform the power iteration method for 300000 iterations and store the PEV after each 1500 steps. 49
- 3.7 We depict the evolution of the steady-state vector of the RNA neutral network population dynamical model on the WRR model network where we rewire an edge connected to the hub node. Starting from a uniform state vector, we perform the power iteration method to reach the steady-state vector. Due to the delocalized PEV, there exists a drastic change in the steady-state of the dynamical process. Model parameters are same as in Fig. 3.6 but $\lambda_1^W < \lambda_1^R$ and $Y_{x_1} = 0.002$ 50
- 3.8 In the cubic equation for the coefficient $n = 1000$, $\epsilon = 0.00002$ and for different values of m in the range given by Eq. (3.24). (a) One can observe nature of three unequal real roots for $\Delta < 0$. (b) Behavior of the wheel graph component size calculated from Eq. (3.6) and for three different roots denoted as $n_1^{\kappa_1}$, $n_1^{\kappa_2}$ and $n_1^{\kappa_3}$ respectively. We can observe that for sparse network $n_1^{\kappa_1}$ is larger than n . On the other hand as network becomes dense, $n_1^{\kappa_3}$ becomes larger than n . $n_1^{\kappa_2}$ is always lesser than n 55
- 4.1 Localization transition in the PEV for hub node size being larger than the square of the average degree of the networks ($k_{max} > \kappa(\kappa + 1)$) [24]. For k_{max} being much larger, IPR value shows a drastical increase leading to a non-zero constant value. We consider a connected random graph of size $n = 100000$ and average degree $\kappa = 10$, where n^{th} node acts as a hub node and degree of the n^{th} node varies from 10 to 300. 61

4.2 Sorted localized PEV entries $((x_1)_i$ for $i = 1, 2, \dots, n$) for different network size. The average degree ($\kappa = 10$) and maximum degree ($k_{max} = 130$) remains fixed and which satisfies $k_{max} > \kappa(\kappa + 1)$. The PEV entries corresponding to the hub node (marked with a circle) and its adjacent nodes receive large constant weights as $n \rightarrow \infty$. The PEV entries corresponding to the nodes which are not connected to the hub node (after dotted vertical lines) gradually show a decrease, eventually becoming close to zero as $n \rightarrow \infty$ 62

4.3 Schematic representation of the wheel-random-regular model networks (\mathcal{G}_{WRR}). Here, n_1 is the number of nodes in the wheel graph and n_2 is the number of nodes in the random regular network having an average degree of κ . With an increase in the number of nodes in the random regular network, while fixing κ , the hub node size of wheel graph remains unchanged. 63

4.4 Value of localized PEV entries of (a) network constructed by combining a wheel graph (\mathcal{W}) with a random regular (\mathcal{R}) graph. We choose $n_1 = 1938$, $n_2 = 470$ and $\kappa = 45$ satisfying $\lambda_1^{\mathcal{W}} = \lambda_1^{\mathcal{R}} + \epsilon$, $\epsilon = 0.00002$ and yielding a network (\mathcal{G}_{WRR}) with $n = 2408$ nodes and $m = 14806$ edges. For \mathcal{G}_{WRR} , IPR value of PEV is equal to 0.2389. Next, by fixing size of \mathcal{W} , we increase size of \mathcal{R} by keeping κ constant. This arrangement leads to $\lambda_1^{\mathcal{W}} = \lambda_1^{\mathcal{R}} + \epsilon$ and keeps the PEV entries same for the hub as well as its adjacent nodes as $n \rightarrow \infty$. (b) The same network but by removing an edge connected to the hub node in \mathcal{W} and adding it between a pair of nodes in \mathcal{R} . This rewiring yields delocalization transition in PEV. By increasing the size of \mathcal{G}_{WRR} by including nodes to \mathcal{R} keeping the κ fixed, and the eigenvalue relation $\lambda_1^{\mathcal{W}} < \lambda_1^{\mathcal{R}}$ holds true, and PEV entries take very less values for the hub and its neighboring nodes as $n \rightarrow \infty$. (c) IPR values of PEV (Y_{x_1}) for the wheel-random-regular (WRR) graph as a function of combined network size n . For each value of n , we consider two WRR graphs, first WRR graph is generate by holding the relation in Eq. (6) and PEV is localized (■). The second WRR graph has an edge rewired, and PEV becomes delocalized (●). For reference to a delocalization, we plot $1/n$ (○) as a function of n 65

4.5	(a) Measure the difference between $\delta = \lambda_1^W - \lambda_1^{\tilde{W}}$ as a function of wheel graph size (n_1) after removing hub edge (●) and peripheral edge (○). IPR value of the combined network and the largest eigenvalue of the individual component as a function of ϵ to demonstrate that a particular value of ϵ is required to witness sudden change in the IPR value as a consequence of a single edge rewiring. (b) IPR of localized and delocalized graph and (c) plot λ_1^W & λ_1^R and (d) plots $\lambda_1^{\tilde{W}}$ & $\lambda_1^{\tilde{R}}$. The size of the wheel graph is calculated from Eq. (4.5), where parameters of the random graph is $n_2 = 500$ and $\kappa = 6$	67
4.6	(a) IPR values of PEV (Y_{x_1}) for the star-random-regular (SRR) graph as a function of combined network size n . For each value of n , we consider two SRR graphs, first SRR graph is generate by holding $\lambda_1^S > \lambda_1^R$ and PEV is localized (■). The second SRR graph has delocalized PEV by holding $\lambda_1^S < \lambda_1^R$ (●). For reference to a delocalization, we plot $1/n$ (○) as a function of n . (b) Same as (a) but for the friendship-random-regular (FRR) networks; (c) Same as (a) but for the scalefree-regular (SFRR) networks.	69
4.7	Pearson correlation between normalized degree vector and PEV of WRR (●), corresponding to the random regular component of WRR (○) and corresponding to wheel component of WRR (□), respectively as a function of n for (a) localized PEV state; (b) delocalized PEV state.	70
5.1	Schematic representation of the evolution of a multilayer network using the single-layer optimized edge rewiring scheme. A rewiring is accepted if it increases the IPR value of PEV of the multilayer networks.	81
5.2	IPR value of monolayer and multilayer model networks for different combinations. The size of the monolayer networks; $n_1 = n_2 = 200$ and $\langle k_1 \rangle = \langle k_2 \rangle = 10$. Thus, size and the average degree of the MN is $N = 400$ and $\langle k \rangle = 11$ respectively.	83
5.3	Optimized evolution of an initial ER-ER multilayer network for 50,000 edge rewirings for single-layer (■) and both-layers (▲). Size of the MN is $N = 400$, $\langle k \rangle = 7$, and $\langle k_1 \rangle = \langle k_2 \rangle$	86
5.4	Degree distribution of the initial multilayer network of (a) ER-ER ($N = 400$, $\langle k_1 \rangle = \langle k_2 \rangle = 6$) and (b) SF-SF ($N = 400$, $\langle k_1 \rangle = \langle k_2 \rangle = 6$). (c) and (d) depict the degree distribution of the optimized MN achieved through the both-layers rewiring protocol.	87

5.5	Cytoscape diagram of optimized MN obtained for (a) both-layers and (b) single-layer rewirings. For both the protocols, $N = 120$ and $\langle k \rangle = 3$, where $\langle k_1 \rangle = \langle k_2 \rangle$. A smaller size MN is considered here for a clear illustration of the optimized network structure. . . .	89
5.6	Changes in the IPR values (Y_{x_1}) with the evolution. (a) Single-layer rewiring protocol (PI) does not show IPR drops in the saturation region. (b) Both-layers rewiring protocol (PII) shows drops in the IPR value in the saturation region. (c) The behavior of the largest two eigenvalues of the single-layer and (d) both-layer rewiring protocols. Here, $N = 400$, $\langle k \rangle = 7$, and $\langle k_1 \rangle = \langle k_2 \rangle$	90
5.7	(a) Change in the IPR value during the evolution of MNs with various combinations of the initial networks for single-layer rewiring protocol (PI) and both-layer rewiring protocol (PII). (b) Value of $C_{x_1^{\mathcal{L}_1}}$ and $C_{x_1^{\mathcal{L}_2}}$ as two layers are multilayered and evolved. The initial multilayer network takes two different combinations; ER-ER and ER-SF with $N = 400$, $\langle k \rangle = 7$, and $\langle k_1 \rangle = \langle k_2 \rangle$. The rewiring has been done in the first layer (i.e., ER layer). The contribution of the rewired ER layer is represented by $C_{x_1^{\mathcal{L}_1}}$. (\bullet) and (\blacktriangle) represents this contribution for ER-ER, and ER-SF multiplex networks, respectively. Similarly, the fixed layer contribution ($C_{x_1^{\mathcal{L}_2}}$) for ER-ER and ER-SF multiplex network is depicted by (\circ) and (\triangle), respectively.	92
5.8	The IPR value ($Y_{x_1}^{\mathcal{M}}$) of (a) three layers and (b) four layers MN. The simulation is performed for (a) three and (b) four layers rewiring protocols. Each layer of \mathcal{M} contains 100 nodes and $\langle k_\alpha \rangle = 5$	93
6.1	An initial star network structure having $Y_{x_1}^{\mathcal{S}} \approx 0.25$. However, optimized edge rewiring process leads to a network structure having $Y_{x_1} \approx 0.267$ and network structure is substantially different than star network structure. Here, $n = 500$ nodes and $m = 499$ edges. . .	108
6.2	Changes in IPR values of all eigenvectors (Y_{x_j}) of ER as initial network is rewired using the scheme depicted in section 2.3. Here, only those edge rewirings in the r_3 region are allowed which lead to an increase in Y_{x_1} value. Network size $n = 500$ and $\langle k \rangle = 10$. The color scheme is generated through the code in Ref. [158].	114
6.3	Overall behavior of all the eigenvalues during the network evolution process started from ER network. Network parameters are same as in Fig. (6.2).	115

6.4	Changes in IPR values of all eigenvectors (Y_{x_j}) of SF as initial network is rewired using the scheme depicted in section 2.3. Network size $n = 500$ and $\langle k \rangle = 10$	115
6.5	Overall behavior of all the eigenvalues during the network evolution process started from SF network. Network parameters are same as in Fig. (6.4).	115
6.6	IPR as a function of edge-rewiring. The networks with large IPR value in r_3 region consists of few edge-rewiring, which leads to a sudden drop in the IPR value. Rewiring of the first 50,000 edges is depicted for SF as initial network. Here, $n = 500$ and $\langle k \rangle = 10$. . .	116

List of Tables

3.1	Largest three eigenvalues and IPR values of two largest eigenvectors of the optimized networks (\mathcal{G}_i) as well as its two components (\mathcal{C}_1^i and \mathcal{C}_2^i). After rewiring of an edge connected to the hub node in \mathcal{G}_i , the new network is denoted as \mathcal{G}_{i+1} and its two components are denoted with \mathcal{C}_1^{i+1} and \mathcal{C}_2^{i+1}	41
3.2	We portray various structural and spectral properties of two individual components (\mathcal{C}_1 and \mathcal{C}_2), as well as the combined network achieved by connecting them through a link. We consider ER random graph, Scalefree (SF), wheel (\mathcal{W}), and random regular (\mathcal{R}) networks as an individual component. Satisfying $\lambda_1^{\mathcal{C}_1} > \lambda_1^{\mathcal{C}_2}$ leads to a localized PEV and for $\lambda_1^{\mathcal{C}_1} < \lambda_1^{\mathcal{C}_2}$ yields delocalized PEV of the combined graph.	42
3.3	Various network parameters and IPR values of PEV for a given n and m . From the analytical derivations in Eq. (3.11), we decide κ , n_1 and n_2 . Thereupon, we construct a wheel graph of size n_1 and a random regular graph of size n_2 and join them with a node. This method leads to a highly localized PEV. We consider here $\epsilon = 0.02$	48
4.1	We portray various network parameters of wheel-random regular (WRR), stat-random regular (SRR), Friendship random regular (FRR) and scale-free random regular (SFRR) networks which provides localized PEV state.	70

5.1 Various properties of real-world social (first seven) and biological (last ten) multilayer networks. Inverse participation ratio (Y_{x_1}), maximum degree (k_{max}), average clustering coefficient ($\langle CC \rangle$), degree-degree correlation ($r_{deg-deg}$), PEV-degree correlation ($r_{pev-deg}$), PEV-cc correlation (r_{pev-cc}), the largest eigenvalue (λ_1), and the second-largest eigenvalue (λ_2) of few real-world MNs. Ref. [131] is used to calculate IPR and eigenvalues of MNs having large network size. The IPR values of the corresponding random networks are very close to $3/N$, which is predicted by the random matrix theory [52]. First, six networks with l layers are constructed based on the Twitter data with different exceptional events ranging from sports, politics to scientific discovery of Higgs boson. The layers represent retweet, reply, and mention on twitter [132] network. The CKM is a multilayer social network of a sample of physicians in US [133]. The *Drosophila* and *Homo* are the multilayer genetic and protein interaction networks where layers are the physical association, direct interaction, colocalization, association respectively [134–136]. The rest of the networks are also multilayer genetic and protein interaction networks, where we consider only the first four layers when the number of layers is more. We consider the largest connected component to calculate various properties and treat all the edges undirected and unweighted. Moreover, we measure the clustering coefficient value for all the nodes of the multiplex network having degree 2 or more, as nodes with degree 1 have zero clustering coefficient. 94

6.1 Results are shown for the average over 31 realizations with 6,00,000 edge rewiring steps. \mathcal{G}_{opt} denotes the optimized network achieved through the network evolution from the initial base network being \mathcal{G}_{init} network. \mathcal{G}_{opt}^{conf} refers to the network constructed from the configuration model having the same degree sequence as of the \mathcal{G}_{opt} network. \mathcal{G}_{opt}^{cc} refers to the network constructed with the same $\langle CC \rangle$ and degree sequence as in the \mathcal{G}_{opt} network. Finally, $\mathcal{G}_{opt}^{r_{deg-deg}}$ refers to the network having the degree-degree correlation as in the \mathcal{G}_{opt} network. 113

6.2	Various spectral properties of different synthetic and real-world networks [134, 159, 160]. We consider symmetric adjacency matrices corresponding to the connected networks having binary entries. For the networks largest two eigenvalues are close to each other however having a delocalized PEV.	116
6.3	Various network parameters and IPR values of PEV for a given n and m . From the analytical derivations in Eq. (3.11), we decide κ , n_1 and n_2 . Thereupon, we construct a wheel graph of size n_1 and a random regular graph of size n_2 , and join them with a node. We rewire an edge connected to the hub node and connect in random regular network. This leads to a delocalized PEV denoted as $Y_{x_1}^d$. We consider here $\epsilon = 0.02$	117

Chapter 1

Introduction

1.1 Overview

Networks are composed of interconnected units that interact with each other forming the infrastructure for different dynamical systems [1]. The exact pattern of interconnection between these units can take on various forms that dictate the functionality of a system [2]. The relationship between the interconnected architecture and functionality is essential to understand the questions pertaining to how the virus spreads nationwide, how information spreads through the social networks or how neurons interact to perform specific functions over the brain networks [1, 3]. An important microscopic question concerns whether some units of a system participate significantly and the rest of the others have a tiny contribution, or all the units have the same amount of contribution to a dynamical process [4, 5]. For instance, during the disease spread, it is important to investigate whether a portion of the network is affected more than other parts, whether perturbation remains restricted to the vicinity of the source unit or reaches to the remote units, which properties of a network allow different regions to process information over different timescales [4–

7]. Spectral (eigenvalues and eigenvectors) properties provide important clues on the interplay between interconnection architecture and network dynamics [8–10].

A promising paradigm that assists in understanding the above phenomena is the localization behavior of eigenvectors of matrices associated with the networks [4, 5, 7, 11–20]. Localization of an eigenvector refers to a state when a few components of the vector take very high values while the rest of the components take small values independent of the network size. Specifically, the eigenvector corresponding to the largest eigenvalue referred to as principal eigenvector (PEV) of the adjacency matrix approximate the steady-state behavior of linear-dynamical process on the network [9]. On characterizing the network properties that enhance the localization of PEV, it is found that a few interconnected units participate significantly and the rest of the units contribute very less in the linear-dynamical process [4, 11, 12]. Understanding the relationship between the interconnection architecture and PEV localization in a system could improve the efficiency and robustness of the system performance [11, 21, 22].

Existing research expressed that network properties such as the presence of high degree unit, the existence of a dense subnetwork, and a power-law degree distribution are a few factors known to make a PEV localized [4, 23–25], however basic intuitions about the network properties that enhance localization of PEV have remained elusive. We formulate an optimized network evolution process and reveal some important network properties which enhance the PEV localization in networks. Finally, we develop an analytical framework assisting the construction of a localized network structure and avoiding the optimized evolution process. Although our primary focus lies in the characterization of network properties which enhance localization, in order to validate our results, we use linear-dynamical processes. Our analysis on model networks formalism aids in understanding the steady-state behavior of a broad range of linear-dynamical processes, from epidemic spreading to biochemical dynamics, associated with the adjacency matrices. Our results offer fundamental insights into the network properties with the localization behavior of PEV in adjacency matrices.

We devote the next few sections in discussing basic definitions of networks, the importance of eigenvector localization, the motivation behind this thesis, and finally, a brief sketch of our works elaborated in the individual chapters.

1.2 Networks and basic definitions

A graph or network can be represented as $\mathcal{G} = (V, E)$ where $V = \{v_1, v_2, \dots, v_n\}$ is the set of units (nodes or vertices) and $E = \{e_1, e_2, \dots, e_m\}$ is the set of interconnections (edges or links) among them [26]. We denote $|V| = n$ as the number of nodes and $|E| = m$ being the number of edges of \mathcal{G} . Here, we consider undirected (if there is an edge between nodes v_i to v_j , then there must be an edge between v_j to v_i), unweighted (edge weights are always one), and connected networks. The present work restricts to simple networks, i.e., the network without multiple connections and self-loop. In a graph, two or more edges joining the same pair of vertices are multiple edges. An edge joining a vertex to itself is a self-loop. Hence, the corresponding adjacency matrix can be denoted as \mathbf{A} and represented easily as

$$a_{ij} = \begin{cases} 1 & \text{if nodes } v_i \text{ and } v_j \text{ are connected} \\ 0 & \text{Otherwise} \end{cases} \quad (1.1)$$

Degree: In a graph, the degree of a vertex v_i is the number of edges incident with v_i , denoted as $k_{v_i} = \sum_{j=1}^n a_{ij}$ or simple k_i

Degree sequence: The degree sequence $(\{k_i\}_{i=1}^n)$ of a graph \mathcal{G} is the sequence obtained by listing the vertex degrees of \mathcal{G} in increasing order, with repeats as necessary.

Average degree: The average degree of the network is denoted by $\langle k \rangle = \frac{1}{n} \sum_{i=1}^n k_i$.

Maximum degree: We refer the maximum degree node or the hub node of \mathcal{G} as $k_{max} = \max_{1 \leq i \leq n} k_i$.

Degree distribution: Degree distribution of a network is represented as $p(k)$ which says fraction of vertices having degree k . We can calculate $p(k) = \frac{\Gamma_k}{n}$, where Γ_k is the number of nodes having degree k [27].

Clustering Coefficient: Clustering coefficient [28] of node i is calculated by

$$C_i = \frac{2\Delta_i}{k_i(k_i - 1)}$$

where k_i denotes the degree of node i , and Δ_i is the number of edges between the k_i neighbors of node i . C_i is the “probability that two neighbors of a node link to each other” and also called as local clustering coefficient. The average clustering coefficient is represented as,

$$\langle CC \rangle = \frac{1}{n} \sum_{i=1}^n C_i$$

and $\langle CC \rangle$ is the “probability that two neighbors of a randomly selected node link to each other [28]”.

Degree-degree correlation: The degree-degree correlation is measured by the Pearson correlation coefficient and denoted as [29]

$$r_{deg-deg} = \frac{[m^{-1} \sum_{i=1}^m j_i k_i] - [m^{-1} \sum_{i=1}^m \frac{1}{2}(j_i + k_i)]^2}{[m^{-1} \sum_{i=1}^m \frac{1}{2}(j_i^2 + k_i^2)] - [m^{-1} \sum_{i=1}^m \frac{1}{2}(j_i + k_i)]^2}$$

where m is the total number of edges in the network and j_i, k_i are the degrees of nodes with i^{th} edge and $r_{deg-deg}$ value varies in between -1 to 1 . When high degree nodes connected to other high degree nodes in a network, then $r_{deg-deg}$ values become positive and referred to as an assortative network. In case of high degree nodes connected to lower degree nodes, then $r_{deg-deg}$ becomes negative, and the network is said to be disassortative.

Node centrality: Centrality of a node measures how important a particular node is with respect to some properties. There exist different centrality measures based on the degree of a node or eigenvector entry corresponding to a node, for instance, degree centrality, eigenvector centrality, Katz centrality, PageRank [27].

1.2.1 Spectral properties

Here, we consider undirected network, thus the adjacency matrix of the network, \mathbf{A} is a real symmetric matrix, and it has a spectral decomposition $\mathbf{A} = \mathbf{X}\mathbf{\Lambda}\mathbf{X}^T$. The $\mathbf{X} \in \mathbb{R}^{n \times n}$ contains orthonormal eigenvectors $\{\mathbf{x}_1, \mathbf{x}_2, \dots, \mathbf{x}_n\}$ i.e. $\|\mathbf{x}_i\|_2^2 = 1$ and the diagonal matrix $\mathbf{\Lambda} \in \mathbb{R}^{n \times n}$ contains corresponding eigenvalues $\{\lambda_1, \lambda_2, \dots, \lambda_n\}$ and called the *spectrum* of \mathcal{G} . The eigenvalues are real and in the order $\lambda_1 \geq \lambda_2 \geq \dots \geq \lambda_n$ and corresponding orthonormal set of eigenvectors are denoted as

$$\mathbf{x}_i = ((x_i)_1, (x_i)_2, \dots, (x_i)_n)^T$$

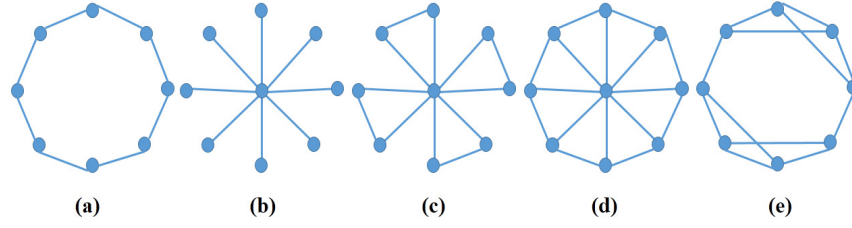


Figure 1.1: Schematic diagram of (a) cycle (b) star (c) friendship (d) wheel and (e) regular graphs.

for $i = 1, 2, \dots, n$. \mathbf{A} has n real eigenvalues, and some eigenvalues may be repeated (degenerate). The algebraic multiplicity of an eigenvalue λ of \mathbf{A} is the number of times that λ is repeated. If $\text{alg mult}_{\mathbf{A}}(\lambda) = 1$, then λ is said to be a simple (non-degenerate) eigenvalue. The geometric multiplicity of an eigenvalue λ of \mathbf{A} is the number of linearly independent eigenvectors that are associated with \mathbf{A} . The set $\{\mathbf{x} \in \mathbb{R}^n | \mathbf{A}\mathbf{x} = \lambda\mathbf{x}\}$ corresponding to λ is a subspace of \mathbb{R}^n and is called eigenspace of λ and is denoted as $\mathcal{E}(\lambda)$ [30]. Further, \mathbf{A} is a non-negative ($a_{ij} \geq 0$) and irreducible (connected network) matrix and it follows from the Perron-Frobenius theorem [27] that there exists a positive and simple eigenvalue, λ_1 . The eigenvector corresponding to λ_1 is a unique positive eigenvector (\mathbf{x}_1) referred as the principal eigenvector (PEV).

1.2.2 Model Networks

In the following, we briefly explain the basic graph models [26] that are used in the later chapters.

Cycle graph: A cycle graph is a graph consisting of a single cycle of vertices and edges, represented as $\mathcal{C} = \{V_{\mathcal{C}}, E_{\mathcal{C}}\}$ where $|V_{\mathcal{C}}| = n$ and $|E_{\mathcal{C}}| = n$ (Fig. 1.1(a)).

Star graph: In a star graph one node is connected to all other nodes and denoted as $\mathcal{S} = \{V_{\mathcal{S}}, E_{\mathcal{S}}\}$ where $|V_{\mathcal{S}}| = n$ and $|E_{\mathcal{S}}| = n - 1$ (Fig. 1.1(b)).

Friendship network: A friendship graph ($\mathcal{F} = \{V_{\mathcal{F}}, E_{\mathcal{F}}\}$) can be constructed by merging l copies of the cycle graph of length 3 with a common vertex (Fig. 1.1(c)). For friendship graph $|V_{\mathcal{F}}| = n = 2l + 1$ is the number of nodes and $|E_{\mathcal{F}}| = 3l$ is the number of edges in \mathcal{F} .

Wheel graph: A wheel graph is denoted as $\mathcal{W} = \{V_{\mathcal{W}}, E_{\mathcal{W}}\}$ and is formed by connecting one node to all the nodes of a cycle graph of size $n - 1$ (Fig. 1.1(d)). Here, $|V_{\mathcal{W}}| = n$ is the number of nodes and $|E_{\mathcal{W}}| = 2(n - 1)$ is the number of edges in \mathcal{W} .

Regular graph: A graph is said to be regular if each node has same degree and denoted as $\mathcal{R} = \{V_{\mathcal{R}}, E_{\mathcal{R}}\}$ (Fig. 1.1(e)). Therefore, degree of each node is k which is equal to the average degree i.e. $\langle k \rangle = k$. We denote $|V_{\mathcal{R}}| = n$ and $|E_{\mathcal{R}}| = \frac{nk}{2}$.

Erdős-Rényi random network: For the above models, structure of the graph is fixed. In the following, we discuss about the network models which can be generated randomly. One of the important random graph model is the Erdős-Rényi (ER) random graph or $\mathcal{G}(n, p)$ model [27]. To generate the ER random networks, we provide two parameters, one is the network size (n) and another is the probability (p). For each pair of nodes, we connect an edge with a probability p , where $p = \frac{\langle k \rangle}{n}$. Hence, the expected number of edges $\langle m \rangle = \binom{n}{2}p$ and $\langle k \rangle = (n - 1)p$. The degree distribution of ER random network follows binomial distribution $p(k) = \binom{n-1}{k} p^k (1 - p)^{n-1-k}$ and for $n \rightarrow \infty$ degree distribution can be approximated to Poisson distribution $p(k) = e^{-\langle k \rangle} \frac{\langle k \rangle^k}{k!}$.

Scalefree networks: A scale-free (SF) network is another random graph model where degree distribution of the network obeys power-law ($p(k) \sim k^{-\gamma}$) [27]. The SF network is constructed using the Barabasi-Albert preferential attachment model [27]. Many real-world networks follow power-law degree distribution and one of the main reasons for the popularity of this model network.

Configuration model: The ER random or SF networks have a specific degree distribution. However, the configuration model [27] plays a significant role to generate a network randomly while fixing the degree sequence. It is known that the generated networks through the configuration model having a fixed degree sequence, however, allow for self-loops and multiple edges. In this dissertation, we have used a similar kind of model devised by *Genio et al.* to generate networks randomly when avoiding multiple edges and self-loops [31]. For the model, we always provide a non-increasing degree sequence, and for the details, we refer to Ref. [31].

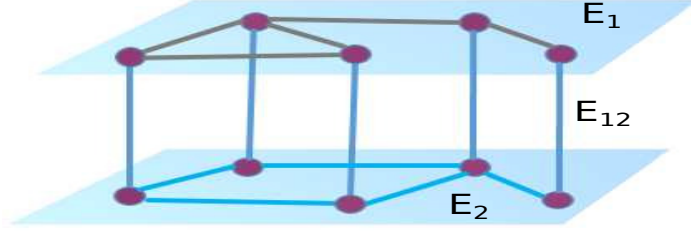


Figure 1.2: Schematic diagram of a multilayer network having two layers. Here, intra-layer edge set are denoted by E_1 , E_2 and inter-layer edge set as E_{12} respectively.

1.3 Multilayer networks:

The traditional monolayer network framework offers only a limited representation of complex systems having different layers of interactions. Recent years have witnessed the emergence of the multilayer network (MN) framework, which provides more accurate insights into the behaviors of complex systems possessing multiple types of relations among the same units [32–41]. In contrast, all the above model networks discussed above are referred to as monolayer networks.

We represent a multilayer network (MN), $\mathcal{M} = (\mathcal{G}, \mathcal{C})$ [34], where $\mathcal{G} = \{\mathcal{L}_\alpha; \alpha \in \{1, 2, \dots, l\}\}$ is the family of connected monolayer network $\mathcal{L}_\alpha = \{V_\alpha, E_\alpha\}$, where $V_\alpha = \{v_1^\alpha, v_2^\alpha, \dots, v_n^\alpha\}$ is the set of vertices and $E_\alpha = \{e_1^\alpha, e_2^\alpha, \dots, e_{m(\alpha)}^\alpha\}$ is the set of edges in the α layer of the MN. In addition, $\mathcal{C} = \{E_{\alpha\beta} \subseteq V_\alpha \times V_\beta : \alpha, \beta \in \{1, 2, \dots, l\}, \alpha \neq \beta\}$ is the set of edges between \mathcal{L}_α and \mathcal{L}_β layers. We refer E_α as the set of all intra-layer edges and $E_{\alpha\beta} = \{e_1^{\alpha\beta}, e_2^{\alpha\beta}, \dots, e_n^{\alpha\beta}\}$ as the set of all inter-layer edges of \mathcal{M} . Here, we consider each node in one layer connected to its mirror node in the other layers of the MN, and all the layers consist of exactly the same number of nodes.

We denote the adjacency matrices corresponding to \mathcal{L}_α as $\mathbf{A}^\alpha \in \mathbb{R}^{n \times n}$ constructed using the above relation (1.1). We represent degree of a node v_i^α in layer α as $k_{v_i^\alpha} = \sum_{j=1}^{n_\alpha} (a^\alpha)_{ij}$ and the average degree of α layer as $\langle k_\alpha \rangle = \frac{1}{n_\alpha} \sum_{i=1}^{n_\alpha} k_{v_i^\alpha}$. The average degree of the MN is denoted as $\langle k \rangle = 1 + \frac{\sum_{\alpha=1}^l \langle k_\alpha \rangle}{l}$. For instance a schematic diagram of a two layers MN is portrayed in Fig. 1.2, with $\mathcal{L}_1 = \{V_1, E_1\}$

and $\mathcal{L}_2 = \{V_2, E_2\}$, where $|V_1| = |V_2| = n$, $|E_1| = m_1$, $|E_2| = m_2$, and $|E_{12}| = n$. Hence, the total number of nodes in \mathcal{M} is $|V| = 2n = N$ and edges $|E| = m_1 + m_2 + n = M$. The supra-adjacency matrix [34] of the two layer MN is a block matrix and can be defined as:

$$\mathbf{A}_{\mathcal{M}} = \begin{bmatrix} \mathbf{A}^1 & \mathbf{I} \\ \mathbf{I} & \mathbf{A}^2 \end{bmatrix}$$

where \mathbf{I} is an $n \times n$ identity matrix. The layer of a multilayer network can be any above model networks (i.e., regular, star, ER random or SF networks). The analysis of the multilayer networks needs different measurements than monolayer networks and for the details readers are refer to some interesting articles [32–41]. In this dissertation, model multilayer networks are unweighted, and the number of nodes in each layer is same. In chapter 5, we discuss more on the structural and spectral properties of multilayer networks.

1.3.1 Eigenvectors in networks

The graph isomorphism has applications in many areas of science, including Feynman diagrams, biometrics, molecular modeling, and cryptography [42–45]. It is well known that a pair of isomorphic graphs are cospectral (two graphs have the same spectrum). Two graphs are isomorphic if there exists a one-to-one correspondence between their vertex sets which preserves adjacency [46]. However, the existence of non-isomorphic cospectral graphs indicates that eigenvalues of the adjacency matrices are not enough for characterizing the corresponding graphs, additional information of the eigenspace (eigenvectors) is necessary to find the isomorphism pairs in cospectral graphs [30]. In addition to the graph isomorphism, there exists other problems in network science which includes ranking of vertices [47], detection of communities [48, 49], perturbation analysis [7, 22, 50], vibration confinement [51], identification of important genes [52], detecting anomaly in computer systems [53] where investigations of eigenvectors provide understanding to the behaviors of the underlying systems. Particularly, PEV of the adjacency matrices plays a crucial role in the characterization of various structural as well as dynamical properties of the underlying graphs [9, 25, 54]. For instance, a connected non-

bipartite graph having the largest eigenvalue λ_1 and $\mathbf{x}_1 = ((x_1)_1, (x_1)_2, \dots, (x_1)_n)^T$, the number of walks of length k between a pair of vertices i and j is asymptotic to $\lambda_1^k (x_1)_i (x_1)_j$ as $k \rightarrow \infty$ (see Theorem 2.2.5 of Ref. [30]). Further, for various linear-dynamical processes on networks, for instance, epidemic spreading, population dynamics of Ribonucleic acid (RNA) neutral networks, rumor spreading, brain network dynamical models the steady-state vector has been approximated using the PEV [9, 11, 12]. To understand how an individual entity is infected or how information spreads in a network in the steady-state, it is sometimes enough to analyze the PEV of the corresponding adjacency matrices.

Existing research on networks has focused on connecting the steady-state vector of linear-dynamical systems to the PEV with a prime focus to understand the role of largest eigenvalue [55–57], and little is known about the behavior of PEV of adjacency matrices [58, 59]. In this dissertation, we focus on understanding the localization behavior of PEV and its relation with the network properties (structural and spectral).

1.3.2 Eigenvector localization in networks

Roots of the eigenvector localization trace back to the Anderson localization which describes the diffusion of electrons in a random, disordered medium [60, 61]. Localization of an eigenvector refers to a state when a few components of the vector take very high values while the rest of the components take small values regardless of the system size. Anderson model was used in various scientific disciplines and received remarkable success in understanding behaviors of many complex systems [62–68], driving interest to investigate localization transition in complex networks [62, 69, 70]. Motivated from the success of the Anderson localization in understanding the behavior of complex systems, we focus on exploring eigenvector localization to gain insight into the behavior of corresponding complex systems of network’s adjacency matrices. Note that we consider binary irreducible symmetric matrices with zero diagonal elements and investigation of Anderson localization associated with Hamiltonian matrices having non-zero diagonal elements [61].

Existing research on eigenvector localization in networks unveiled that PEV of the adjacency matrix is helpful in getting insight into the propagation or localization of information in the underlying systems [4, 11, 12]. One key factor of our interest is to understand the properties of networks which may help in spreading or restricting information in networks [7]. For instance, during a disease outbreak, one will be interested in knowing if the disease will spread through the underlying network leading to the pandemic or will be restricted to a smaller section of the network [4, 71]. Similarly, one may be interested in spreading a piece of particular information, for instance, awareness of vaccination at the time of disease outbreak, or may wish to restrict a rumor propagation [72]. Furthermore, the eigenvector centrality (EC) measure has been very popular due to its ability in measuring the importance of the nodes based on not only the number of interactions they acquire but also particular structural positions they have in the networks. It was found that EC measure may fail upon the consequence of PEV localization [24]. Note that EC measures and the PEV localization have two different perspectives. The former is used to rank the nodes, and the latter stands as a particular phenomenon which predicts difficulties associated with the EC measure. Moreover, Arruda et al. extended the PEV localization concepts for multilayer networks (MNs) [73] and identified that PEV localization behaviors for MNs could be different from the monolayer networks. Specifically, in the monolayer networks, localization can happen on a few nodes [4] whereas, in MNs, a layer can be localized [73]. These investigations shed light on the properties of the multilayer networks and their relations with the PEV. The PEV localization of network is confirmed if there exists a particular arrangement of nodes and edges such that few entries of the PEV take very large values with rest of the entries taking tiny values, and this arrangement should hold good irrespective of the network size. Network properties which enhance the PEV localization remain elusive, and we attempt to understand in this dissertation. Note that an eigenvector or a set of eigenvectors associated with a matrix corresponding to a network might be localized and simultaneously it might be possible that an eigenvector or a set of eigenvectors are delocalized.

1.3.3 Inverse Participation Ratio

We use the inverse participation ratio (IPR) to measure the extent of PEV localization [24, 25]. This measure had been introduced to quantify the participation of atoms in a normal mode of vibration and is similar to the fourth moment in statistics [74, 75]. Later on, IPR had been used as an effective measure to quantify the localized and the delocalized eigenvectors in complex networks [9, 15, 16, 17, 18, 19, 21, 22, 24]. We calculate the IPR value ($Y_{\mathbf{x}_i}$) of an orthonormal eigenvector ($\mathbf{x}_i = ((x_i)_1, (x_i)_2, \dots, (x_i)_j, \dots, (x_i)_n)^T$) corresponding to nondegenerate eigenvalue of \mathbf{A} as follows [60]:

$$Y_{\mathbf{x}_i} = \sum_{j=1}^n (x_i)_j^4 \quad (1.2)$$

where $(x_i)_j$ is the j^{th} component of \mathbf{x}_i . A delocalized eigenvector ($\mathbf{x}_i = (\frac{1}{\sqrt{n}}, \frac{1}{\sqrt{n}}, \dots, \frac{1}{\sqrt{n}})^T$) has $Y_{\mathbf{x}_i} = \frac{1}{n}$, whereas the most localized eigenvector ($\mathbf{x}_i = (1, 0, \dots, 0)^T$) yields an IPR value equal to $Y_{\mathbf{x}_i} = 1$. These are two extreme cases for the eigenvector localization and thus IPR lies in the range $\frac{1}{n} \leq Y_{\mathbf{x}_i} \leq 1$.

It is known that for any connected regular graph, $\mathbf{x}_1 = (\frac{1}{\sqrt{n}}, \frac{1}{\sqrt{n}}, \dots, \frac{1}{\sqrt{n}})^T$ (Theorem 6 [26]) and thus, $Y_{\mathbf{x}_1} = \frac{1}{n}$. Therefore, for a regular network IPR value of PEV provides the lower bound. Hence, a sparse as well as a dense regular network both will have a delocalized PEV. For instance, if we consider a graph where each node is isolated without having any interaction with any one and having a self-loop, adjacency matrix will be nothing but an identity matrix and for which we can choose $\mathbf{x}_1 = (1, 0, \dots, 0)^T$ leading to $Y_{\mathbf{x}_1} = 1$. Additionally, for any disconnected network, PEV entries might be zeros. For instance,

$$\mathbf{A} = \begin{pmatrix} 0 & 1 & 0 & 0 \\ 1 & 0 & 0 & 0 \\ 0 & 0 & 0 & 1 \\ 0 & 0 & 1 & 0 \end{pmatrix}$$

has eigenvalues $\{-1, -1, 1, 1\}$. Hence, the largest eigenvalue is repeated (degenerate) and thus we can choose PEV as a linear combination of basis eigenvectors $c_1(1, 1, 0, 0)^T + c_2(0, 0, 1, 1)^T$ or eigenspace of λ_1 , $\mathcal{E}(\lambda_1) = 2$. We can choose $\mathbf{x}_1 = (1, 1, 1, 1)$ as PEV by taking $c_1 = 1$ and $c_2 = 1$ or $\mathbf{x}_1 = (1, 1, 0, 0)$ by taking

$c_1 = 1$ and $c_2 = 0$. Now, if we calculate the IPR value for these two PEVs, we get two different IPR values. One can observe that the former IPR value is lesser than the later one. Therefore, to get a unique PEV, we consider irreducible and non-negative matrices in our study. Hence, from the Perron-Frobenius theorem all the entries of the PEV is positive. Therefore, IPR value of the PEV should be in the range $1/n \leq Y_{x_1} < 1$ for $n \geq 2$. However, to test whether the PEV is localized or not for IPR being in the range $1/n < Y_{x_1} < 1$, we adopt the procedure proposed for the detection of the Anderson localization [60] and which was recently used to measure the eigenvector localization in complex networks [23–25]. According to this procedure, one should calculate the IPR value of PEV for different network sizes. If Y_{x_1} tends to have a constant value as $n \rightarrow \infty$, PEV is localized, otherwise it is delocalized [25]. In other words, for a network, PEV is said to be localized if $Y_{x_1} = \mathcal{O}(1)$ and delocalized if $Y_{x_1} \rightarrow 0$ as $n \rightarrow \infty$ [4].

1.4 Motivation behind this thesis

We represent an undirected network by an adjacency matrix which encodes the interactions or relations among n entities (nodes) of a real-world complex system. The adjacency matrix is real symmetric, and spectral decomposition exists [93] as follows.

$$\mathbf{A} = \mathbf{X}\mathbf{\Lambda}\mathbf{X}^T \quad (1.3)$$

Therefore, we have n number of eigenvectors which represent n different solutions of the system. We can think of as eigenvectors entries acting as a function on nodes. Hence, by knowing the behavior of the eigenvectors (\mathbf{X}), we can provide information about the underlying systems represented in terms of the adjacency matrix. Moreover, each eigenvector has different meaning corresponding to the underlying system [5]. It is straightforward to find eigenvalues and eigenvectors of a matrix but challenging to interpret the meaning of the eigenvector entry behavior and its relation with the network structure. We know that PEV approximate the steady-state of linear dynamical processes which include information spreading, rumor spreading, emotional spreading in emergencies, a spread of cultural norms, knowledge & in-

novations, epidemic spreading [3, 9]. The epidemic spreading phenomenon is the basis for all of the models, and a cornerstone feature of epidemic processes is the presence of the so-called epidemic threshold [3]. Below the threshold, the disease does not spread, and above the threshold, the disease spreads across the population. It is well known that the threshold is inversely proportional to the largest eigenvalue of the adjacency matrix [3, 76]. In other words, the largest eigenvalue provides a threshold for such spreading process, but it can not say about the behavior of the spreading process in the steady-state, means how do the nodes of a network is affected during the disease spread. Analyzing the localization behavior of PEV plays a significant role in understanding the behavior of a linear-dynamical process in the steady-state [4, 11]. For instance, A linear-dynamical system represented by a network having a localized PEV indicates, a few nodes have significant contribution and rest of other nodes have a tiny contribution. Similarly, for a delocalized PEV, all the nodes have the same amount of contribution to a linear-dynamical process. Hence, network properties which enhance PEV localization can implicitly restrict the linear-dynamics in a smaller section of the network in the steady-state. A fundamental question at the core of the structural-dynamical relation is that of optimization [22]: How can we optimize the underlying graph structure to affect the outcome of the dynamical process in the desired way? Optimizing the largest eigenvalue of the adjacency matrix by edge manipulation to control the threshold of the spreading process has been analyzed [21, 77]. However, finding network structure optimizing the localization behavior of PEV remains elusive and an open challenge. Understanding the network properties of optimized structures helps us to engineer the system architecture, enhance robustness, as well as can provide insights into the underlying mechanism of their evolution [22]. Therefore, we have an interest in the network properties and its relations with the PEV localization of adjacency matrices.

Considering any connected undirected and unweighted regular network structure, we have a delocalized PEV. We even do not know for which kind of network structure one can get a delocalized PEV which is different from the regular network

structure. On the other hand, for a star network $\mathbf{x}_1^S = \left(\frac{1}{\sqrt{2}}, \frac{1}{\sqrt{2(n-1)}}, \dots, \frac{1}{\sqrt{2(n-1)}} \right)$ and hence, $Y_{\mathbf{x}_1^S} = \frac{1}{4} + \frac{1}{4(n-1)}$. Considering a same size wheel graph, we have $\mathbf{x}_1^W = \left(\frac{1}{\beta}, \frac{\alpha}{\beta}, \dots, \frac{\alpha}{\beta} \right)$ where $\alpha = \frac{\sqrt{n+1}}{n-1}$, $\beta = \sqrt{1 + \frac{(\sqrt{n+1})^2}{n-1}}$ [78] and $Y_{\mathbf{x}_1^W} = \frac{1}{4} \frac{(n-1)^2}{(n+\sqrt{n})^2} + \frac{(\sqrt{n+1})^4}{4(n-1)(n+\sqrt{n})^2}$. Hence, for $n \rightarrow \infty$, we get $Y_{\mathbf{x}_1^S} = Y_{\mathbf{x}_1^W} \approx 0.25$, and PEVs are localized for both of the star and wheel networks. Further, for any model networks, it is difficult to find a closed functional form of PEV directly and thus difficult to find the IPR value. It has been reported that for ER random network each node having the same expected degree, and hence we get delocalized PEV [79]. In contrast, for SF networks presence of hub nodes and power-law degree distribution lead some amount of localization in the PEV and IPR value is larger than ER random networks and much lesser than the star networks [4, 23–25]. Indeed, we do not know there is any possibility to get different structure than a star, a wheel, or even an SF network structure which provides a more localized network structure. By understanding network properties, one can artificially construct network structure to have control over the linear-dynamical processes on the networks. The entire thesis revolves around to find the answers to the following questions for PEV of the adjacency matrix and few places explicitly mention the other eigenvectors. How can we understand the role of the PEV entry behavior in networks? How do PEV entries and network structure is related? What are the structural and spectral properties which lead to most localized PEV? How can we perform an optimization process to find the network structure?

1.5 Thesis Overview

- In chapter 2, we address the challenges by formulating the problem as for a given number of nodes and edges; we aim to construct a connected network structure which has the most localized PEV. We devise an optimized network evolution method and identifies several network properties which lead to highly localized PEV. Our inspection unveils that PEV localization is not a consequence of the existence of an individual network property, and prefer-

ably involves the cumulative impact of changes in various structural features. We succeed in constructing a blueprint of the network topology corresponding to a highly localized PEV which possesses a distinctive architecture. It consists of two subgraph components of different sizes which are connected via a single node. We reveal that for highly localized PEV, the hub node should be connected to a small set of nodes, not to all the nodes. For the most localized network, we find a set of edges rewiring any one of them leads to complete delocalization of the PEV. We observe that this emergence of sensitivity in the PEV and shifting of λ_2 close to λ_1 happens simultaneously, suggesting a relation between the special structure of the optimized network and the second largest eigenvalue of the network.

- In chapter 3, we investigate the origin of the occurrence of the sensitivity of PEV in highly localized networks and show that the high localization of PEV is related to the behavior of the largest eigenvalue of the subgraph components. Taking a clue from the subgraphs eigenvalue relation, we develop an analytical framework which assists for construction of highly localized networks without performing an optimization scheme. To address the challenges, we introduce wheel random regular (WRR) model network and propose a scheme for partitioning a given network parameter. To achieve subgraph components size, we analytically solving the roots of a cubic equation built up from the network properties required for localized PEV. Analysis of the discriminant of the cubic equation reveals another important result that for a wheel random regular network, one can achieve a localized PEV in two different ways either by connecting a sparse random regular subgraph with a small wheel subgraph or connecting by a dense random regular subgraph with a large wheel subgraph structure.
- Chapter 4 explores the investigation involves the problems associated with the eigenvector centrality (EC) measure. Despite the considerable success of EC in ranking the nodes of a network, using the WRR model, we show that

along with the occurrence of localized PEV state, the existence of delocalization of PEV can also affect weights assignment to the higher degree nodes based on EC, thereby creating difficulties in accessing relative importance of the nodes, causing the failure of EC. While it is evident that random regular networks have delocalized PEV as all the nodes carry the same information in the network, investigations of the WRR model reveals that graphs consisting of heterogeneous degrees can also have delocalized PEVs.

- Chapter 5 extends the optimized edge rewiring on monolayer networks to multilayer networks. Starting with a multilayer network corresponding to a delocalized PEV, we rewire the network edges using an optimization technique such that the PEV of the rewired multilayer network becomes localized. For two layers MN, we implement two different edge rewiring protocols; (1) by rewiring edges in both-layers or (2) by rewiring edges in only one layer. We reveal that for both the rewiring protocols, though there is an emergence of various specific structural features, the different rewiring protocols lead to a noticeable difference in the spectral properties of the optimized MN. For the both-layers rewiring protocol, PEV is sensitive to a single edge rewiring in the optimized MN; however, interestingly, we get rid of this sensitivity of PEV for the single-layer rewiring protocol. This sensitivity in the localization behavior of PEV is accompanied by the second largest eigenvalue lying very close to the largest one. Furthermore, analysis of multilayer networks constructed using real-world social and biological data show that the localization properties of these real-world multilayer networks are in good agreement with the simulation results for the model multilayer network.
- Finally, Chapter 6 provides the conclusion of the study and discusses open problems for future research.

Chapter 2

Numerical schemes for the construction of PEV localized networks

2.1 Introduction

Networks provide a simple framework to understand and predict the properties of complex real-world systems by modeling them in terms of interacting units [80]. This framework is successful in explaining various mechanisms behind the emergence of collective behaviors of systems arising due to the local interaction patterns of their components. Principal eigenvector (PEV) corresponding to the maximum eigenvalue of the network's adjacency matrix is helpful in getting insight into the propagation or localization of information in the underlying systems [4]. One key factor of our interest is to understand the properties of networks which may help in spreading or restricting information in networks captured by PEV localization [7]. Localization of PEV refers to a state when a few components of the vector take very high values while the rest of the components take small values. For instance, during a disease outbreak, one will be interested in knowing if the disease will spread through the underlying network leading to the pandemic or will be restricted to a

smaller section of the network [4, 71]. Similarly, one may be interested in spreading a piece of particular information, for instance, awareness of vaccination at the time of disease outbreak, or may wish to restrict information like rumor propagation [72]. It is known that PEV of an adjacency matrix approximates the steady-state vector of many linear-dynamical systems [4, 9, 12]. Therefore, a network structure which maximizes the localization behavior of PEV can have a few nodes contributing more in a linear-dynamical process and the rest of the nodes having a tiny contribution. Analyzing structural and spectral properties of such networks can help us to engineer the system architecture, enhance robustness, as well as can provide insights into the underlying mechanism of their evolution [22].

There have been some investigations attempting to relate one or more structural properties of a network with PEV of the network's adjacency matrix. For example, the eigenvector localization properties have been related to the scaling parameter of scale-free networks [23]. Goltsev *et al.* reported that PEV localization of scale-free networks exists only for the power-law exponent being greater than a critical value [4]. On the contrary, Pastor-Satorras *et al.* have shown that PEV of all the power-law degree distributed networks are localized to some extent, with the existence of two different types of localization based on the degree of the nodes [23]. Nevertheless, they noted that these two different types of localization are not so evident in real-world networks [23]. Furthermore, localization has been investigated for eigenvector centrality defining the score of each node based on its neighborhood properties and is a standard measure for determining the importance of nodes in networks. However, it was also found that the eigenvector centrality may fail upon the consequence of PEV localization [24]. Network properties such as the presence of hubs, the existence of dense subgraph, and a power-law degree distribution are few factors known to make a PEV localized [4, 24]. However, we show that the presence of these features in a network does not guarantee a highly localized PEV of the corresponding adjacency matrix. In other words, for a given network size and number of connections, if we construct a network which possesses one or more of these structural features, the PEV of underlying matrix may be more localized

than the corresponding random network built using, say, the Erdős-Renyi algorithm, but may not be *the most localized* for the given network parameters. Here, we ask a reverse question: for a given network size and a number of connections if we construct a network which has the most localized PEV, what particular structural features the network will possess? We address this issue in this chapter.

We organize the chapter as follows: Section 2.2 describes the notations and definitions used in the later discussion. In addition, section 2.3 contains a brief explanation of the optimization procedure used in our work. Section 2.4 illustrates various numerical results including degree and eigenvector entry distribution of the initial as well as of the optimized network. Moreover, this section exhibits the results for the initial network taken as SF and real-world networks. Section 2.5 uses SIS disease spreading model to validate our results. Finally, in section 2.6, we summarize the current study.

2.2 Background

For the completeness of our discussion, we again provide backgrounds of networks, symmetric matrix, and IPR value, respectively. We represent a graph (network), $\mathcal{G} = \{V, E\}$, where $V = \{v_1, v_2, \dots, v_n\}$ is the set of vertices and $E = \{e_1, e_2, \dots, e_m | e_p = (v_i, v_j), p = 1, 2, \dots, m\} \subseteq U$ is the set of edges. We define the universal set $U = V \times V = \{(v_i, v_j) | v_i, v_j \in V \text{ and } i \neq j\}$ which contains all possible unordered pairs of vertices excluding the self-loops and $|U| = \frac{n(n-1)}{2}$ denotes the size of the universal set. The complementary set of the edges can be defined as $E^c = U - E = \{(v_i, v_j) | (v_i, v_j) \in U \text{ and } (v_i, v_j) \notin E\}$ i.e., $E \cap E^c = \emptyset$ and $E \cup E^c = U$. The $|V| = n$ and $|E| = m$ represent the number of nodes and number of edges in \mathcal{G} , respectively, and thus $|E^c| = \frac{n(n-1)}{2} - m$. We denote the adjacency matrix corresponding to \mathcal{G} as $\mathbf{A} \in \mathbb{R}^{n \times n}$ which can be defined as

$$a_{ij} = \begin{cases} 1 & \text{if nodes } i \text{ and } j \text{ are connected} \\ 0 & \text{Otherwise} \end{cases}$$

Here, $k_i = \sum_{j=1}^n a_{ij}$ denotes the degree of node v_i and $\{k_i\}_{i=1}^n$ stands for the degree sequence of \mathcal{G} . The average degree of the network is denoted by $\langle k \rangle = \frac{1}{n} \sum_{i=1}^n k_i$.

We refer the maximum degree node or the hub node of \mathcal{G} as $k_{max} = \max_{1 \leq i \leq n} k_i$.

Here, network is undirected, thus \mathbf{A} is a real symmetric matrix, and hence all the eigenvalues are real. The spectrum of \mathcal{G} is a set of eigenvalues $\{\lambda_1, \lambda_2, \dots, \lambda_n\}$ of \mathbf{A} where $\lambda_1 \geq \lambda_2 \geq \dots \geq \lambda_n$, and the corresponding eigenvectors are $\{\mathbf{x}_1, \mathbf{x}_2, \dots, \mathbf{x}_n\}$. We quantify the localization of i^{th} eigenvector ($\mathbf{x}_i = ((x_i)_1, (x_i)_2, \dots, (x_i)_n)^T$) using the IPR [4] and is defined as,

$$Y_{\mathbf{x}_i} = \sum_{j=1}^n (x_i)_j^4 \quad (2.1)$$

where $(x_i)_j$ is the j^{th} component of the normalized eigenvector, \mathbf{x}_i is in the Euclidean norm. For any connected regular graph, $\mathbf{x}_1 = (\frac{1}{\sqrt{n}}, \frac{1}{\sqrt{n}}, \dots, \frac{1}{\sqrt{n}})^T$ (Theorem 6 [26]) and thus, $Y_{\mathbf{x}_1} = \frac{1}{n}$. Hence, a sparse as well as a dense regular network both will have a delocalized PEV. Next, if we consider a disconnected graph where each node is isolated without having any interaction with any one and having a self-loop, adjacency matrix will be an identity matrix and for which we can choose $\mathbf{x}_1 = (1, 0, \dots, 0)^T$ leading to $Y_{\mathbf{x}_1} = 1$. However, as \mathbf{A} is a nonnegative matrix and \mathcal{G} is always connected, thus from the Perron-Frobenius theorem [27], all the entries of PEV are positive ($(x_1)_j > 0$). Therefore, for a simple, connected, undirected and unweighted network, \mathbf{x}_1 never be $(1, 0, \dots, 0)^T$. Hence, for connected networks PEV is said to be localized when a large number of components take value near to zero and only a few have large values. In other words, IPR value of the PEV should be in the range $1/n \leq Y_{\mathbf{x}_1} < 1$ for $n \geq 2$.

For any connected and regular networks, we can easily get delocalized PEV; however, it becomes challenging to find connected networks having highly localized PEV. By maximizing the IPR of PEV as an objective function, we attempt to get a network structure which has a few nodes contributing significantly to a linear-dynamical process with the rest of the nodes having a tiny contribution.

2.3 Methods

For a given n and m , we aim to get a connected network which has the most localized PEV corresponding to the maximum IPR value. For a particular value of

n and m , if we can enumerate all the possible network configurations, the network corresponding to the maximum IPR value will be our desired network. The number of possible network configurations for a given n and m is of the order $\mathcal{O}(n^{2m})$ [46]. Therefore, we formulate this problem through an optimization method as follows.

Given an input graph \mathcal{G} with n vertices, m edges and a function $\zeta : \mathbb{R}^n \rightarrow \mathbb{R}$, we want to compute the maximum possible value of $\zeta(\mathbf{x}_1)$ over all the simple, connected, undirected, and unweighted graph \mathcal{G} . Thus, we are maximizing the objective function $\zeta(\mathbf{x}_1) = Y_{\mathbf{x}_1} = \sum_{i=1}^n (x_1)_i^4$ subject to the constraints that $\sum_{i=1}^n (x_1)_i^2 = 1$, and $0 < (x_1)_i < 1$. The first constraint simply says that the PEV of \mathbf{A} is normalized to the Euclidean norm. The second constraint implicitly stipulates that the network must be connected (from Perron-Frobenius theorem) in the optimization process.

Starting from an initial connected random network, we use an edge rewiring approach [81, 82] based on a Monte Carlo algorithm to obtain the optimized network iteratively. For a single edge rewiring process, we choose an edge $e_i \in E$ uniformly at random from \mathcal{G} and remove it. At the same time, we introduce an edge in the network from E^c , which preserves the total number of edges during the network evolution. The new network and the corresponding adjacency matrix are denoted as \mathcal{G}' and \mathbf{A}' , respectively. The eigenvalues and eigenvectors of \mathbf{A}' are indicated as $\{\lambda'_1, \lambda'_2, \dots, \lambda'_n\}$ and $\{\mathbf{x}'_1, \mathbf{x}'_2, \dots, \mathbf{x}'_n\}$, respectively. It is important to remark that during the network evolution, there is a possibility that an edge rewiring makes the network disconnected. We only approve those rewiring steps which yield a connected graph through the depth-first search algorithm [83]. We calculate the IPR value of PEV from \mathbf{A} and \mathbf{A}' . If $Y_{\mathbf{x}'_1} > Y_{\mathbf{x}_1}$, \mathbf{A} is replaced with \mathbf{A}' . Therefore, in each time step, we get a network which has the PEV more localized than the previous network. We repeat the above steps until we obtain the maximum IPR value corresponding to the optimized network, \mathcal{G}_{opt} . We refer the initial network as \mathcal{G}_{init} and the optimized network as \mathcal{G}_{opt} . Additionally, the optimization process helps us in assessing the impact of structural and spectral properties of networks on IPR value of PEV as networks evolve from the delocalized to a localized state.

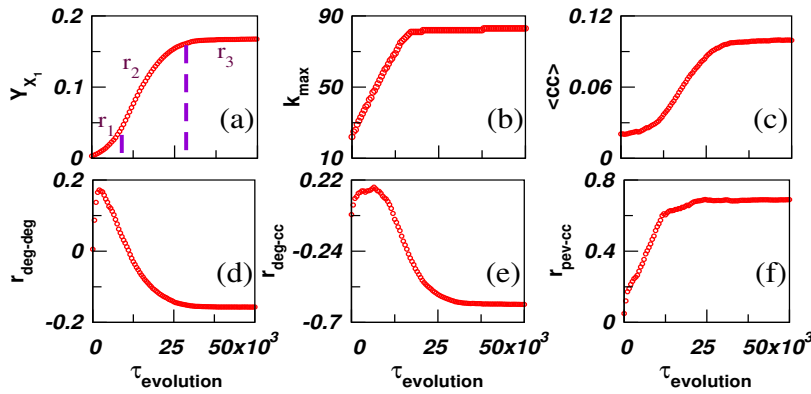


Figure 2.1: Network size is $n = 500$, $\langle k \rangle = 10$ and we iterate the rewiring process for 600,000 times and store the network after each 100^{th} steps. Changes of various network properties (a) IPR value of PEV (b) maximum degree (c) average clustering coefficient (d) degree-degree correlation (e) correlation between degree vector and clustering coefficient vector and (f) correlation between PEV and clustering coefficient vector during the evolution ($\tau_{evolution}$).

2.4 Results

2.4.1 Network evolution

Starting with an initial connected random network generated using Erdős-Rényi (ER) random graph model [27], the evolution process based on the PEV localization forces a change in the initial network structure. The ER random network is generated with an edge probability $\langle k \rangle/n$, where $\langle k \rangle$ is the average degree of the network. The choice of an ER random network at the beginning of the evolution provides a delocalized PEV to start with [79].

Based on the nature of changes in the IPR value, we can divide the evolution into three different regions; r_1 , r_2 , and r_3 . In the first region, each rewiring yields a small change in the IPR value, whereas, in the r_2 region, changes in the IPR values are much larger. The r_3 region represents the saturation state (Fig. 2.1(a)). This is also referred to as the critical region, explained later. At the beginning of the optimization process, the evolution of the IPR with rewiring is slow as there exist many nodes with degree close to each other (Fig. 2.2(a)). Consequently, for an optimized rewiring, there exist several options for the edges, rewiring which leads to an enhancement in the IPR value. Once, a node becomes a clear hub by attaining

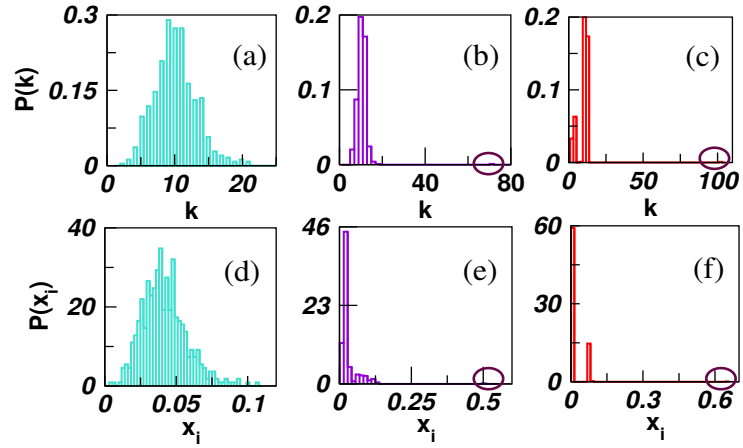


Figure 2.2: ER network as an initial network. Degree distribution of the (a) initial (b) intermediate and (c) optimized network. PEV entry distribution of the (d) initial (e) intermediate and (f) optimized network.

considerable larger degree than the rest of the nodes (region r_2 and Fig. 2.2(b)), the PEV entries corresponding to that node keeps on becoming larger (Fig. 2.2(e)) and those of all other nodes becoming considerably smaller, yielding a fast growth in the IPR value for each rewiring.

2.4.2 Analyzing network properties during network evolution

We have already described in section 2.3, the total number of edges is fixed throughout evolution. Therefore, it is rearrangements of the links which affect the localization properties of the network (i.e., network properties which lead to localized PEV). Moreover, we know that as PEV gets localized, it affects many structural properties of the corresponding network, such as the largest degree (k_{max}), average clustering coefficient ($\langle\langle CC \rangle\rangle$), degree distribution, etc. [4, 24, 62]. We keep a record of all these properties during the evolution and observe that k_{max} starts rising as IPR value increases (Fig. 2.1(a)) and reaches its maximum value much before the IPR achieves its maxima (Fig. 2.1(b)). This indicates that these two quantities affect each other positively but are not strongly related. Nevertheless, to study a possible relationship between k_{max} and IPR value of PEV, we use the configuration model [31] to generate a network which has the same degree sequence as of the \mathcal{G}_{opt} . However, the configuration networks have IPR value much smaller than

the optimal IPR value even though both the networks have the same k_{max} and the degree sequence. This finding indicates that presence of a hub node or a particular degree sequence is important for making PEV of the network more localized than the corresponding ER random network, however, may not be the only requirement for achieving a localized PEV. Therefore, we analyze possible correlations of IPR with other structural properties which are known to contribute to the localization.

The clustering coefficient is known to play a significant role in localization transition in complex networks [62]. We investigate $\langle CC \rangle$ vs. IPR during the evolution process. We find that the IPR value increases slowly in the r_1 region, while the $\langle CC \rangle$ remains almost constant (Fig. 2.1(c)). In the r_2 region, $\langle CC \rangle$ increases rapidly with the evolution and finally gets saturated to a particular value in r_3 region. It suggests that IPR and $\langle CC \rangle$ have a relation. One possible way to check this relationship is by constructing a network with the same $\langle CC \rangle$ as for \mathcal{G}_{opt} and to compare the IPR values of both the networks. In fact, we also preserve the degree sequence of the optimized network while creating such a network by an algorithm adopted from Ref. [84]. Interestingly, these networks, which have a degree sequence and average clustering exactly the same as those of the optimized network, have IPR values, considerably higher than that of the corresponding ER random network but far lower than that of \mathcal{G}_{opt} . This experiment indicates that regulating the $\langle CC \rangle$ leads to a localization of PEV but does not bring it as high as \mathcal{G}_{opt} . We continue our investigations with other structural properties which might contribute to the PEV localization. One such property is the degree-degree correlation of the networks which we measure using the Pearson product-moment correlation coefficient [27]. The degree-degree correlation has been reported to affect several dynamical and spectral features of corresponding systems [85, 86].

During the network evolution process, the degree-degree correlation ($r_{deg-deg}$) exhibits an increment in the beginning when there is a small change in the IPR value (r_1) and decreases rapidly with a further increase in the IPR value (r_2). Finally, both become saturated (Fig. 2.1(d)) and \mathcal{G}_{opt} is a disassortative network. To check the importance of disassortativity for the localization, we perform an experiment by

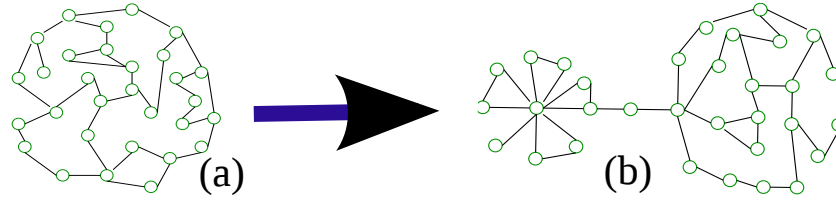


Figure 2.3: Schematic diagram representing the (a) initial and the (b) optimized networks.

constructing a network using Sokolov algorithm [87] which yield the same $r_{deg-deg}$ as of the \mathcal{G}_{opt} . However, this construction also fails to produce the IPR value as high as for \mathcal{G}_{opt} . Furthermore, in the optimized network, the degree and local clustering coefficient vectors manifest a negative correlation (Fig. 2.1(e)) whereas local clustering coefficient vector and PEV indicates a high positive correlation (Fig. 2.1(f)). These two measurements do provide us information about the possible structure of the networks but do not tell what the structure exactly is.

2.4.3 Revealing Optimized network structure

The most intriguing result of our investigation is that we get a special network topology corresponding to the optimized IPR value concerning PEV. The optimized network consists of two components of different sizes which are connected via a single node (Fig. 2.3). In the beginning of the evolution process (starting at r_1 region), the degree distribution of the network follows Poisson law (Fig. 2.2 (a)). The evolution process forces the network structure to change in a very typical manner. The degree of one node attains a much higher value than that of the rest of the nodes in the network at the intermediate stage (Fig. 2.2(b)). In the r_3 region, the degree distribution of the optimal structure, which has the most localized PEV is depicted in Fig. 2.2(c). One can notice that it consists of two peaks at lower k values, besides there exists one data point corresponding to the hub node lying very far from these two peaks. The first smaller peak is contributed by the nodes lying in the smaller part of the network (Fig. 2.3(b)), and the larger peak comes from, the larger component having an optimized network structure. Similarly, the distribution of the PEV entries during the network evolution takes shape in such a manner that at the r_2 and

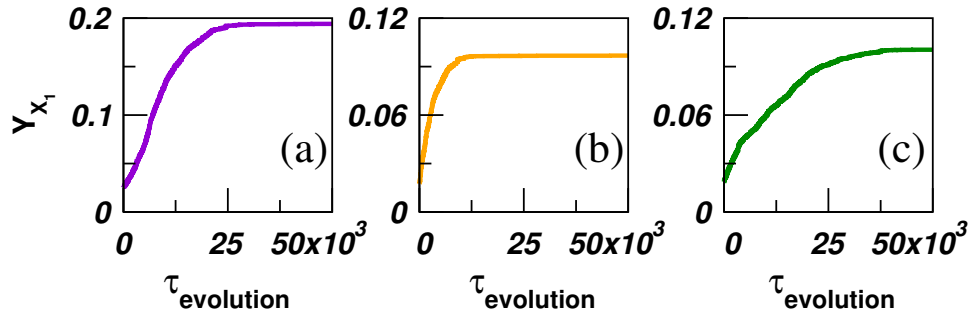


Figure 2.4: Change in IPR value as a function of network evolution ($\tau_{evolution}$). (a) SF networks with $n = 500$ and $\langle k \rangle = 10$ (b) *C. elegans* frontal network with $n = 131$ and $\langle k \rangle = 11$ (c) *C. elegans* neural network with $n = 297$ and $\langle k \rangle = 14$. We consider crude approximations that edges are undirected and unweighted for *C. elegans* networks.

r_3 regions (in Fig. 2.2(e) and Fig. 2.2(f)) more number of nodes have tiny weights at corresponding PEV entries, and less number of nodes have an enormous weight which is an indication of a highly localized PEV (Fig. 2.2(d)). Further, it is visible in Fig. 2.2(f) that each node belonging to the smaller component (Fig. 2.3(b)) of the \mathcal{G}_{opt} has large PEV weight whereas those belonging to the larger component has smaller PEV weights.

2.4.4 Impact of initial network structure and size on evolution

To check the robustness of the emerged localized network structure against changes in the initial network, we start the evolution process on the scale-free (SF) network considered as the initial structure. The SF network is constructed using the Barabasi-Albert preferential attachment model [27]. The network gets evolved through the similar r_1, r_2 region of slow and fast changes in IPR values, and finally, leads to the saturation region r_3 . The final optimal structure remains the same as depicted by Fig. 2.3. There exist few changes occurring before the network reaches to the final optimized structure. A prime change is that reaching to the saturation state (r_3) is faster when one starts with an SF network structure. The reason behind this slightly faster convergence is that the PEV of the SF network is already slightly localized due to the presence of a hub node. Moreover, the optimization process acts on a network already having a hub node which causes shrinkage in the

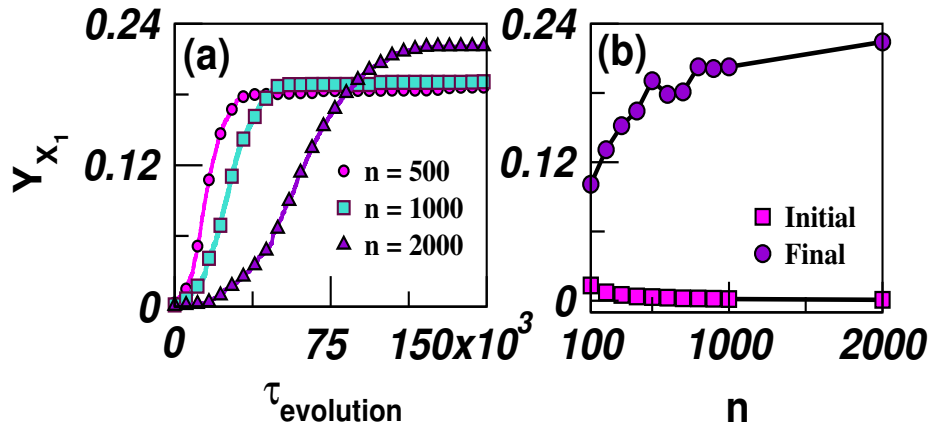


Figure 2.5: (a) Evolution ($\tau_{\text{evolution}}$) of IPR values for different network size. As network size increases, it takes more evolution time for a network to reach the optimized state. (b) IPR value of the initial ER and the final optimized networks as a function of n .

slow evolution region (r_1). Additionally, we consider a few real-world networks as our starting initial network structure, and again the final optimal network structure remains the same as found earlier with the existence of critical region r_3 . For example, we consider *C. elegans* frontal [88] and *C. elegans* neural [89] network as the initial network structure and achieve the similar structure as obtained from the ER and SF networks through the evolution process (Figs. 2.3(b) and 2.4).

Further, we consider the impact of changes in the network size on the properties of the optimized network evolution process. As network size increases, the evolution process remains the same as depicted by Fig. 2.5(a). The final optimized network structure achieves through the intermediate stage and attains the same structure (Fig. 2.3). However, as n increases, it takes more evolution time for a network to be optimized (Fig. 2.5(a)). It is not surprising as Goltsev et al. have provided theoretical bounds on the maximum IPR values for the Bethe lattices and have shown its dependency on n [4]. Fig. 2.5(b) depicts IPR values of the initial and the optimized network for various values of n .

2.4.5 Sensitivity of PEV in r_3 region

Note that, in between any two increments in the IPR values as evolution progresses, there exist several edge rewiring which does not lead to an increase in the IPR

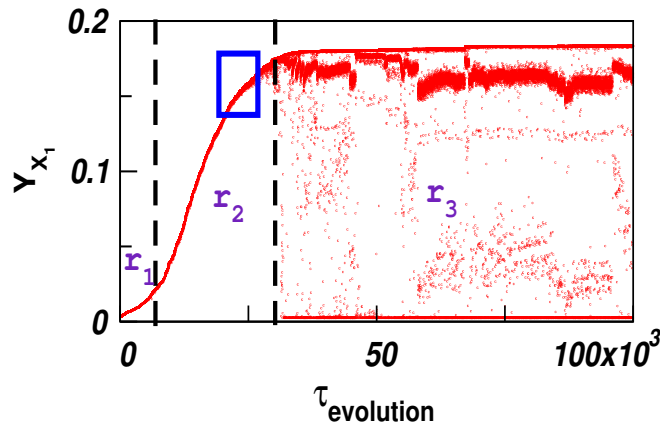


Figure 2.6: IPR as a function of edge-rewiring. The networks with large IPR value in r_3 region consists of few edge-rewiring, which leads to a sudden drop in the IPR value. Rewiring of the first 1,00,000 edges is depicted. The marked square indicates the regime where the networks attain IPR values which are very close to the optimized network. However, in this regime rewiring an edge does not have a significant impact on the IPR values.

value. If we consider rewiring of all the edges, and not only those which lead to an increase in the IPR value, we get surprising results in the r_3 region (Fig. 2.6). For this region, the IPR value gets almost saturated, and there exists only a subtle increment in its value with a further evolution of the network. Though the network in this region has the maximum IPR value, there exist few edges, rewiring them leads to a sudden drop in the IPR value resulting in the complete delocalization of PEV from a highly localized state. It reveals that only a single edge rewiring makes the most localized PEV to the delocalized one, and this phenomenon is observed for sparse networks in r_3 region (Fig. 2.6). We look forward to identifying the set of special edges and the rewiring locations, perturbing which, lead to delocalization of PEV. It turns out that in the optimized network if we remove an edge connected to the hub node inside the smaller component (Fig. 2.3(b)) the IPR value drops down leading to a complete delocalization of PEV. Interestingly, just before the saturation (in the r_2 region) if we rewire an edge which is connected to the hub, no sudden drop is observed in the IPR value. This is a region highlighted within a square in (Fig. 2.6), where IPR value is much larger than the initial ER random network as well as is robust against the edge rewiring. Whereas in the r_3 region, though the

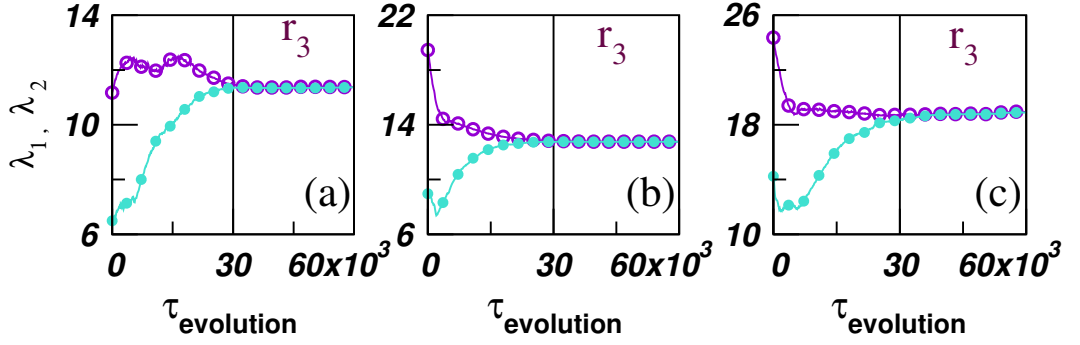


Figure 2.7: Behavior of λ_1 (\circ) and λ_2 (\bullet) during the network evolution ($\tau_{evolution}$). Initial network as (a) ER random network (b) SF network (c) *C. elegans* neural network.

network achieves the maximum IPR value, it becomes very sensitive to the single edge rewiring. Most importantly, by controlling a few edges, we can control the PEV localization of the entire network. This sensitivity of PEV in the r_3 region can also be observed if we change the initial network structure to SF network and consider all the edge rewiring during the network evolution process (Appendix Fig. 6.6).

In the following, we attempt to understand the emergence of the special structure as a consequence of optimization as well as the sensitivity of PEV in the critical region. The eigenvalues of a network adjacency matrix lie in a bulk region separated from extremal eigenvalues at both the side which lies outside the bulk. It is known that the extremal eigenvalues, particularly the largest one, may follow completely different statistical properties than those lying in bulk [55, 56]. Furthermore, the number of eigenvalues lying outside the bulk is known to be equal to the number of communities in the network [57]. For a random network without any community structure, there exists only one eigenvalue which lies outside the bulk region and all other eigenvalues including the second-largest λ_2 are part of the bulk region [57]. As depicted in Fig. 2.7, the value of λ_2 is much smaller than the value of λ_1 in the initial network structure corresponding to ER, SF, and *C. elegans* neural networks. During the evolution, λ_2 starts shifting towards λ_1 , i.e., λ_2 starts drifting away from the bulk region. This drift in λ_2 is not surprising as we know that the final optimized structure consists of two parts or communities, and hence there

should be two eigenvalues which lie outside the bulk. However, the interesting observation is that for the optimized network, λ_2 not only drift away from the bulk but becomes very close to λ_1 , however, following the Perron-Frobenius theorem λ_1 is simple (non-degenerate). Almost the same values for both the eigenvalues might be a reason behind the sensitivity of PEV for a single edge rewiring. Markov chain and its associated transition matrix have been extensively studied in network science. It has been reported that when the two largest eigenvalues of a transition matrix become very close to each other, PEV which is known as the stationary probability distribution vector becomes sensitive to a small perturbation in the transition matrix [90]. Consequently, the associated Markov chain becomes decomposable [91]. The transition matrices are different from the adjacency matrices considered here; nevertheless, largest two eigenvalues being close to each other and sensitivity of PEV occurring at the same evolution time is brings forward an insight into the behavior of PEV localization. When PEV becomes highly localized resulting in λ_1 close to λ_2 , the network structure becomes very sensitive for rewiring and may lead to a complete delocalization of PEV even for a single edge rewiring (Fig. 2.6). In the next section, we use the most localized PEV state to approximate the steady-state behavior of the susceptible-infected-susceptible (SIS) disease spreading model [4].

2.5 Disease spreading in localized networks

Starting from the ER random or SF networks as an initial network, we can achieve an optimized network structure which has highly localized PEV. To demonstrate the efficiency of these artificially constructed network structures for a dynamic process, we use the standard SIS disease spreading model. We observe the behavior of a spreading process at different stages of the optimization process. In the SIS model, each susceptible vertex becomes infected with the infection rate γ , and infected vertices become susceptible with the unit rate. The probability $\rho_i(t)$ that vertex i is infected at time t is described by the evolution equation [4]

$$\frac{d\rho_i(t)}{dt} = -\rho_i(t) + \gamma[1 - \rho_i(t)] \sum_{j=1}^n a_{ij}\rho_j(t) \quad (2.2)$$

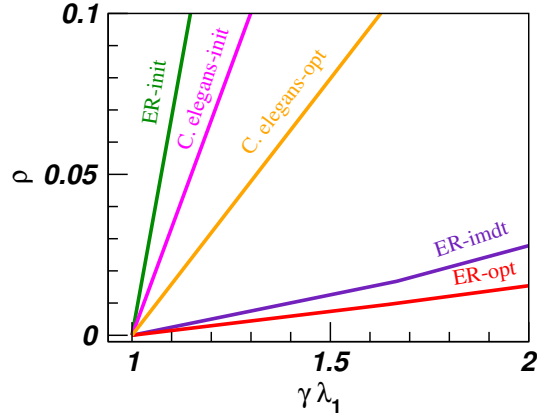


Figure 2.8: Spreading process of SIS model on the initial ER random network ($\lambda_1^{init} \approx 11.34$, $Y_{x_1}^{init} \approx 0.0007$), an intermediate network ($\lambda_1^{imdt} \approx 11.14$, $Y_{x_1}^{imdt} \approx 0.21$) and an optimized network ($\lambda_1^{opt} \approx 10.77$, $Y_{x_1}^{opt} \approx 0.22$) and the *C. elegans* neural network ($\lambda_1^{init} \approx 24.36$, $Y_{x_1}^{init} \approx 0.019$ and $\lambda_1^{opt} \approx 17.18$, $Y_{x_1}^{opt} \approx 0.1$) have been depicted. ER network has $n = 2000$ nodes with $\langle k \rangle = 10$.

and in the steady state, at $t \rightarrow \infty$, $\rho_i \equiv \rho_i(t)$. Hence,

$$\rho_i = \frac{\gamma \sum_{j=1}^n a_{ij} \rho_j}{1 + \gamma \sum_{j=1}^n a_{ij} \rho_j} \quad (2.3)$$

Therefore, in steady-state with probability ρ_i , a vertex i infected by its neighbours, and the prevalence is given by $\rho = \sum_{i=1}^n \rho_i / n$. It has been shown that ρ_i is approximated to PEV entries of adjacency matrix i.e. $\rho_i \approx c_1(x_1)_i$, where $c_1 \in \mathbb{R}$ [4]. We know that when the infection rate γ cross the epidemic threshold i.e. $\gamma > \gamma_c = \frac{1}{\lambda_1}$ [76] the disease will spread over the networks. However, if the PEV of the network's adjacency matrix is localized, in the vicinity of the epidemic threshold $\gamma_c + \epsilon$, $\epsilon > 0$ the disease infects a small number of vertices and spreading process becomes slow. As a result, it requires a larger value of γ for spreading the disease over the network. Fig. 2.8 manifests that for the initial network, for a value of γ , which is slightly larger than γ_c , the disease infects a large number of vertices. Whereas, for the networks corresponding to the intermediate and the optimized states, there exist very few vertices which get infected.

2.6 Conclusion

In this chapter, starting from an initial random network, we achieve a network structure through a Monte Carlo based network evolution method. The optimized net-

work possesses a highly localized PEV quantified by the IPR value. We analyze various structural and spectral properties of the optimized network as well as the networks at the intermediate state before the optimized structure is reached. We demonstrate that PEV localization is not a consequence of a single network property and rather requires the collective impact of several structural features. The final optimized network possesses a special structure and which we have shown to be robust against changes in the initial network structure. We demonstrate the robustness of the results by considering various popular network models as well as real-world networks as an initial network structure. Furthermore, we characterize the evolution regime into different stages. In the intermediate stage, we identify an evolution regime which corresponds to the PEV localization almost the same as that of the optimized network, but the localization property is robust against the edge rewiring. Whereas, PEV is sensitive against single edge rewiring in the critical (saturation) region. Our analysis identifies a special set of edges which are essential for the localization of PEV in the optimized network structure. Rewiring any one edge of this set leads to a complete delocalization of PEV. We observe that this emergence of sensitivity in the PEV and shifting of λ_2 close to λ_1 happens simultaneously suggesting a relation between the special structure of the optimized network and the second largest eigenvalue of the network.

It may not always be feasible to rewire a real-world network to such an extent to get a desired PEV localization behavior. However, the results and approach used here will be more useful in constructing an artificial network with the desired localization behavior. Though the prime concern of our analysis to have insights into the network structure and PEV localization, using disease spread model, we verify that network structure in the optimal and the intermediate stages spreading of disease is much slower than the initial random structure. Our study provides a more in-depth insight into the PEV localization on synthetic as well as on empirical networks.

This chapter mainly concentrates on the numerical investigation to find network structure and properties leading to high localization of PEV through the network evolution process. In the next chapter, by analyzing the sub-component eigenval-

ues relation of the optimized network structure, we explore the reason behind the sensitive behavior of PEV in the optimized network structure. Finally, based on the behavior of the eigenvalues, we devise an analytical formulation which assists in constructing PEV localized network structure and avoid the network evolution process.

Chapter 3

Analytical construction of PEV localized networks

3.1 Introduction

In Chapter 1, we have presented an optimized edge rewiring algorithm to construct networks having highly localized PEV's (Fig. 3.1). The optimized network was shown to consist of subgraphs connected via a node (Fig. 3.1(b)). Furthermore, the optimized networks were shown to have the largest two eigenvalues being very close to each other. Importantly, the optimized network was shown to contain few special edges, rewiring one of them leads to a delocalization of the PEV from a highly localized state which was referred to as sensitivity of PEV [92].

Although chapter 1 successfully concluded that PEV localization depends on several network parameters; however, the following observation was not precise. Before the single edge rewiring, two largest eigenvalues in the critical region (r_3 region) are close as well as after the rewiring they are also close (discussed in Table 3.1), which indicates that closeness is necessary but not a sufficient condition to get sensitivity in highly localized PEV. Besides, there exist real-world networks

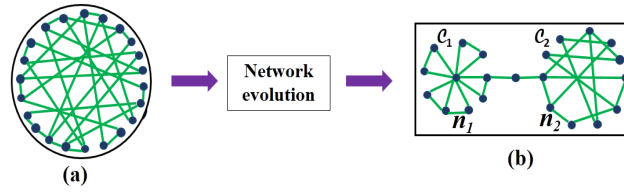


Figure 3.1: Schematic diagram of (a) initial network and (b) the optimized network structure having two components evolved through the network evolution process discussed in chapter 2, section 2.3.

for which the largest two eigenvalues are close, and PEV is delocalized (Appendix Table 6.2). Hence, it is not clear the reason behind the sensitivity in PEV of an optimized network structure. Understanding the origin of sensitivity in PEV, one can construct a highly localized PEV network structure without using any optimization process.

In this chapter, we focus on identifying the origin of sensitivity behavior of PEV localization as well as devise a method based on an analytical derivation of network parameters for direct construction of a highly localized network without using any evolution scheme. The current investigation can be summarized as follows: First, we show that the eigenvalue crossing phenomenon which takes place when an edge is rewired in the localized network structure is an essence of the sensitivity behavior of PEV localization. Second, taking a clue from this eigenvalue crossing phenomenon, we establish a relationship between the largest eigenvalues of the individual subgraph of the optimized network structure. Using this relation, we analytically derive the network parameters required for direct construction of PEV localized networks. Ergo, our investigation identifies the necessary structural and spectral properties for highly localized networks. Third, we substantiate the eigenvalue crossing phenomenon by using the RNA neutral network population dynamical model [58].

The chapter is designed as follows: Section 3.2 describes the notations and definitions of the mathematical terms. Section 3.3.1 illustrates the numerical results demonstrating the relationships between the PEV localization and the second-largest eigenvector, which is required for eigenvalue crossing. The analytical treat-

ment is given in subsection 3.3.2 provides us a method for direct construction of PEV localized network without performing a network evolution method. Section 3.4 describe the results for the steady-state behavior on a linear-dynamical system. Finally, section 3.5 summarizes our work.

3.2 Background

In this section, we again briefly discuss the underlying matrix representation and IPR definition. We represent a network as $\mathcal{G} = \{V, E\}$, where V and E represent the set of nodes and edges, where n and m denote the size of V and E , respectively. We refer $E^c = \{e_1^c, e_2^c, \dots, e_{(n(n-1)/2)-m}^c\}$ as the set of edges which are not present in \mathcal{G} . In this dissertation, we restrict to simple networks, i.e. the network without multiple connections and self-loop. The adjacency matrix (\mathbf{A}) corresponding to \mathcal{G} is defined as,

$$a_{ij} = \begin{cases} 1 & \text{if nodes } i \text{ and } j \text{ are connected} \\ 0 & \text{Otherwise} \end{cases}$$

Here, $k_i = \sum_{j=1}^n a_{ij}$ denotes the degree of node v_i and the average degree of the network is denoted by $\langle k \rangle = \frac{1}{n} \sum_{i=1}^n k_i$. We refer the maximum degree node or the hub node of \mathcal{G} as $k_{max} = \max_{1 \leq i \leq n} k_i$. Here, \mathbf{A} is a real symmetric matrix, hence, it has a set of orthonormal eigenvectors $\{\mathbf{x}_1, \mathbf{x}_2, \dots, \mathbf{x}_n\}$ corresponding to the real eigenvalues $\{\lambda_1, \lambda_2, \dots, \lambda_n\}$. Moreover, the edge weights of \mathbf{A} are 1, and network is always connected. Thus, \mathbf{A} is a non-negative and irreducible matrix. Hence, we know from the Perron-Frobenius theorem that all the entries in PEV of \mathbf{A} are positive and λ_1 is simple (non-degenerate) [93].

The inverse participation ratio (IPR) quantifies the localization as well as delocalization behavior of eigenvectors in complex networks [4, 7, 11, 12, 25, 94]. We calculate the IPR value ($Y_{\mathbf{x}_i}$) of an orthonormal eigenvector ($\mathbf{x}_i = ((x_i)_1, (x_i)_2, \dots, (x_i)_n)^T$) of \mathbf{A} as follows:

$$Y_{\mathbf{x}_i} = \sum_{j=1}^n (x_i)_j^4 \quad (3.1)$$

where $(x_i)_j$ is the j^{th} component of \mathbf{x}_i . A delocalized eigenvector ($\mathbf{x}_i = (\frac{1}{\sqrt{n}}, \frac{1}{\sqrt{n}}, \dots, \frac{1}{\sqrt{n}})^T$) has $Y_{\mathbf{x}_i} = \frac{1}{n}$, whereas the most localized eigenvector ($\mathbf{x}_i = (1, 0, \dots, 0)^T$)

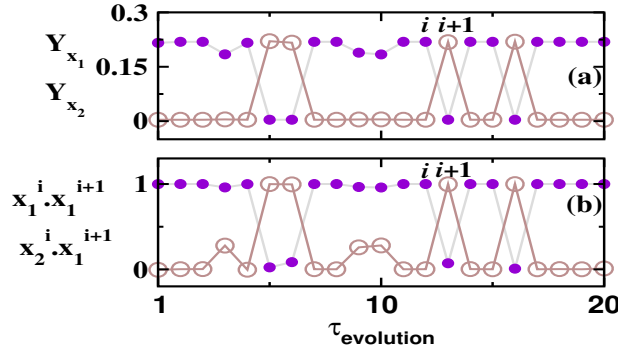


Figure 3.2: (a) Flipping behavior of IPR values of the largest (●) and second largest (○) eigenvectors. (b) Detection of eigenvalue crossing through dot products $(x_1^i)^T x_1^{i+1}$ (●) and $(x_2^i)^T x_1^{i+1}$ (○) in the r_3 region during the network evolution. Network parameters are same as in Fig. 3.

yields an IPR value equal to $Y_{x_i} = 1$. For a connected, undirected and unweighted network, the IPR values of PEV lies between $1/n \leq Y_{x_1} < 1$, $n \geq 2$.

3.3 Results

3.3.1 Analysis of eigenvectors angles: signature of eigenvalue crossing

To capture the sensitive behavior of PEV in the optimized network structure ($\mathcal{G}_1 \equiv \mathcal{G}_{opt}$), we consider random edge rewiring in the optimized network. We choose an edge $e_p \in E$ ($p = 1, 2, \dots, |E|$) uniformly at random from \mathcal{G}_i and remove it and at the same time, we introduce an edge uniformly at random in \mathcal{G}_i from $e_q^c \in E^c$ ($q = 1, 2, \dots, |E^c|$). The new network and the corresponding adjacency matrix are denoted as \mathcal{G}_{i+1} and \mathbf{A}_{i+1} , respectively. Starting from a optimized network structure (constructed using optimized edge rewiring algorithm discussed in section 2.3), the random edge rewiring process yields a sequence of networks $\{\mathcal{G}_1, \mathcal{G}_2, \dots, \mathcal{G}_i, \mathcal{G}_{i+1}, \dots, \mathcal{G}_\tau\}$ and the corresponding adjacency matrices as $\{\mathbf{A}_1, \mathbf{A}_2, \dots, \mathbf{A}_i, \mathbf{A}_{i+1}, \dots, \mathbf{A}_\tau\}$ where τ is the total number of edge rewiring performs. Notably, during an edge rewiring, there is a possibility that the network becomes disconnected. However, we allow only those edge rewirings which yield a connected network. Note that the optimized rewiring process described in section 2.3 and the random rewiring process used here is different.

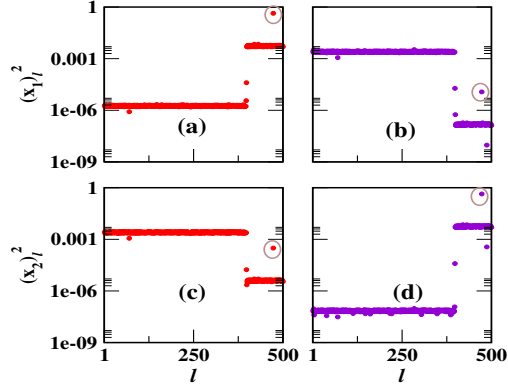


Figure 3.3: Largest two eigenvectors entries in (a) & (c) optimized network where the entry corresponding to the hub node is marked with circle, (b) & (d) after a single edge rewiring of the optimized network which is connected to the hub node. Network parameters are same as in Fig. 3.2. Due to Perron-Frobenius theorem, PEV entries are all positive, however second-largest eigenvector entries are both positive and negative. Hence, to observe the pattern of the eigenvectors entries, we take square of each entries.

We find that there exists few edges, rewirings them bring PEV from a highly localized to a delocalized state (Fig. 3.2 (a)) as also discussed in section 2.4.5. Additionally, there exists abrupt changes in the IPR value of second-largest eigenvector (x_2). In other words, there exists abrupt changes in the Y_{x_1} and Y_{x_2} values due to a single edge rewiring of such edges. To elaborate this aspect of the abrupt changes in the IPR value as a consequence of a single edge rewiring, we focus on two consecutive networks, say, \mathbf{A}_i and \mathbf{A}_{i+1} such that \mathbf{A}_{i+1} is achieved after a single edge rewiring on \mathbf{A}_i . We observe that x_1^{i+1} reaches to a delocalized state, from a highly localized state, at $(i+1)^{th}$ time step (Fig. 3.2 (a)). This abrupt change in IPR value of x_1^{i+1} is accompanied with a high localization of x_2^{i+1} from a delocalized state (x_2^i) (Fig. 3.2 (a)). Scrutinizing the entries of the largest and the second largest eigenvectors in these two consecutive steps, we find that there exist radical changes in the eigenvector entries (Fig. 3.3). One can observe that, x_1^i is highly localized with maximum entry value corresponding to the hub node (marked with a circle in Fig. 3.3(a)). However, after a single edge rewiring on \mathbf{A}_i , \mathbf{A}_{i+1} has the same structure (except single edge rewired), x_1^{i+1} becomes delocalized (Fig. 3.2 (a)). The entry corresponding to the hub node for this delocalized x_1^{i+1} takes a very

small value (Fig. 3.3(b)). Notably, for \mathbf{x}_2^{i+1} , the entry corresponding to the hub node takes the same value as that of the \mathbf{x}_1^i (Figs. 3.3(a) and (d)). This clear flip in the entries of the largest two eigenvectors (\mathbf{x}_1^{i+1} and \mathbf{x}_2^{i+1}) affect the IPR value of both of them in \mathbf{A}_{i+1} .

Further, an examination of relative positions of the two largest eigenvectors provide insight into the sensitive behavior of the PEV in the optimized network structure. To trace the relative position of the largest two eigenvectors in the vector space, we track the angle by computing the dot product of two vectors, i.e.,

$$(\mathbf{x}_1^i)^T \mathbf{x}_1^{i+1} \text{ and } (\mathbf{x}_2^i)^T \mathbf{x}_1^{i+1} \text{ for } i = 1, 2, \dots, \tau$$

during the random edge rewiring process. One can see that presence of the flips in IPR values (Fig. 3.2(a)) are reflected in the similar abrupt changes in the dot product values (Fig. 3.2(b)). These abrupt changes in $(\mathbf{x}_1^i)^T \mathbf{x}_1^{i+1}$ and $(\mathbf{x}_2^i)^T \mathbf{x}_1^{i+1}$ manifest a signature of the eigenvalue crossing. The rewiring of an edge connected to the hub node leads to rotation of \mathbf{x}_1 and \mathbf{x}_2 by approx. 90° (Fig. 3.2(b)). It has already been reported that abrupt changes in the eigenvector entries carry information of the eigenvalue crossing [95–97]. Moreover, it has also been noted that just after the crossing, the eigenvectors become orthogonal to the eigenvectors before the crossing. The largest two eigenvectors satisfy these two criteria mentioned above during the flipping of the IPR values. Further, to confirm the eigenvalue crossing phenomenon, we perform the following experiments. We separate two graph components (\mathcal{C}_1^i and \mathcal{C}_2^i) of \mathcal{G}_i corresponding to \mathbf{A}_i by breaking the existing connection between them, and record the largest two eigenvalues (Fig. 3.1(b)). We observe that the largest two eigenvalues of the \mathcal{G}_i remain almost the same as of the largest eigenvalue of the two subgraph components separately (Table 3.1)

$$\lambda_1^{\mathcal{C}_1^i} \approx \lambda_1^{\mathcal{G}_i}, \quad \lambda_1^{\mathcal{C}_2^i} \approx \lambda_2^{\mathcal{G}_i}$$

Further, one can also notice that

$$\lambda_1^{\mathcal{C}_1^i} > \lambda_1^{\mathcal{C}_2^i} \tag{3.2}$$

In an another experiment, if we remove an edge from \mathcal{G}_i , which is connected to the hub node in \mathcal{C}_1^i , and add it between a randomly selected pair of nodes in \mathcal{C}_2^i , there exists an abrupt change in the localization behavior of PEV. The modified network

\mathcal{G}	n	k_{max}	m	Y_{x_1}	Y_{x_2}	λ_1	λ_2	λ_3
\mathcal{G}_i	500	101	2512	0.19059	0.00253	11.48807	11.47669	6.28379
\mathcal{C}_1^i	102	101	236	0.19075	0.02251	11.48764	2.65329	2.63804
\mathcal{C}_2^i	397	12	2274	0.00253	0.00657	11.47660	6.28334	6.10097
\mathcal{G}_{i+1}	500	100	2512	0.00253	0.19084	11.48227	11.42444	6.29319
\mathcal{C}_1^{i+1}	102	100	235	0.19075	0.02251	11.42401	2.65315	2.63839
\mathcal{C}_2^{i+1}	397	13	2275	0.00253	0.00643	11.48217	6.29273	6.11759

Table 3.1: Largest three eigenvalues and IPR values of two largest eigenvectors of the optimized networks (\mathcal{G}_i) as well as its two components (\mathcal{C}_1^i and \mathcal{C}_2^i). After rewiring of an edge connected to the hub node in \mathcal{G}_i , the new network is denoted as \mathcal{G}_{i+1} and its two components are denoted with \mathcal{C}_1^{i+1} and \mathcal{C}_2^{i+1} .

is denoted as \mathcal{G}_{i+1} . This reshuffling of an edge makes x_1^{i+1} to be in a delocalized and x_2^{i+1} to be in a highly localized state (Fig. 3.2 (a)). Next, if we separate two components of \mathcal{G}_{i+1} , we observe (Table 3.1) that

$$\lambda_1^{\mathcal{C}_2^{i+1}} \approx \lambda_1^{\mathcal{G}_{i+1}}, \lambda_1^{\mathcal{C}_1^{i+1}} \approx \lambda_2^{\mathcal{G}_{i+1}}$$

The transition between localized and delocalized state for x_1^{i+1} and x_2^{i+1} respectively in \mathcal{G}_{i+1} is accompanied with a change in the $\lambda_1^{\mathcal{C}_1^{i+1}}$ value leading to

$$\lambda_1^{\mathcal{C}_1^{i+1}} < \lambda_1^{\mathcal{C}_2^{i+1}} \quad (3.3)$$

For both the experiments, the largest eigenvalues of \mathcal{G}_i and \mathcal{G}_{i+1} are always greater than the corresponding second largest eigenvalues i.e.,

$$\lambda_1^{\mathcal{G}_i} > \lambda_2^{\mathcal{G}_i} \text{ and } \lambda_1^{\mathcal{G}_{i+1}} > \lambda_2^{\mathcal{G}_{i+1}}$$

which also satisfy the Perron-Frobenius theorem [93]. However, changes occur in the largest eigenvalue of the individual components in \mathcal{G}_i and \mathcal{G}_{i+1} (Eqs. (3.2) and (3.3)) occurs due to the eigenvalue crossing. In other words, for the case of the highly localized PEV the component containing the hub node has prime contribution in the largest eigenvalue.

To summarize, we can think of the optimized network evolution process (in section 2.3) acts as a black box which takes a given network of size n and m as input and produces an optimized structure (\mathcal{G}_i) having two components (\mathcal{C}_1^i and \mathcal{C}_2^i) connected via a node, where \mathcal{C}_1^i contains a hub node, and \mathcal{C}_2^i has almost a regular structure. Additionally, $\lambda_1^{\mathcal{G}_i} > \lambda_2^{\mathcal{G}_i}$ and $\lambda_1^{\mathcal{C}_1^i} > \lambda_1^{\mathcal{C}_2^i}$. On the otherhand, upon a single edge rewiring leading to a delocalized PEV in \mathcal{G}_{i+1} yielding $\lambda_1^{\mathcal{G}_{i+1}} > \lambda_2^{\mathcal{G}_{i+1}}$

and $\lambda_1^{c_1^{i+1}} < \lambda_1^{c_2^{i+1}}$. Importantly, for both the cases, eigenvalues of the combined networks are close enough, but they are distinct (non-degenerate) (details is in Appendix 6.5). In other words, optimization process provides a partition to a given network of n number of nodes and m number of edges into two components such that $n = n_1 + n_2 + 1$, $m = m_1 + m_2 + 2$ and $\lambda_1^{c_1} > \lambda_1^{c_2}$ where $|E_{c_1}| = m_1$ and $|E_{c_2}| = m_2$. Next, we ask a question that can we use one or all of these pieces of information to directly construct a network, without performing the optimized network evolution process. Note that, combining any two components with one of them containing a hub node and another having a regular structure, does not produce a localized PEV, thereby making the problem more challenging. For instance, by combining two components where one of them contains a hub node and another has a regular structure, one can bring the largest two eigenvalues of \mathcal{G} close enough (e.g., ER random and scalefree (SF) networks). However, this way of the network construction while yields close enough $\lambda_1^{\mathcal{G}}$ and $\lambda_2^{\mathcal{G}}$, may not lead to a localized PEV (Table 3.2 (No. 1,2)) indicating that closeness of largest two eigenvalues is a necessary but not a sufficient condition. It turns out, for a localized PEV a particular eigenvalue relation ($\lambda_1^{c_1} > \lambda_1^{c_2}$) between the individual component should hold true (Table 3.2 (No. 3,4)). In the following we analytically calculate the subgraph component size which satisfy the particular subgraph eigenvalue relation.

No.	\mathcal{G}	n_1	n_2	$\lambda_1^{\mathcal{G}}$	$\lambda_2^{\mathcal{G}}$	k_{max}	$Y_{x_1}^{\mathcal{G}}$	$\lambda_1^{c_1}$	$\lambda_1^{c_2}$
1.	ER-SF	500	500	11.03	10.09	69	0.003	11.03	10.09
2.	\mathcal{R} - \mathcal{W}	500	24	6	5.9	23	0.002	6	5.89
3.	ER-SF	500	500	10.27	9.59	68	0.08	9.58	10.24
4.	\mathcal{R} - \mathcal{W}	500	26	6.1	5.99	25	0.17	6	6.09

Table 3.2: We portray various structural and spectral properties of two individual components (\mathcal{C}_1 and \mathcal{C}_2), as well as the combined network achieved by connecting them through a link. We consider ER random graph, Scalefree (SF), wheel (\mathcal{W}), and random regular (\mathcal{R}) networks as an individual component. Satisfying $\lambda_1^{c_1} > \lambda_1^{c_2}$ leads to a localized PEV and for $\lambda_1^{c_1} < \lambda_1^{c_2}$ yields delocalized PEV of the combined graph.

3.3.2 Analytical construction of localized network using wheel and random regular graph

From the numerical simulations, we learn that in the optimized networks, \mathcal{C}_1^i contains a hub node while \mathcal{C}_2^i has almost a regular structure. Hence, we choose structures which resemble to \mathcal{C}_1^i and \mathcal{C}_2^i components. The closest structures corresponds to \mathcal{C}_1^i is a star or wheel graph (Fig. 3.1 (b)). For \mathcal{C}_2^i component, we choose a random regular structure.

It turns out that one can recreate the spectral properties of the optimized network by replacing \mathcal{C}_1 with a wheel graph and \mathcal{C}_2 with a random regular network. A wheel graph is denoted as $\mathcal{W} = \{V_{\mathcal{W}}, E_{\mathcal{W}}\}$ where $|V_{\mathcal{W}}| = n_1$ is the number of nodes and $|E_{\mathcal{W}}| = 2(n_1 - 1)$ is the number of edges in \mathcal{W} . Further, the random regular (or regular) graph is denoted as $\mathcal{R} = \{V_{\mathcal{R}}, E_{\mathcal{R}}\}$ where $|V_{\mathcal{R}}| = n_2$ is the number of nodes and $|E_{\mathcal{R}}| = \frac{n_2\kappa}{2}$ is the number of edges with each node having degree κ . We generate the random regular graph using the algorithm in [98]. Further, we know that for a wheel and random regular graph, the largest eigenvalues are as follows [78]

$$\lambda_1^{\mathcal{W}} = 1 + \sqrt{n_1} \text{ and } \lambda_1^{\mathcal{R}} = \kappa \quad (3.4)$$

Interestingly, to connect a wheel graph with a random regular network such that $\lambda_1^{\mathcal{W}} > \lambda_1^{\mathcal{R}}$ (learn from analyzing optimized network structure in subsection 3.3.1), we need the information about the size of the individual component (n_1 , n_2 and κ) of the combined network (\mathcal{G}_{new}). By using the relation $\lambda_1^{\mathcal{W}} > \lambda_1^{\mathcal{R}}$, we consider,

$$\lambda_1^{\mathcal{W}} = \lambda_1^{\mathcal{R}} + \epsilon \text{ where } 0 < \epsilon < 1 \quad (3.5)$$

Here, we use $\epsilon < 1$ to observe the single edge rewiring effect; however, we generalize to $\epsilon > 0$ in the next chapter. Moreover, we provide a proof (in section 4.6) which says that holding $\lambda_1^{\mathcal{W}} > \lambda_1^{\mathcal{R}}$, one can have a combined network structure where wheel subgraph has a prime contribution to the PEV of the combined network structure. From Eqs. (3.4) and (3.5), we obtain the size of the wheel graph as

$$n_1 = \lceil (\kappa - 1 + \epsilon)^2 \rceil \quad (3.6)$$

where ($\lceil \cdot \rceil$) is the ceiling function and Eq. (3.6) tells that for a particular value of κ if

we take $\lceil(\kappa - 1 + \epsilon)^2\rceil$ as a number of nodes for the wheel graph, then the combined graph will satisfy Eq. (3.5). Importantly, in Eq. (3.6) the number of nodes in the \mathcal{W} component of \mathcal{G}_{new} depends on the average degree of the \mathcal{R} component in \mathcal{G}_{new} . Therefore, to construct \mathcal{G}_{new} , we are free to choose any arbitrary number of nodes and average degree ($3 \leq \kappa \leq n_2 - 2$) for the random regular component such that κn_2 is even. Note that for $\kappa = 2$ and $\epsilon \ll 1$, we get $n_1 = 2$ and which is not a valid size to construct a \mathcal{W} component. The smallest value to construct a \mathcal{W} component is $n_1 = 4$ and to satisfy Eq. (3.5), we consider $\kappa = 3$. On the other hand, to observe delocalization in PEV due to single edge removal from \mathcal{W} component and add it to the \mathcal{R} component, we should take κ at most $n_2 - 2$.

From the above investigation, we learn that we can construct a PEV localized network without having any restriction on κ and n_2 . In other words, there is no restriction on the number of nodes and edges for the combined networks. However, to avoid the optimized rewiring process, the partition of a given set of n and m should be such that it satisfies Eq. (3.5) as well as holds the following two relations

$$n = n_1 + n_2 + 1 \quad (3.7)$$

and

$$m = |E_{\mathcal{W}}| + |E_{\mathcal{R}}| + 2 = \frac{4n_1 + n_2\kappa}{2} \quad (3.8)$$

simultaneously. From Eqs. (3.6) and (3.7) we know that

$$n_2 = n - \lceil(\kappa - 1 + \epsilon)^2\rceil - 1 \quad (3.9)$$

To find a κ value for any given set of n and m such that they satisfy Eqs. (3.5), (3.7) and (3.8), we rearrange Eq. (3.8) with the help of Eqs. (3.6) and (3.9), and reach to a cubic equation of the form

$$\kappa^3 + b\kappa^2 + c\kappa + d = 0 \quad (3.10)$$

where $b = (-4 - 2(1 - \epsilon))$, $c = ((1 - \epsilon)^2 + 8(1 - \epsilon) + 1 - n)$, and $d = (2m - 4(1 - \epsilon)^2)$ are the coefficient of the cubic equation. Next, roots of the cubic equation can be

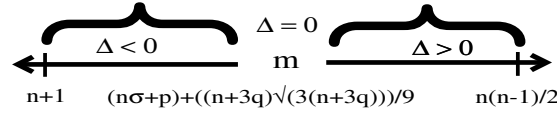


Figure 3.4: Separation of range of m value based on the behavior of the discriminant value (Δ) of the cubic equation (in Eq. 3.11) for a particular value of n . For sparse network $\Delta < 0$ and $\Delta \geq 0$ as network becomes dense. Here, $\sigma = (1 - \frac{\epsilon}{3})$, $p = \frac{\epsilon^3 + 9\epsilon^2 + 36\epsilon}{27}$, $q = \frac{\epsilon^2 + 6\epsilon + 6}{9}$ and we consider $n \geq 49$.

written from the Cardano's formula [99–101] as follows,

$$\begin{aligned}\kappa_1 &= \Delta_1 + \Delta_2 - \frac{b}{3} \\ \kappa_2 &= -\frac{1}{2}(\Delta_1 + \Delta_2) - \frac{i\sqrt{3}}{2}(\Delta_1 - \Delta_2) - \frac{b}{3} \\ \kappa_3 &= -\frac{1}{2}(\Delta_1 + \Delta_2) + \frac{i\sqrt{3}}{2}(\Delta_1 - \Delta_2) - \frac{b}{3}\end{aligned}\quad (3.11)$$

such that

$$\Delta_1 = \sqrt[3]{-\beta/2 + \sqrt{\Delta}} \text{ and } \Delta_2 = \sqrt[3]{-\beta/2 - \sqrt{\Delta}} \quad (3.12)$$

where $\Delta = \frac{\beta^2}{4} + \frac{\alpha^3}{27}$, $\alpha = \frac{1}{3}(3c - b^2)$, $\beta = \frac{1}{27}(2b^3 - 9bc + 27d)$ and $i^2 = -1$. Therefore, given a set of n and m , we obtain three different possible values for κ to partition n and m between two subgraphs. There is a possibility to get complex values for κ . The following analysis presents bounds to avoid complex numbers as well as few other unnecessary situations.

We know that the behavior of the discriminant (Δ) leads to a change in the nature of the roots. One can notice from Eq. (3.13) that Δ is a function of n and m . Furthermore, we know that for a given n , value of m can vary between $n + 1$ to $n(n - 1)/2$. Hence, by varying m , we get Δ as a function of n . It turns out that as m varies, the nature of the roots changes yielding real or complex values for κ_i 's. However, we do not know the exact relation between m and Δ . It is known that (a) $\Delta = 0$ yields three real roots in which at least two are equal, (b) $\Delta > 0$ gives one real root and other two complex conjugate roots, (c) $\Delta < 0$ yields three unequal real roots [99–101]. To know the behavior of the discriminant as m changes for a particular value of n , we analyze Δ in Eq. (3.12) of the cubic equation as;

$$\Delta = (m - n\sigma - p)^2 - \left(\frac{n}{3} + q\right)^3 \quad (3.13)$$

where $\sigma = (1 - \frac{\epsilon}{3})$, $p = \frac{\epsilon^3 + 9\epsilon^2 + 36\epsilon}{27}$, $q = \frac{\epsilon^2 + 6\epsilon + 6}{9}$ and we consider $n \geq 49$ (details is in Appendix section 3.6). Analyzing the discriminant reveals that for

$$m = (n\sigma + p) + \frac{(n + 3q)\sqrt{3(n + 3q)}}{9} \quad (3.14)$$

we get (a) $\Delta = 0$. Further, from the above equation, we find the lower and upper bounds of m , for which $\Delta < 0$ and $\Delta > 0$ as follows

$$\begin{aligned} n + 1 \leq m \leq \left\lceil (n\sigma + p) + \frac{(n + 3q)\sqrt{3(n + 3q)}}{9} \right\rceil - 1 \\ \left\lfloor (n\sigma + p) + \frac{(n + 3q)\sqrt{3(n + 3q)}}{9} \right\rfloor + 1 \leq m \leq \frac{n(n - 1)}{2} \end{aligned}$$

The ranges of m illustrate that as the network becomes dense, Δ becomes greater or equal to zero (Fig. 3.4). One can notice from Eq. (3.13) that $\Delta = 0$ appears when m is a real with fractional part (Eq. (3.14)). However, in our case, m represents the number of edges in \mathcal{G}_{new} and is a positive integer. Hence, $\Delta = 0$ can never appear. Further analysis of the discriminant reveals that for (b) $\Delta > 0$, n_1 calculated from κ_1 (Eq. (3.6)) is always larger than the given value of n . Hence, we can not use κ_1 to find n_1 and n_2 in Eqs. (3.6) and (3.9) for the construction of \mathcal{G}_{new} (details is in Appendix section 3.6). Finally, we investigate the case (c) which corresponds to three unequal real roots in Eq. (3.11). We have achieved two different ways to divide the number of nodes in two different groups such that the entire network has a localized PEV (see Appendix section 3.6 for details). The first way is that we consider a sparse regular structure with a smaller size wheel graph, and the second way is to consider a dense regular structure with a larger size wheel graph. Similar to the network evolution process, coefficients of the cubic equation take n , m and ϵ as the input parameter and produce the subgraph parameters for direct construction of the PEV localized network (Fig. 3.5).

Table 3.3 verifies the theoretical approach of arranging the graph components into two different ways. For a given value of n and m , we calculate the average degree of a regular graph (κ_1) from Eq. (3.11). Next, from Eqs. (3.6) and (3.9), we calculate n_1 and n_2 values, which in turn provide us the size of the wheel and the random regular graphs while satisfying Eq. (3.5). This combined graph has a

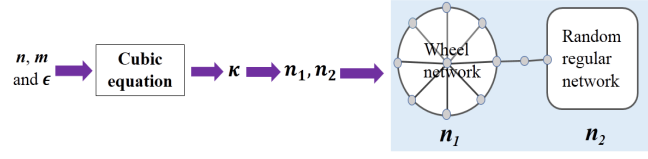


Figure 3.5: A method to direct construction of PEV localized network through the solution of a cubic equation. Given the input parameters (number of nodes (n), connections (m) and $\epsilon \ll 1$) to the coefficients of the cubic equation provide the roots (average degree κ), from which we calculate the size of wheel (\mathcal{W}) and random regular (\mathcal{R}) networks (Eqs. (3.6) and (3.9)). Finally, connecting \mathcal{W} and \mathcal{R} yields the PEV localized network.

localized x_1 and a delocalized x_2 . Similarly, the root κ_2 can be calculated by the same procedure, and we can calculate n_1 and n_2 . The Y_{x_1} value obtained from the analysis comes out to be the same as the value obtained from the optimized edge rewiring process (Table 3.3). Similarly, removing an edge connected to the hub node in \mathcal{W} component and add it to the \mathcal{R} component leading to a delocalization of PEV and second-largest eigenvector becomes highly localized as observed in the optimized network structure in section 3.3.1 (Appendix Table 6.3).

The method simplifies our understanding to the origin of peculiar spectral properties of the optimized structure, as well as provides us a simple method to achieve a large size PEV localized network without performing any optimized edge rewiring process. To conclude, investigation of an optimized network structure obtained through the network evolution reveals that the high localization of the PEV is accompanied with a relation between the eigenvalue of individual components ($\lambda_1^{e_1} > \lambda_1^{e_2}$). The analysis presented in this section is an attempt to solve the problem in a reverse manner. It shows that by considering two subgraphs where one of them has a hub node and another has a regular structure and $\lambda_1^{\mathcal{W}} > \lambda_1^{\mathcal{R}}$, one can produce a network structure having a highly localized as well as sensitive PEV.

3.4 Localization behavior on linear-dynamical system

In sections 3.3.2, we investigate eigenvalue crossing and its relation with the sensitivity behavior of PEV corresponding to the adjacency matrices without using any

n	m	κ_1	n_1	n_2	Y_{x_1}	κ_2	n_1	n_2	Y_{x_1}
500	2512	18	290	209	0.22	13	145	354	0.21
520	2630	19	325	194	0.22	13	145	374	0.21
2448	14806	46	2027	420	0.23	13	145	2302	0.21
4720	13712	69	4627	92	0.24	6	26	4693	0.17
10498	52490	101	10005	492	0.24	11	101	10396	0.20
20422	163376	138	18775	1646	0.24	17	257	20164	0.22

Table 3.3: Various network parameters and IPR values of PEV for a given n and m . From the analytical derivations in Eq. (3.11), we decide κ , n_1 and n_2 . Thereupon, we construct a wheel graph of size n_1 and a random regular graph of size n_2 and join them with a node. This method leads to a highly localized PEV. We consider here $\epsilon = 0.02$.

optimization scheme. Next, we turn our attention to show the impact of eigenvalue crossing phenomenon, caused by single edge rewiring, on the steady-state behavior of a linear-dynamical system. We consider RNA neutral network population linear dynamical model [9, 58, 102–104], which represents a set of genotypes, mapping to the same phenotype form a neutral network. Nodes in the neutral network correspond to genotypes (sequences), and two nodes are said to be connected if the corresponding sequences differ by a single point mutation. Each node i holds a number $x_i(t)$ from the sequence at time t . At each time step each sequence replicates at a rate $f > 1$ and each daughter sequence mutate to one of the $3L$ nearest neighbors with a probability μ and does not mutate with a probability $1 - \mu$. L is the sequence length and $0 < \mu < 1$. The equations illustrating the dynamics of the population on the network can be given by [104]

$$x_i(t+1) = f(1 - \mu)x_i(t) + \frac{f\mu}{3L} \sum_{j=1}^n a_{ij}x_j(t) \quad (3.15)$$

In the matrix form

$$\begin{aligned} \mathbf{x}(t+1) &= f(1 - \mu)\mathbf{I}\mathbf{x}(t) + \frac{f\mu}{3L}\mathbf{A}\mathbf{x}(t) \\ &= \left[f(1 - \mu)\mathbf{I} + \frac{f\mu}{3L}\mathbf{A} \right] \mathbf{x}(t) \\ &= \mathbf{M}\mathbf{x}(t) \end{aligned} \quad (3.16)$$

where $\mathbf{M} = f(1 - \mu)\mathbf{I} + \frac{f\mu}{3L}\mathbf{A}$, \mathbf{I} , and \mathbf{A} are the transition, identity, and adjacency matrix respectively. For the above model, the steady-state vector obtains from the PEV of the transition matrix [102]. Importantly, all the eigenvectors of \mathbf{A} and \mathbf{M}

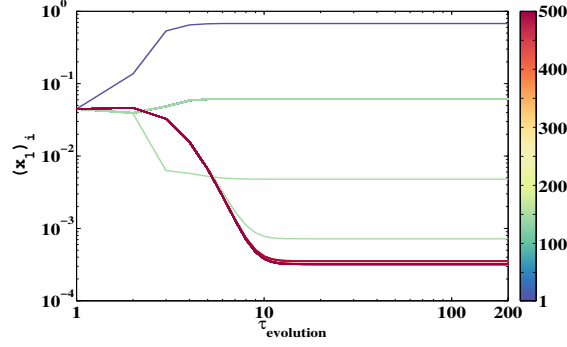


Figure 3.6: We portray the evolution of steady-state vector of the RNA neutral network model population dynamical model on WRR model network. Starting from a uniform state vector, we perform the power iteration method to reach the steady-state vector. Due to the localized PEV in WRR model, the hub node contributes more to the dynamical process, and the rest of them have very less contribution. Here, $n = 500$, $\mu = 0.5$, $f = 2.6$, $L = 18$. For the wheel random regular combined network $\lambda_1^W > \lambda_1^R$ and $Y_{x_1} = 0.22$. We perform the power iteration method for 300000 iterations and store the PEV after each 1500 steps.

are the same which can easily be shown from Eq. (3.16) as follows

$$\begin{aligned}
 \mathbf{M}\mathbf{x}_i^{\mathbf{A}} &= f(1 - \mu)\mathbf{I}\mathbf{x}_i^{\mathbf{A}} + \frac{f\mu}{3L}\mathbf{A}\mathbf{x}_i^{\mathbf{A}} \\
 &= f(1 - \mu)\mathbf{x}_i^{\mathbf{A}} + \frac{f\mu}{3L}\lambda_i^{\mathbf{A}}\mathbf{x}_i^{\mathbf{A}} \\
 &= \lambda_i^{\mathbf{M}}\mathbf{x}_i^{\mathbf{A}}
 \end{aligned} \tag{3.17}$$

where $\lambda_i^{\mathbf{M}} = f(1 - \mu) + \frac{f\mu}{3L}\lambda_i^{\mathbf{A}}$, $\lambda_i^{\mathbf{M}}$ and $\lambda_i^{\mathbf{A}}$ denotes the eigenvalues and $\mathbf{x}_i^{\mathbf{M}}$ and $\mathbf{x}_i^{\mathbf{A}}$ are the eigenvectors of \mathbf{M} and \mathbf{A} respectively. Further, $\lambda_1^{\mathbf{M}}$ is the asymptotic growth rate of the population and from Eq. (3.17) one can observe that limit distribution of population or the steady-state vector of the transition matrix is solely determined by the PEV of the adjacency matrix [9, 58].

We perform the power iteration method on \mathbf{M} with an initial population distribution vector having all the entries same. Considering \mathbf{A} as the adjacency matrix corresponding to the wheel-random structure with $\lambda_1^W > \lambda_1^R$, maximum contribution to the dynamical process comes from a few nodes (Fig. 3.6). In other words, few nodes contribute more to the linear-dynamical process, and the rest of them have very less contribution.

In the wheel-random network, we rewire an edge connected to the hub node and

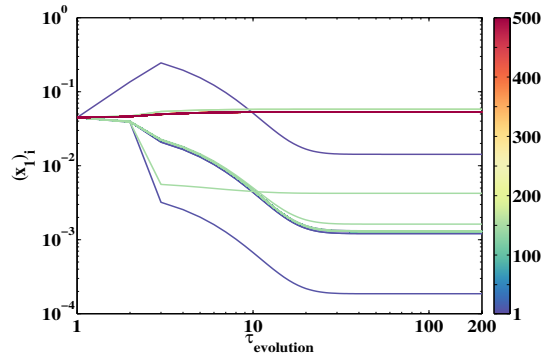


Figure 3.7: We depict the evolution of the steady-state vector of the RNA neutral network population dynamical model on the WRR model network where we rewire an edge connected to the hub node. Starting from a uniform state vector, we perform the power iteration method to reach the steady-state vector. Due to the delocalized PEV, there exists a drastic change in the steady-state of the dynamical process. Model parameters are same as in Fig. 3.6 but $\lambda_1^W < \lambda_1^R$ and $Y_{x_1} = 0.002$.

add it to the random regular structure, and the new transition matrix is denoted by M' . We again perform the power iteration method on M' with the initial population distribution vector which has all the entries same. One can observe (Figs. 3.6 and 3.7) drastic changes in the steady-state vector of the RNA model arising due to the eigenvalue crossing phenomenon. The two largest eigenvalues of the combined network remain close to each other, but there exist changes in the subgraph eigenvalue relation ($\lambda_1^W < \lambda_1^R$) leading to change in the behavior of the steady-state. To avoid this sensitive dependence of the steady-state arising due to a single edge rewiring, we either increase the largest eigenvalue of the wheel graph component by increasing the size, or we can decrease the average degree of the regular graph component which we learned from the analytical approach discussed in subsection 3.3.2.

Although the wheel-random structure is quite special, it provides us an understanding of the localization behavior observed for the networks evolved through the optimized evolution process. Note that the dynamical system used here is a simplified and discrete-time version of the Eigen's molecular-evolution model [58].

3.5 Conclusion

Our investigation reveals that eigenvalue crossing along with the presence of a hub node is the prime reason behind the sensitivity of the PEV in the optimized network. We found that a single edge rewiring in the optimized network structure leads to an eigenvalue crossing, which is detected through the dot product of the two largest eigenvectors. We show that the eigenvalue crossing leads to a change in the eigenvalue relation of the individual components and in turn, governs the sensitivity of the PEV localization.

From the observation of the eigenvalue crossing phenomenon, we develop an analytical framework which assists for the construction of a network structure having high localization as well as sensitive PEV. Importantly, this structure is obtained without performing an optimization scheme. In other words, we use the information of spectral properties of the optimized network to perform reverse engineering to construct a network structure having a highly localized PEV. By mapping the eigenvalue relation of the individual components to a cubic equation and solving it analytically, we find the component size for the direct construction of PEV localized networks.

In the next chapter, we use the wheel random regular model network and the subgraph eigenvalue relation to understand the failure of eigenvector centrality measure. Finally, we extend the WRR model for other networks and provides a detailed discussion of choosing the ϵ values on IPR.

3.6 Appendix: Discriminant analysis

The section analyzes the discriminant of Eq. (3.12) and provides the bounds for the wheel graph size (n_1) as a function of n . To achieve, we first find the range of m values and their relations with the behavior of discriminant (Δ). Then, we calculate the bounds for the roots and calculate the bounds for n_1 . We rewrite the

discriminant in Eq. (3.12)

$$\begin{aligned}\Delta &= \frac{\beta^2}{4} + \frac{\alpha^3}{27} \\ &= (m - n\sigma - p)^2 - \left(\frac{n}{3} + q\right)^3\end{aligned}\quad (3.18)$$

where $\sigma = (1 - \frac{\epsilon}{3})$, $p = \frac{\epsilon^3 + 9\epsilon^2 + 36\epsilon}{27}$, and $q = \frac{\epsilon^2 + 6\epsilon + 6}{9}$. We consider connected network and choose m in between $n + 1$ to $n(n - 1)/2$ where $n \geq 49$.

Case (i) [$\Delta = 0$]: To find out the value of m for which $\Delta = 0$, we solve,

$$(m - n\sigma - p)^2 - \left(\frac{n}{3} + q\right)^3 = 0 \quad (3.19)$$

Solving the quadratic equation of m , we get $m = (n\sigma + p) \pm \frac{(n+3q)\sqrt{3(n+3q)}}{9}$ for which $\Delta = 0$. We know that m should always be a positive quantity, hence we consider

$$m = (n\sigma + p) + \frac{(n + 3q)\sqrt{3(n + 3q)}}{9} \quad (3.20)$$

Moreover, in our case, m is always be a positive integer but from Eq. (3.20), m is a real value with fractional part. Hence, $\Delta = 0$ can never appear for our case.

Case (ii) [$\Delta > 0$]: Now, as m should be a positive integer we add 1 to Eq. (3.20) and get the lower bound for m value as follows

$$\left[(n\sigma + p) + \frac{(n + 3q)\sqrt{3(n + 3q)}}{9} \right] + 1 \leq m \leq \frac{n(n - 1)}{2} \quad (3.21)$$

for which $\Delta > 0$. Now, we substitute Eq. (3.18) in Eq. (3.12), and we have

$$\begin{aligned}\Delta_1 &= \left[-(m - n\sigma - p) + \sqrt{(m - n\sigma - p)^2 - \left(\frac{n}{3} + q\right)^3} \right]^{1/3} \\ \Delta_2 &= \left[-(m - n\sigma - p) - \sqrt{(m - n\sigma - p)^2 - \left(\frac{n}{3} + q\right)^3} \right]^{1/3}\end{aligned}$$

Further, for the range of m values mentioned in Eq. (3.21), $(m - n\sigma - p) > \sqrt{(m - n\sigma - p)^2 - (\frac{n}{3} + q)^3}$, thus $\frac{\sqrt{(m - n\sigma - p)^2 - (\frac{n}{3} + q)^3}}{m - n\sigma - p} < 1$ and hence using binomial approximation we get

$$\begin{aligned}\Delta_1 &\approx -(m - n\sigma - p)^{1/3} \left[1 - \frac{\sqrt{(m - n\sigma - p)^2 - (\frac{n}{3} + q)^3}}{3(m - n\sigma - p)} \right] \\ \Delta_2 &\approx -(m - n\sigma - p)^{1/3} \left[1 + \frac{\sqrt{(m - n\sigma - p)^2 - (\frac{n}{3} + q)^3}}{3(m - n\sigma - p)} \right]\end{aligned}$$

Therefore, from Eq. (3.11) and using the above two relations we get,

$$\kappa_1 = -2(m - n\sigma - p)^{1/3} + \frac{6 - 2\epsilon}{3} \quad (3.22)$$

Further, from Eq. (3.22) with the help of inequality in Eq. (3.21), we get lower bound for κ_1 using the binomial approximation as follows

$$\begin{aligned} \kappa_1 &> -2\left(\frac{n(n-1)}{2} - n\sigma - p\right)^{\frac{1}{3}} + \frac{6 - 2\epsilon}{3} \\ &= -2\left(\frac{n^2}{2} - \frac{n(9-2\epsilon)}{6} - p\right)^{\frac{1}{3}} + \frac{6 - 2\epsilon}{3} \\ &\text{for } 0 < \epsilon \ll 1 \\ &\approx -2^{2/3}n^{2/3}\left(1 - \frac{1}{n}\right) + 2 \\ &\text{for } n \rightarrow \infty \\ &\approx -(2n)^{2/3} + 2 \end{aligned} \quad (3.23)$$

Similarly, we calculate the upper bound for κ_1 from Eqs. (3.21) and (3.22) as follows

$$\kappa_1 < -\frac{2}{\sqrt{3}}\sqrt{n} + 2$$

Hence, combining the above two cases for $\Delta > 0$ we have

$$-(2n)^{2/3} + 2 < \kappa_1 < -\frac{2}{\sqrt{3}}\sqrt{n} + 2$$

and finally from Eq. (3.6), we get bounds for n_1 as follows

$$\frac{4}{3}n - \frac{4}{\sqrt{3}}\sqrt{n} < n_1^{\kappa_1} < (2n)^{4/3} - 4n^{2/3}$$

From the above, we conclude that for a given n value as m varies in the range given in Eq. (3.21), size of the wheel graph varies in the above range. Finally, we show that $\frac{4}{3}n - \frac{4}{\sqrt{3}}\sqrt{n} > n$ for $n \geq 49$ and $(2n)^{4/3} - 4n^{2/3} > n$ for $n \geq 4$. Hence, for $n \geq 49$, size of the wheel graph exceeds the given n . Thus, we can not use κ_1 for the wheel graph size calculation from Eq. (3.6).

Case (iii) [$\Delta < 0$]: Subtracting 1 from Eq. (3.20), we get upper bound for m

$$n + 1 \leq m \leq \left[(n\sigma + p) + \frac{(n + 3q)\sqrt{3(n + 3q)}}{9} \right] - 1 \quad (3.24)$$

for which $\Delta < 0$. Now, following the inequality in Eq. (3.24), from Eq. (3.12) we get

$$\Delta_1 = z_1^{1/3} \text{ and } \Delta_2 = z_2^{1/3}$$

where

$$\begin{aligned} z_1 &= \left[-(m - n\sigma - p) + i\sqrt{\left(\frac{n}{3} + q\right)^3 - (m - n\sigma - p)^2} \right] \\ z_2 &= \left[-(m - n\sigma - p) - i\sqrt{\left(\frac{n}{3} + q\right)^3 - (m - n\sigma - p)^2} \right] \end{aligned} \quad (3.25)$$

Hence, Δ_1 and Δ_2 are the cubic roots of complex numbers z_1 and z_2 respectively.

Therefore, in the polar form

$$z_1 = r_{z_1} [\cos \theta_{z_1} + i \sin \theta_{z_1}]$$

$$z_2 = r_{z_2} [\cos \theta_{z_2} + i \sin \theta_{z_2}]$$

and the cubic roots of z_1 and z_2 can be calculated as

$$\begin{aligned} \Delta_1^s &= \sqrt[3]{r_{z_1}} \left[\cos \frac{2\pi s + \theta_{z_1}}{3} + i \sin \frac{2\pi s + \theta_{z_1}}{3} \right], \quad s = 0, 1, 2 \\ \Delta_2^s &= \sqrt[3]{r_{z_2}} \left[\cos \frac{2\pi s + \theta_{z_2}}{3} + i \sin \frac{2\pi s + \theta_{z_2}}{3} \right], \quad s = 0, 1, 2 \end{aligned}$$

and hence from Eq. (3.11) we get

$$\begin{aligned} \kappa_1 &= \Delta_1^s + \Delta_2^s - \frac{b}{3} \\ &= \sqrt[3]{r_{z_1}} \left[\cos \frac{2\pi s + \theta_{z_1}}{3} + i \sin \frac{2\pi s + \theta_{z_1}}{3} \right] + \\ &\quad \sqrt[3]{r_{z_2}} \left[\cos \frac{2\pi s + \theta_{z_2}}{3} + i \sin \frac{2\pi s + \theta_{z_2}}{3} \right] - \frac{b}{3} \end{aligned} \quad (3.26)$$

To simplify the above equation, we perform the following steps. From Eq. (3.25), we calculate

$$\begin{aligned} r_{z_1} &= \sqrt{(-(m - n\sigma - p))^2 + \left(\sqrt{\left(\frac{n}{3} + q\right)^3 - (m - n\sigma - p)^2}\right)^2} \\ &= \left(\frac{n}{3} + q\right)^{\frac{3}{2}} \end{aligned}$$

Similarly, from Eq. (3.25) we also get, $r_{z_2} = \left(\frac{n}{3} + q\right)^{\frac{3}{2}}$. Hence,

$$r_{z_1} = r_{z_2} = \left(\frac{n}{3} + q\right)^{\frac{3}{2}} \quad (3.27)$$

Now, one can see that for the range of m value in Eq. (3.24), $(m - n\sigma - p) > 0$ and $\sqrt{\left(\frac{n}{3} + q\right)^3 - (m - n\sigma - p)^2} > 0$ for $0 < \epsilon \ll 1$. Hence, z_1 and z_2 in Eq. (3.25) belongs to the second and third quadrant of the Argand plane and complex

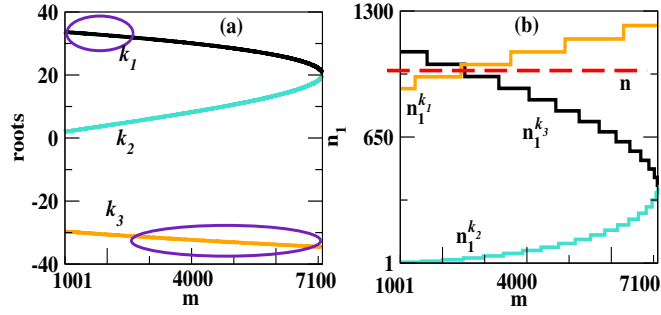


Figure 3.8: In the cubic equation for the coefficient $n = 1000$, $\epsilon = 0.00002$ and for different values of m in the range given by Eq. (3.24). (a) One can observe nature of three unequal real roots for $\Delta < 0$. (b) Behavior of the wheel graph component size calculated from Eq. (3.6) and for three different roots denoted as $n_1^{\kappa_1}$, $n_1^{\kappa_2}$ and $n_1^{\kappa_3}$ respectively. We can observe that for sparse network $n_1^{\kappa_1}$ is larger than n . On the other hand as network becomes dense, $n_1^{\kappa_3}$ becomes larger than n . $n_1^{\kappa_2}$ is always lesser than n .

conjugate to each other. We find the principal value for the argument in the range of $(-\pi, \pi]$ [105]. Hence, the argument becomes

$$\theta_{z_2} = -\theta_{z_1} \quad (3.28)$$

Now, from Eq. (3.26) by using the relations in Eqs. (3.27) and (3.28) we get

$$\kappa_1 = 2\sqrt[3]{r_{z_1}} \cos \frac{\theta_{z_1}}{3} \left[\cos \frac{2\pi s}{3} + i \sin \frac{2\pi s}{3} \right] - \frac{b}{3} \quad (3.29)$$

Further, it is known $\Delta < 0$ provides three unequal real roots, hence, κ_1 should be a real value [99–101]. One can see that we get a real value for $s = 0$ and complex number for other s values. Finally, for $s = 0$, from Eq. (3.29) we get

$$\kappa_1 = 2 \left(\frac{n}{3} + q \right)^{\frac{1}{2}} \cos \frac{\theta_{z_1}}{3} + \frac{6 - 2\epsilon}{3} \quad (3.30)$$

and similarly from Eq. (3.11) by using the relation in Eqs. (3.27), (3.28) and for $s = 0$, we get

$$\begin{aligned} \kappa_2 &= 2 \left(\frac{n}{3} + q \right)^{\frac{1}{2}} \sin \left(\frac{\theta_{z_1}}{3} - \frac{\pi}{6} \right) + \frac{6 - 2\epsilon}{3} \\ \kappa_3 &= -2 \left(\frac{n}{3} + q \right)^{\frac{1}{2}} \sin \left(\frac{\theta_{z_1}}{3} + \frac{\pi}{6} \right) + \frac{6 - 2\epsilon}{3} \end{aligned} \quad (3.31)$$

Next, we calculate the lower and upper bounds for the roots in the range of m for a given n in Eq. (3.24). We know that z_1 is in second quadrant, thus, $\frac{\pi}{2} < \theta_{z_1} < \pi$, implies $\frac{\pi}{6} < \frac{\theta_{z_1}}{3} < \frac{\pi}{3}$, hence, $\frac{1}{2} < \cos \frac{\theta_{z_1}}{3} < \frac{\sqrt{3}}{2}$ and which is positive. Further, $0 < \frac{\theta_{z_1}}{3} - \frac{\pi}{6} < \frac{\pi}{6}$ implies that $0 < \sin \left(\frac{\theta_{z_1}}{3} - \frac{\pi}{6} \right) < \frac{1}{2}$. Finally, $\frac{\pi}{3} < \frac{\theta_{z_1}}{3} + \frac{\pi}{6} < \frac{\pi}{2}$

implies that $\frac{\sqrt{3}}{2} < \sin(\frac{\theta_{z_1}}{3} + \frac{\pi}{6}) < 1$. Further, we find the lower and upper bound for the roots from Eqs. (3.30) and (3.31) using the binomial approximation for $0 < \epsilon \ll 1$ and $n \rightarrow \infty$ as follows

$$\begin{aligned} \frac{1}{\sqrt{3}}\sqrt{n} + 2 &< \kappa_1 < \sqrt{n} + 2 \\ 2 &< \kappa_2 < \frac{1}{\sqrt{3}}\sqrt{n} + 2 \\ -\frac{2}{\sqrt{3}}\sqrt{n} + 2 &< \kappa_3 < -\sqrt{n} + 2 \end{aligned}$$

Finally, use the lower and upper bounds of κ_i and calculate the bounds of n_1 in Eq. (3.6) as follows

$$\begin{aligned} \frac{1}{3}n + \frac{2}{\sqrt{3}}\sqrt{n} &< n_1^{\kappa_1} < n + 2\sqrt{n} \\ 1 &< n_1^{\kappa_2} < \frac{1}{3}n + \frac{2}{\sqrt{3}}\sqrt{n} \\ n - 2\sqrt{n} &< n_1^{\kappa_3} < \frac{4}{3}n - \frac{4}{\sqrt{3}}\sqrt{n} \end{aligned}$$

From the above $\frac{1}{3}n + \frac{2}{\sqrt{3}}\sqrt{n} > n$ for $n < 3$, $n + 2\sqrt{n} > n$ for $n > 0$, and finally $\frac{4}{3}n - \frac{4}{\sqrt{3}}\sqrt{n} > n$, $n \geq 48$. Hence, if we choose $n \geq 49$, $n_1^{\kappa_2}$ will always be less than n .

We numerically vary m in the range in Eq. (3.24) and examine the behavior of three different roots (Fig. 3.8(a)) and their corresponding n_1 values (Fig. 3.8(b)). One can observe that for a small region, size of $n_1^{\kappa_1}$ and $n_1^{\kappa_3}$ exceeds the given n (depicted by a horizontal dotted line in Fig. 3.8(b)). Importantly, the bounds obtained from the analysis are in good agreement with the numerical results and indicate that for sparse networks small portion of the κ_1 cannot be used to find wheel graph size (Fig. 3.8(a) marked with an ellipse). Consequently, for dense networks, κ_3 can not be used for the wheel graph size calculation (Fig. 3.8(a) marked with an ellipse) and κ_2 always works well. Hence, we use κ_1 and κ_2 to calculate the wheel and random regular component size to construct \mathcal{G}_{new} .

Chapter 4

Impact of PEV localization on Eigenvector centrality measure

4.1 Introduction

Complex networks or graphs provide a powerful framework to understand the importance of individuals and their interactions in real-world complex systems [2, 106]. For instance, in a transportation system, cities represent the nodes and the routes among them represent the links or edges. Social media like Facebook can also be seen as edges of friendship where people are the nodes. It is often essential to have the information of “most influential” or “central nodes” in a network. For example, assuming a population of a city as a social network where we want to spread news, spreading of information will be faster if we pass the news to the central person or a group of people having more connections. To understand the relevance of a node in a network, different types of centrality measures have been proposed [9, 27]. Particularly, measures based on degree centrality, betweenness centrality, closeness centrality, and eigenvector centrality (EC), are successful in assigning centrality weights to the nodes in a network. The degree centrality identi-

fies a node as a central node based on the number of edges connected to it, whereas, EC measures devised by Bonacich is based on how important its neighboring nodes are and is calculated by taking into account the weights of the neighboring nodes as well [107]. Further, the EC value for each node in a network can easily be calculated from the PEV entry of the corresponding adjacency matrix [27]. In other words, the EC vector of a network corresponds to the PEV of the network's adjacency matrix.

Despite considerable success of EC in ranking the nodes of a network [108–115], Martin *et al.* demonstrated that under certain circumstances PEV might undergo a localization transition where most of the weights get concentrated on a few nodes leading to a failure of EC [24, 116]. Note that PEV is said to be localized when independent of the network size few entries of the vector take large constant weights while rest of the entries receive tiny weights. There exists another extreme case for PEV, i.e., the delocalized state. PEV is said to be delocalized when all the entries in PEV receive almost the same weight independent of the network size [23, 24].

Using random matrix theory, Ref. [24] proposed a structural relationship ($k_{max} > \kappa(\kappa + 1)$) between the average degree (κ) and maximum degree (k_{max}) of a network to observe the localization of PEV, thereafter imposing severe problems to the EC measure. These studies concentrated on finding constraints for a localized PEV and its impact on the EC measures. However, it is not clear what impact a delocalized PEV state has on the EC measure. Additionally, if there exists a relationship between the network's parameters governing its structure, ensuring a delocalized PEV?

Using wheel-random-regular (WRR) model network introduced in chapter 3, we show that not only PEV localization can lead to a problem for the EC, but delocalization in PEV can also create problems to the EC measure. We know that for a connected regular graph, PEV is delocalized (Theorem 6 [26]), and therefore the degree centrality and EC provide the same information [107]. It is evident that for the regular or random regular network have delocalized PEV as all the nodes carry the same information in the network. However, investigations of the WRR

model reveal that graphs consisting of heterogeneous degrees can also have delocalized PEVs. In this chapter, using the WRR model, we show that along with the occurrence of localization state, the occurrence of delocalization of PEV can also affect weights assignment to the higher degree nodes, thereby creating difficulties in accessing relative importance of the nodes, causing the failure of EC.

We fabricate the chapter as follows: Section 4.2 describes the notations and definitions of the mathematical terms. Section 4.3.2 illustrates the results demonstrating PEV localization-delocalization for wheel-random regular, star-random regular, friendship-random regular, and scalefree-random regular networks. It also contains a subsection which discusses the failure of EC measure due to the localization-delocalization transition of PEV. Finally, section 4.5 summarizes our work.

4.2 Background

In this section, we again briefly provide the basics of adjacency matrices, EC measure, and IPR. A graph can be represented as $\mathcal{G} = (V, E)$ where V is the set of nodes and E is the set of edges (links) among them. We denote $|V| = n$ as the number of nodes and $|E| = m$ being the number of edges of \mathcal{G} . Here, we consider undirected, unweighted, connected, and simple networks. Hence, the corresponding adjacency matrix can be denoted as \mathbf{A} and represented easily as

$$a_{ij} = \begin{cases} 1 & \text{if nodes } i \text{ and } j \text{ are connected} \\ 0 & \text{Otherwise} \end{cases}$$

The number of edges to a particular node is referred as its degree denoted as $k_i = \sum_{j=1}^n a_{ij}$. The average degree of the network is denoted by $\langle k \rangle = \frac{1}{n} \sum_{i=1}^n k_i$. We refer the maximum degree node or the hub node of \mathcal{G} as $k_{max} = \max_{1 \leq i \leq n} k_i$.

Here, \mathbf{A} is a real symmetric matrix and consequently has a set of real eigenvalues $\{\lambda_1, \lambda_2, \dots, \lambda_n\}$. The corresponding orthonormal set of eigenvectors are $\{\mathbf{x}_1, \mathbf{x}_2, \dots, \mathbf{x}_n\}$ where

$$\mathbf{x}_i = ((x_i)_1, (x_i)_2, \dots, (x_i)_n)^T$$

for $i = 1, 2, \dots, n$. Further, \mathbf{A} is a non-negative matrix and it follows from the Perron-Frobenius theorem [27] that there exists a positive and simple eigenvalue λ_1 .

The eigenvector corresponding to λ_1 is a unique positive eigenvector (\mathbf{x}_1) referred as the principal eigenvector.

The EC vector, $\mathbf{v} = (v_1, v_2, \dots, v_n)^T$ denotes the centrality of all the nodes and v_i can be calculated as

$$v_i = \lambda_1^{-1} \sum_{j=1}^n a_{ij} v_j \quad (4.1)$$

It is well known that \mathbf{v} corresponds to \mathbf{x}_1 [27].

We use the inverse participation ratio (IPR) to measure the PEV localization [24, 25]. The IPR of the PEV can be calculated [4, 23–25] as follows:

$$Y_{\mathbf{x}_1} = \sum_{j=1}^n (x_1)_j^4 \quad (4.2)$$

where $(x_1)_j$ is the j^{th} component of \mathbf{x}_1 . A completely localized PEV with components $\mathbf{x}_1 = (1, 0, \dots, 0)^T$ yields an IPR value, $Y_{\mathbf{x}_1} = 1$, whereas a completely delocalized PEV with component $\mathbf{x}_1 = (\frac{1}{\sqrt{n}}, \frac{1}{\sqrt{n}}, \dots, \frac{1}{\sqrt{n}})^T$ has $Y_{\mathbf{x}_1} = \frac{1}{n}$. In general, PEV is said to be localized if $Y_{\mathbf{x}_1} = \mathcal{O}(1)$ as $n \rightarrow \infty$ and referred to as delocalized if $Y_{\mathbf{x}_1} \rightarrow 0$ as $n \rightarrow \infty$ [4]. It is known that for any connected regular graph, $\mathbf{x}_1 = (\frac{1}{\sqrt{n}}, \frac{1}{\sqrt{n}}, \dots, \frac{1}{\sqrt{n}})^T$ (Theorem 6 [26]) and thus, $Y_{\mathbf{x}_1} = \frac{1}{n}$. Next, if we consider a disconnected graph where each node is isolated without having any interaction with any one and having a self-loop, adjacency matrix will be an identity matrix and for which we can choose $\mathbf{x}_1 = (1, 0, \dots, 0)^T$ leading to $Y_{\mathbf{x}_1} = 1$. However, if we consider a connected network having non-negative entries, all the entries of the PEV is positive (from Perron-Frobenius theorem). Hence, IPR value of the PEV should be in the range $1/n \leq Y_{\mathbf{x}_1} < 1$ for $n \geq 2$. However, to test whether the PEV is localized or not for IPR being in the range $1/n < Y_{\mathbf{x}_1} < 1$, we adopt the procedure proposed for the detection of the Anderson localization [60] and which was recently used to measure the eigenvector localization in complex networks [23–25]. According to this procedure, one should calculate the IPR value of PEV for different network sizes. If $Y_{\mathbf{x}_1}$ tends to have a constant value as $n \rightarrow \infty$, PEV is localized, otherwise it is delocalized [25].

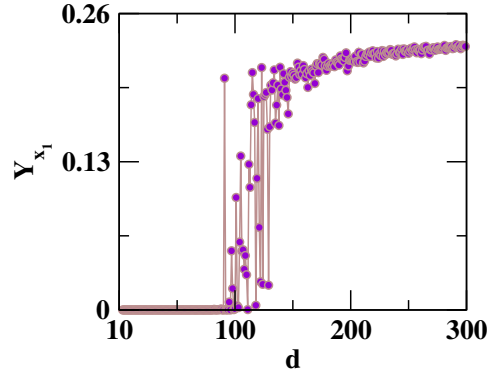


Figure 4.1: Localization transition in the PEV for hub node size being larger than the square of the average degree of the networks ($k_{max} > \kappa(\kappa + 1)$) [24]. For k_{max} being much larger, IPR value shows a drastical increase leading to a non-zero constant value. We consider a connected random graph of size $n = 100000$ and average degree $\kappa = 10$, where n^{th} node acts as a hub node and degree of the n^{th} node varies from 10 to 300.

4.3 Results and Discussion

We first consider a graph model which has only one hub node [24, 116]. This model network has localized PEV. The PEV entries experience minor changes with the change in the network size confirming its localization. Furthermore, using WRR model networks and its variants, we demonstrate that non-regular networks can have localized as well as delocalized PEV. Further, with the help of the WRR model network, we show that the delocalization of PEV can also cause failure to the EC as it does not assign sufficiently large weights to the higher degree nodes. All the data and codes used in this paper are available at GitHub repository [117].

4.3.1 Localization transition in Random Graph Model

In the random graph (RG) model [24], a random subgraph (\mathcal{G}_{RG}) of size $n - 1$ is generated with the connection probability between a pair of vertices being $p = \kappa/(n - 1)$ for $n \rightarrow \infty$. The random subgraph is generated using the algorithm in [118]. Further, n^{th} node is included in \mathcal{G}_{RG} such that it connects to the $n - 1$ existing nodes of the random subgraph with a probability $k_{max}/(n - 1)$, where $k_{max} \gg \kappa$. Hence, the expected number of connections to the n^{th} node should be k_{max} , thereby n^{th} node will be the hub node. Further, using the random matrix

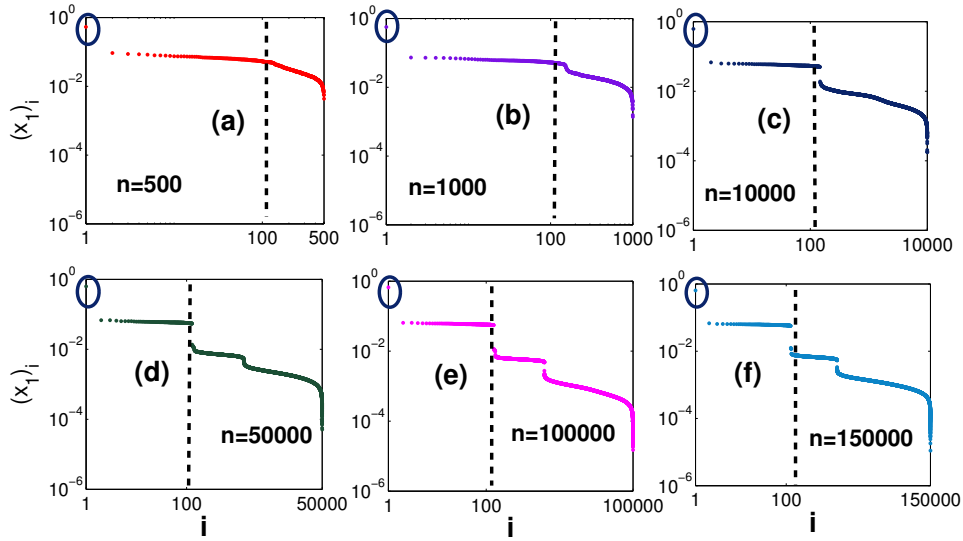


Figure 4.2: Sorted localized PEV entries $((x_1)_i$ for $i = 1, 2, \dots, n$) for different network size. The average degree ($\kappa = 10$) and maximum degree ($k_{max} = 130$) remains fixed and which satisfies $k_{max} > \kappa(\kappa + 1)$. The PEV entries corresponding to the hub node (marked with a circle) and its adjacent nodes receive large constant weights as $n \rightarrow \infty$. The PEV entries corresponding to the nodes which are not connected to the hub node (after dotted vertical lines) gradually show a decrease, eventually becoming close to zero as $n \rightarrow \infty$.

theory, it has been shown in Ref. [24] that if the size of the hub node is larger than $\kappa(\kappa + 1)$, localization transition occurs. Further, the PEV entry corresponding to the hub node and its immediate neighbors are expected to have constant values, and which should only depend on κ and k_{max} . However, rest of the nodes which are not adjacent to the hub node receive a vanishing weight as $n \rightarrow \infty$. Note that κ is the average degree of the random subgraph containing $n - 1$ number of nodes.

Fig. 4.1 indicates that for a hub node of size k_{max} , $k_{max} < \kappa(\kappa + 1)$, IPR value of PEV is small and in fact it lies close to zero. However, as k_{max} becomes greater than $\kappa(\kappa + 1)$, there arises a sudden jump in the IPR value (Fig. 4.1) as also illustrated in [24]. Though, it is evident from Fig. 4.1, that for fix values of n and κ , if we form a hub node of size k_{max} such that it is larger than $\kappa(\kappa + 1)$, IPR value of PEV is large. However, it is not clear that with an increase in the network size by fixing κ and k_{max} , whether IPR value remains fixed to a large value, and how exactly the PEV entries behave?

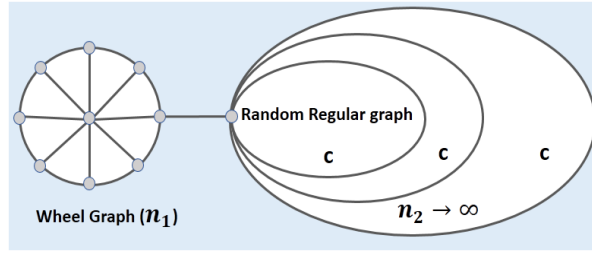


Figure 4.3: Schematic representation of the wheel-random-regular model networks (\mathcal{G}_{WRR}). Here, n_1 is the number of nodes in the wheel graph and n_2 is the number of nodes in the random regular network having an average degree of κ . With an increase in the number of nodes in the random regular network, while fixing κ , the hub node size of wheel graph remains unchanged.

Figure 4.2 plots sorted PEV entries $((x_1)_i)$ for different network sizes by fixing κ and k_{max} such that $k_{max} > \kappa(\kappa + 1)$. For each value of n , the PEV entry corresponding to the hub node adopts a large value (marked with a circle in Fig. 4.2), and successive PEV entries become approximately equal to each other forming a horizontal band (Fig. 4.2). Additionally, we observe that PEV entries in the horizontal band correspond to those nodes which are directly connected to the hub node. After the horizontal band, the PEV entries show a gradually decrease and become close to the zero as $n \rightarrow \infty$ (Fig. 4.2). Hence, in the limit of large n , the size of the hub and its neighboring nodes play a vital role in the occurrence of localization transition of PEV. Note that we choose κ such that the random subgraph is always connected even for large values of n . In the following, we use a few other simple models to demonstrate the localization-delocalization transition as a consequence of single edge rewiring of PEV and relation of this transition with the behavior of EC measure.

4.3.2 Wheel-Random-Regular Model

In this section, we use WRR model network introduced in chapter 3 to provide a simple method, instead of the random matrix theory, to derive a condition to form a model network having the highly localized PEV. Further, the rewiring of a few special sets of edges in this model network is shown to lead the delocalization transition of PEV. This section demonstrates that occurrence of the localization-delocalization

transition of PEV in WRR model networks as a consequence of single edge rewiring creates difficulties in weights assignment to the nodes based on EC, thereby leading to the failure of EC.

As discussed in section 3.3.2, the WRR model consists of a random regular graph and a wheel graph. Let us denote it as \mathcal{G}_{WRR} (Fig. 4.3). This model network manifests both the localization as well as the delocalization of PEV, occurrence of which is decided by the largest eigenvalue relation of the individual graph components. We denote the wheel graph as $\mathcal{W} = \{V_{\mathcal{W}}, E_{\mathcal{W}}\}$ where $|V_{\mathcal{W}}| = n_1$ is the number of nodes and $|E_{\mathcal{W}}| = 2(n_1 - 1)$ is the number of edges in \mathcal{W} . Further, the random regular graph is denoted as $\mathcal{R} = \{V_{\mathcal{R}}, E_{\mathcal{R}}\}$ where $|V_{\mathcal{R}}| = n_2$ is the number of nodes and $|E_{\mathcal{R}}| = \frac{n_2\kappa}{2}$ is the number of edges with each node having degree κ . We generate the random regular graph using the algorithm in [98]. Further, it is known that for a wheel and a random regular graph, the largest eigenvalues are as follows [78]

$$\lambda_1^{\mathcal{W}} = \sqrt{n_1} + 1 \text{ and } \lambda_1^{\mathcal{R}} = \kappa \quad (4.3)$$

We combine a wheel graph and a random regular graph such that

$$\text{(a) } \lambda_1^{\mathcal{W}} > \lambda_1^{\mathcal{R}} \text{ or (b) } \lambda_1^{\mathcal{W}} = \lambda_1^{\mathcal{R}} + \epsilon \text{ where } 0 < \epsilon < 1 \quad (4.4)$$

leading to occurrence of highly localized PEV (learned from chapter 3). To construct \mathcal{G}_{WRR} by holding the relation in Eq. (4.4) requires the network parameters (κ , n_1 and n_2) of \mathcal{W} and \mathcal{R} . One can observe that substitute Eq. (4.3) in Eq. (4.4), one can easily find the size of \mathcal{W} as follows

$$\text{(a) } n_1 > (\kappa - 1)^2 \text{ or (b) } n_1 = \lceil (\kappa - 1 + \epsilon)^2 \rceil \quad (4.5)$$

where ($\lceil \cdot \rceil$) is the ceiling function. For the random regular graph, we can choose any arbitrary size and average degree such that κn_2 is even. Hence, for a particular value of κ , Eq. (4.5) implicitly ensures the validity of Eq. (4.4). In \mathcal{G}_{WRR} all the nodes corresponding to \mathcal{R} component has degree κ except one node having degree $\kappa + 1$ which connects to \mathcal{W} component. Simultaneously, all the peripheral nodes of \mathcal{W} has degree 3 except one node of degree 4 which connects to \mathcal{R} component. From

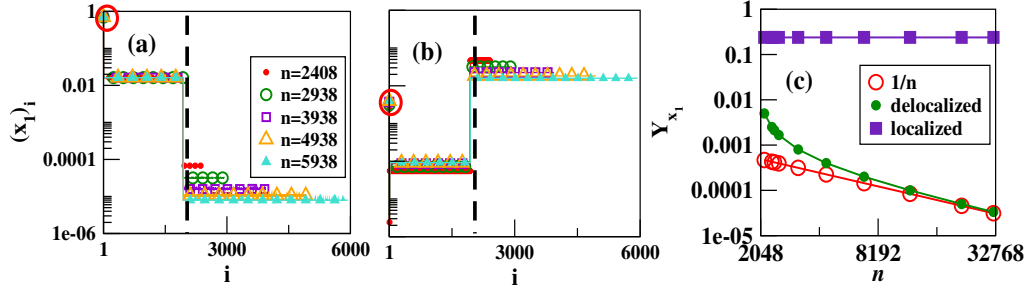


Figure 4.4: Value of localized PEV entries of (a) network constructed by combining a wheel graph (\mathcal{W}) with a random regular (\mathcal{R}) graph. We choose $n_1 = 1938$, $n_2 = 470$ and $\kappa = 45$ satisfying $\lambda_1^{\mathcal{W}} = \lambda_1^{\mathcal{R}} + \epsilon$, $\epsilon = 0.00002$ and yielding a network (\mathcal{G}_{WRR}) with $n = 2408$ nodes and $m = 14806$ edges. For \mathcal{G}_{WRR} , IPR value of PEV is equal to 0.2389 . Next, by fixing size of \mathcal{W} , we increase size of \mathcal{R} by keeping κ constant. This arrangement leads to $\lambda_1^{\mathcal{W}} = \lambda_1^{\mathcal{R}} + \epsilon$ and keeps the PEV entries same for the hub as well as its adjacent nodes as $n \rightarrow \infty$. (b) The same network but by removing an edge connected to the hub node in \mathcal{W} and adding it between a pair of nodes in \mathcal{R} . This rewiring yields delocalization transition in PEV. By increasing the size of \mathcal{G}_{WRR} by including nodes to \mathcal{R} keeping the κ fixed, and the eigenvalue relation $\lambda_1^{\mathcal{W}} < \lambda_1^{\mathcal{R}}$ holds true, and PEV entries take very less values for the hub and its neighboring nodes as $n \rightarrow \infty$. (c) IPR values of PEV (Y_{x_1}) for the wheel-random-regular (WRR) graph as a function of combined network size n . For each value of n , we consider two WRR graphs, first WRR graph is generate by holding the relation in Eq. (6) and PEV is localized (■). The second WRR graph has an edge rewired, and PEV becomes delocalized (●). For reference to a delocalization, we plot $1/n$ (○) as a function of n .

Eq. (4.5), the maximum degree node of the \mathcal{W} component in \mathcal{G}_{WRR} has degree

$$(a) k_{max} > (\kappa - 1)^2 - 1 \text{ or } (b) k_{max} = \lceil (\kappa - 1 + \epsilon)^2 \rceil - 1, \text{ where } k_{max} = n_1 - 1 \quad (4.6)$$

and which is always be greater than κ ($3 \leq \kappa \leq n_2 - 2$). Therefore, Eq. (4.6), establishes a structural relationship between the size of the hub node of \mathcal{G}_{WRR} (k_{max}) and average degree (κ) of random regular graph, which can also be holds true for WRR model networks having the localized PEV. Hence, Eq. (4.6) ensures that the maximum degree node of \mathcal{G}_{WRR} will always come from the wheel graph component of \mathcal{G}_{WRR} .

In the following discussions, we primarily focus on the localization-delocalization transition as a consequence of single edge rewiring and for which we consider $0 < \epsilon < 1$. Importantly, upon changing the bound to $\epsilon > 0$, we get part (a) of

Eqs. (4.4), (4.5) and (4.6). In section 4.6, we analytically show that by holding $\lambda_1^{\mathcal{W}} > \lambda_1^{\mathcal{R}}$, PEV entries of the wheel subgraph contribute more to the PEV of \mathcal{G}_{WRR} as compared to that of the regular graph part.

4.3.2.1 Localization transition in WRR model

First, we perform an experiment to show that \mathcal{G}_{WRR} contains a localized PEV. We construct \mathcal{G}_{WRR} by combining a wheel graph and a random regular graph by satisfying Eq. (4.4) and which gives a large IPR value. Next, to ensure localization of PEV, we fix the average degree of \mathcal{R} and increase the number of nodes in \mathcal{R} , resulting in an increase in the size of \mathcal{G}_{WRR} (Fig. 4.3). In the other words, increasing n_2 leads to an increase in the number of nodes (n) in \mathcal{G}_{WRR} , however, the network keeps satisfying $\lambda_1^{\mathcal{W}} = \lambda_1^{\mathcal{R}} + \epsilon$. We observe that PEV entries remain almost constant for the hub and its adjacent nodes (Fig. 4.4(a)), as well as IPR remains fixed to a constant value (Fig. 4.4(c)) indicating localization of PEV.

4.3.2.2 Delocalization transition in WRR model

Next, to witness the delocalized state, we consider the same model as the above and simply rewire an edge from the \mathcal{W} component to the \mathcal{R} component of \mathcal{G}_{WRR} . We denote the modified graph as $\tilde{\mathcal{G}}_{WRR}$, and the imperfect wheel and random regular component as $\tilde{\mathcal{W}}$ and $\tilde{\mathcal{R}}$, respectively. In \mathcal{G}_{WRR} (Fig. 4.3), just by removing an edge connected to the hub node of \mathcal{W} and adding it between a pair of nodes in \mathcal{R} yields $\tilde{\mathcal{G}}_{WRR}$ with $\lambda_1^{\tilde{\mathcal{W}}} = \lambda_1^{\mathcal{W}} - \delta = \lambda_1^{\mathcal{R}} + \epsilon - \delta$ such that $\delta > \epsilon$. Upon performing one such rewiring, there is a drastic change in the PEV entries (Fig. 4.4(b)) leading to a small IPR value indicating delocalization. However, to ensure this delocalization in PEV upon such rewiring, we increase the size of $\tilde{\mathcal{G}}_{WRR}$ by including more number of nodes to the random regular subgraph without changing the average degree κ leading to an unchanged of the eigenvalue relation for both of the components ($\lambda_1^{\tilde{\mathcal{W}}} = \lambda_1^{\mathcal{R}} + \epsilon - \delta$). The IPR shows a value close to $1/n$ as $n \rightarrow \infty$ which confirms delocalization of PEV (Fig. 4.4(c)). Interestingly, this network has a hub node of the significant size ($k_{max} = \lceil (\kappa - 1 + \epsilon)^2 \rceil - 2$), however, due to an occurrence of the delocalization in PEV, EC is unable to assign high weights to the hub and its

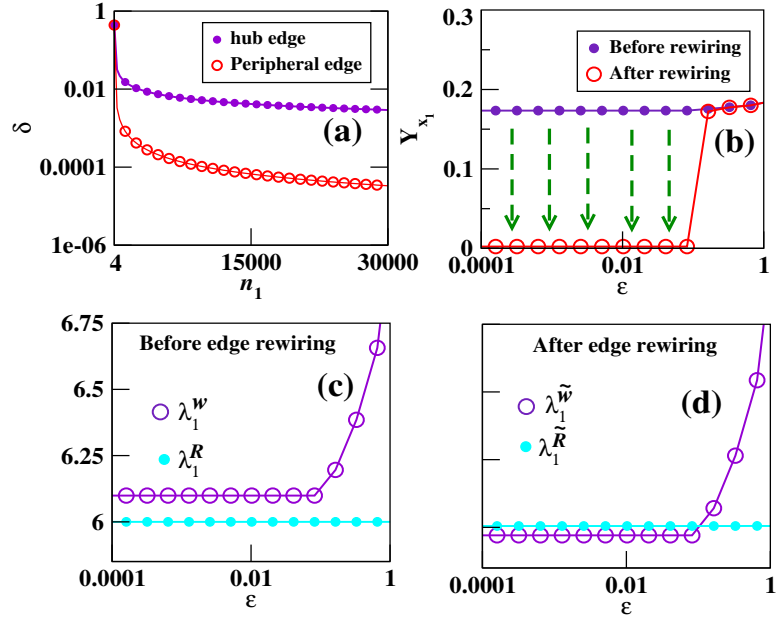


Figure 4.5: (a) Measure the difference between $\delta = \lambda_1^W - \lambda_1^{\tilde{W}}$ as a function of wheel graph size (n_1) after removing hub edge (\bullet) and peripheral edge (\circ). IPR value of the combined network and the largest eigenvalue of the individual component as a function of ϵ to demonstrate that a particular value of ϵ is required to witness sudden change in the IPR value as a consequence of a single edge rewiring. (b) IPR of localized and delocalized graph and (c) plot λ_1^W & λ_1^R and (d) plots $\lambda_1^{\tilde{W}}$ & $\lambda_1^{\tilde{R}}$. The size of the wheel graph is calculated from Eq. (4.5), where parameters of the random graph is $n_2 = 500$ and $\kappa = 6$.

neighboring nodes resulting in a failure of EC measure (Fig. 4.4(b)). Further, one can say that there exists a single point transition for localization-delocalization of PEV. Notably, in the delocalized state, the PEV weights flip between \tilde{W} and \tilde{R} of $\tilde{\mathcal{G}}_{WRR}$, as well as PEV entry weight corresponding to the hub node becomes tiny (Fig. 4.4(b)). To conclude, we have found at least one network structure where the delocalization of PEV creates a problem for EC. Note that chapter 3 illustrates, for such situations, there exists a localized second-largest eigenvector.

4.3.2.3 Impact of ϵ on IPR value

Next let us explain that moving one edge from \mathcal{W} to \mathcal{R} in \mathcal{G}_{WRR} involves two steps (i) removing an edge from \mathcal{W} component and (b) including it in the \mathcal{R} component. We know that removal of an edge from a connected graph always leads to a decrease in the largest eigenvalue, whereas addition of a new edge in a network leads to an

increase the largest eigenvalue (Proposition 1.3.10, [119]). To track the amount of decrement (δ) in $\lambda_1^{\mathcal{W}}$ as a consequence of single edge removal, we perform numerical simulations for different values of n_1 . It is clear from Fig. 4.5(a) that removal of an edge connected to the hub node of \mathcal{W} leads to a significant decrease in $\lambda_1^{\mathcal{W}}$ whereas removal of an edge connected to the peripheral nodes in \mathcal{W} leads to negligible change in $\lambda_1^{\mathcal{W}}$. Therefore, to capture the sudden change in the PEV localization upon a single edge rewiring, we focus on those edges of \mathcal{W} which are connected to the hub node. Further, upon addition the edge to the \mathcal{R} leads to an increment in $\lambda_1^{\mathcal{R}}$ which is negligible because of regularity of the network and we assume $\lambda_1^{\tilde{\mathcal{R}}} = \lambda_1^{\mathcal{R}}$. It indicates that before and after a single edge rewiring, $\lambda_1^{\mathcal{W}}$ is affected substantially. As we have already mentioned that for the localized PEV, $\lambda_1^{\mathcal{W}} = \lambda_1^{\mathcal{R}} + \epsilon$, $0 < \epsilon < 1$ whereas for a delocalized PEV, $\lambda_1^{\tilde{\mathcal{W}}} = \lambda_1^{\mathcal{R}} + \epsilon - \delta$ provided $\delta > \epsilon$ upon a single edge rewiring. Hence, single edge removal leads to a decrement in $\lambda_1^{\mathcal{W}}$ such that δ is greater than ϵ leading to delocalization transition. Fig. 4.5(a) convey that δ itself is a small quantity for large n_1 . Thus, if we consider $\epsilon \ll 1$, δ can easily take value greater than ϵ upon a single edge rewiring leading to the delocalization transition. However, if we consider $\epsilon < 1$ (Fig. 4.5(b)) or $\epsilon > 1$, we have to either remove more number of edges (nodes) from the \mathcal{W} or increases the average degree of \mathcal{R} to adjust the eigenvalue relation between the individual component ($\lambda_1^{\tilde{\mathcal{W}}} < \lambda_1^{\tilde{\mathcal{R}}}$) to witness the delocalization transition. Fig. 4.5(c) and (d) depict the behavior of $\lambda_1^{\mathcal{W}}$ and $\lambda_1^{\mathcal{R}}$ as ϵ value changes. The figures portray that before the rewiring, eigenvalue relation follows as $\lambda_1^{\mathcal{W}} > \lambda_1^{\mathcal{R}}$, and after the rewiring eigenvalue relation changes to $\lambda_1^{\tilde{\mathcal{W}}} < \lambda_1^{\tilde{\mathcal{R}}}$.

Further, we show that instead of WRR model, one can observe the single localization-delocalization transition point for the other models as well. The only condition which holds good should be that one component should have a hub node and another should be random regular such that they satisfy the eigenvalue relation ($\lambda_1^{e_1} > \lambda_1^{e_2}$). In the following, we perform the investigation by replacing \mathcal{W} with a star, friendship and scalefree graph (discussed in chapter 1), and show that regulating the largest eigenvalues of the subgraph components; one can observe the localization-

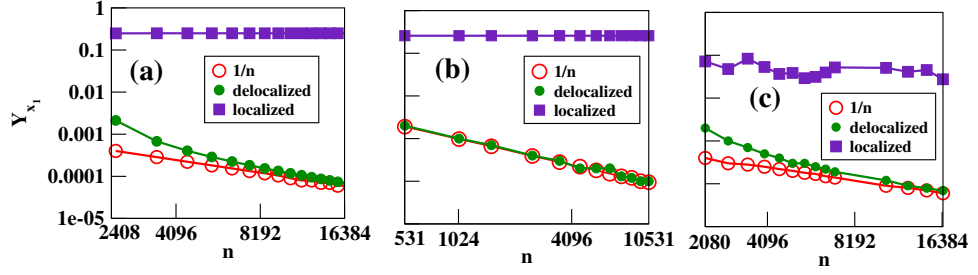


Figure 4.6: (a) IPR values of PEV (Y_{x_1}) for the star-random-regular (SRR) graph as a function of combined network size n . For each value of n , we consider two SRR graphs, first SRR graph is generate by holding $\lambda_1^s > \lambda_1^r$ and PEV is localized (■). The second SRR graph has delocalized PEV by holding $\lambda_1^s < \lambda_1^r$ (●). For reference to a delocalization, we plot $1/n$ (○) as a function of n . (b) Same as (a) but for the friendship-random-regular (FRR) networks; (c) Same as (a) but for the scalefree-random-regular (SFRR) networks.

delocalization transition for the combined network.

4.3.3 Localization transition in other graph models

As demonstrated for the WRR model, we first show that there exists a localized state of PEV for the star random regular model (\mathcal{G}_{SRR}). We consider star graph $\mathcal{S} = \{V_{\mathcal{S}}, E_{\mathcal{S}}\}$ having $|V_{\mathcal{S}}| = n_1$ number of nodes, $|E_{\mathcal{S}}| = n_1 - 1$ number of edges and $\lambda_1^s = \sqrt{n_1 - 1}$. \mathcal{G}_{SRR} is constructed by combining a \mathcal{S} and a \mathcal{R} which satisfies $\lambda_1^s > \lambda_1^r$ and leads to a large IPR value. Next, to ensure the localization of PEV in \mathcal{G}_{SRR} , we fix the average degree of \mathcal{R} and increase the number of nodes in \mathcal{R} resulting in an increase in the size of \mathcal{G}_{SRR} . However, the network keeps satisfying $\lambda_1^s > \lambda_1^r$. We observe that IPR remains fixed to a constant value as n changes (Fig. 4.6(a)) indicating localization of PEV.

Finally, we replace \mathcal{W} in the WRR model with a friendship (\mathcal{F}) and a scale-free network (\mathcal{SF}), respectively. We find that again by holding the eigenvalue relation between the two subgraph component, PEV can be made localized (Fig. 4.6(b) and (c)). Table 1 summarizes the network parameters to construct WRR, SRR, FRR, and SFRR model networks having localized PEV.

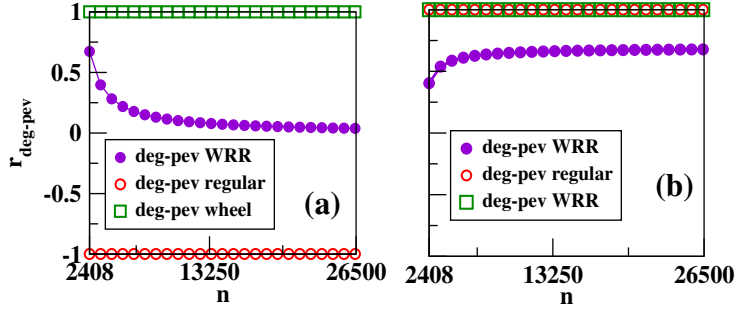


Figure 4.7: Pearson correlation between normalized degree vector and PEV of WRR (\bullet), corresponding to the random regular component of WRR (\circ) and corresponding to wheel component of WRR (\square), respectively as a function of n for (a) localized PEV state; (b) delocalized PEV state.

4.3.4 Delocalization transition in other graph models

In \mathcal{G}_{SRR} , removing an edge connected to the hub node and adding it between a pair of nodes in \mathcal{R} yields $\lambda_1^{\mathcal{S}} < \lambda_1^{\mathcal{R}}$ where $\lambda_1^{\mathcal{S}}$ and $\lambda_1^{\mathcal{R}}$ are eigenvalues of \mathcal{S} and \mathcal{R} , respectively. Upon performing one such rewiring, there exists a drastic change in the PEV entries yielding a small IPR value indicating delocalization of PEV. To ensure the occurrence of the delocalization transition in PEV, we increase the size of \mathcal{G}_{SRR} by including more number of nodes to \mathcal{R} without changing the average degree κ as in the WRR model. The eigenvalue relation for both of the components keep holding true ($\lambda_1^{\mathcal{S}} < \lambda_1^{\mathcal{R}}$) for $n \rightarrow \infty$, and the IPR value comes closer to $1/n$ which confirms the PEV delocalization [Fig. 4.6(b)]. Similarly, for the friendship-random regular and scalefree-random regular models, one can adjust the eigenvalue relation between individual components to make delocalization of PEV [Fig. 4.6(b) and (c)].

\mathcal{G}	WRR	SRR	FRR	SFRR
n_1	$n_1 > (\kappa - 1)^2$	$n_1 > \kappa^2 + 1$	$n_1 > \lceil (\kappa^2 - \frac{1}{2})^2 + \frac{3}{4} \rceil$	n_1
λ_1^{e1}	$\lambda_1^{\mathcal{W}} = 1 + \sqrt{n_1}$	$\lambda_1^{\mathcal{S}} = \sqrt{n_1 - 1}$	$\lambda_1^{\mathcal{F}} = \frac{1}{2} + \frac{1}{2}\sqrt{4n_1 - 3}$ [120]	$\lambda_1^{SF} \approx \max\{\sqrt{k_{max}}, \frac{\langle k^2 \rangle}{\langle k \rangle}\}$ [25]
λ_1^{e2}	$\lambda_1^{\mathcal{R}} = \kappa, \kappa \geq 3$	$\lambda_1^{\mathcal{R}} = \kappa, \kappa \geq 2$	$\lambda_1^{\mathcal{R}} = \kappa, \kappa \geq 2$	$\lambda_1^{\mathcal{R}} = \kappa, \kappa \geq 2$
k_{max}	$k_{max} > (\kappa - 1)^2 - 1$	$k_{max} > \kappa^2$	$k_{max} > \lceil (\kappa^2 - \frac{1}{2})^2 + \frac{3}{4} \rceil - 1$	k_{max}

Table 4.1: We portray various network parameters of wheel-random regular (WRR), stat-random regular (SRR), Friendship random regular (FRR) and scale-free random regular (SFRR) networks which provides localized PEV state.

4.4 Failure of EC measure

The model graph structure demonstrating a peculiar behavior of EC is artificially constructed; however, these investigations, helps in having a better understanding of the effects of PEV localization and delocalization in complex networks. Importantly for all the models (WRR, SRR, FRR, SFRR), there can exist the localized as well as delocalized PEV state is an interesting observation. As EC weights correspond to the PEV entries weights, the localization transition in the PEV is accompanied with assigning almost constant weights to the hub and its neighboring nodes, and very tiny weights to the rest of the nodes in the network. Therefore, it is pre-determined that in the localized environment, EC will always assign a large weight to the hub node, followed by comparatively smaller weights to all its neighboring nodes. Rest of the nodes will receive negligible weights though their degrees can be higher than those of the neighboring nodes of the hub node (Fig. 4.4(a)). Further, calculation of the Pearson correlation coefficient between the normalized degree vector (in Euclidean norm) and PEV which is denoted by $r_{deg-pev}$ reveals that for the WRR model network, having a localized PEV, degree vector and PEV are uncorrelated. Importantly, there exists a negative correlation between those degrees and the PEV entries which correspond to the random regular component of the network, and a positive correlation between the degrees and PEV entries corresponding to the wheel component. These situations arise as the nodes not connected to the hub node are unable to receive centrality weights though their degrees are large as compared to the nodes directly connected to the hub node. Consequently, it leads to the failure of EC measure for the localized PEV. Note that, to avoid the localization effect in PEV of the adjacency matrices, the PEV of non-backtracking matrices has been useful in ranking the nodes in networks [23].

Fig. 4.7(b) reflects that for the case of delocalized PEV, $r_{deg-pev}$ is high (Fig. 4.7(b)). Further, $r_{deg-pev} = 1$ if it is measured by excluding the hub node degree and the corresponding PEV entry weight. It indicates that both the degree vector and PEV is highly correlated in the network having delocalized PEV state and hence

EC is unable to recognize the wheel hub node as an important node. Our study illustrates that for such kind of core-periphery network structures (WRR, SRR, FRR, SFRR model) having delocalized PEV, it is better to use degree centrality instead of EC for measuring the centrality of the nodes as also mentioned in Refs. [107, 121].

4.5 Conclusion

The current study has focused on understanding the relationship between EC and the networks having localized-delocalized PEV in the limit of large n . By using a WRR model network, we have demonstrated that not only the localization transition of PEV can cause difficulties for EC in assigning weights to the nodes, but also the delocalization transition of PEV can also cause a problem to the EC measure. Based on numerical simulations for large size networks, we demonstrate that for PEV being localized, the size of the network imparts minor effects to the PEV entry weights corresponding to the hub and its neighboring nodes.

This work portrays that EC measures and the PEV localization have two different perspectives in which the former is used to rank the nodes and later stands as a particular phenomenon predicting difficulties associated with the EC measure. The PEV localization of network is confirmed if there exists a particular arrangement of the nodes and edges such that few entries of the PEV take very large values with rest of the entries taking tiny values, and this arrangement should hold good independent of the network size. By considering the size of the hub node and average degree fixed, we may not achieve the localized PEV as $n \rightarrow \infty$. Nevertheless, by satisfying a particular relation between the size of the hub node and the average degree of the network (Eq. (4.6)), we may achieve a network which undergoes to the localization transition as demonstrated for the model networks discussed in this chapter.

Though, the WRR model network depicts such a very typical behavior of PEV in the localized-delocalized state, which may be difficult to observe for real-world systems. However, we know that many real-world networks follow power-law degree distributions and thus contain several large degree nodes, naturally forming

imperfect wheel graph (i.e., star, friendship, etc.). Our study offers a platform to understand PEV localization behaviors of real-world systems, as well as to relate them with the network's structural properties by providing fundamental insight to localization and delocalization behavior of eigenvectors of networks [122, 123].

Finally, in the next chapter, we have extended the optimized network evolution process discussed in chapter 2 for the multilayer networks and analyze the network properties.

4.6 Appendix: Wheel-Random-Regular model

Our aim is to interpret PEV and largest eigenvalue of $\mathcal{G} \equiv \mathcal{G}_{WRR}$ in terms of PEV and largest eigenvalue of \mathcal{W} and \mathcal{R} component and find a relation between them. We connect a wheel network (\mathcal{W}) with an edge to a random regular network (\mathcal{R}) such that $\lambda_1^{\mathcal{W}} > \lambda_1^{\mathcal{R}}$ holds true. Hence, from Eq. (4.4 a), $n_1 > (\kappa - 1)^2$, which indicates that for a fixed κ , we can choose a n_1 and we have no restriction on n_2 . Therefore, we get a combined graph \mathcal{G} and the corresponding adjacency matrix ($\mathbf{A} \in \mathbb{R}^{n \times n}$ such that $n = n_1 + n_2$) as follows

$$\mathbf{A}\mathbf{x}_1 = \lambda_1^{\mathcal{G}}\mathbf{x}_1$$

$$\begin{bmatrix} \mathcal{W}_{n_1 \times n_1} & \mathcal{P}_{n_1 \times n_2} \\ \mathcal{P}_{n_2 \times n_1}^T & \mathcal{R}_{n_2 \times n_2} \end{bmatrix} \begin{bmatrix} \mathbf{x}_{1n_1 \times 1}^1 \\ \mathbf{x}_{1n_2 \times 1}^2 \end{bmatrix} = \lambda_1^{\mathcal{G}} \begin{bmatrix} \mathbf{x}_{1n_1 \times 1}^1 \\ \mathbf{x}_{1n_2 \times 1}^2 \end{bmatrix}$$

where \mathcal{P} matrix contains only single one. Hence, we have

$$\mathcal{W}\mathbf{x}_1^1 + \mathcal{P}\mathbf{x}_1^2 = \lambda_1^{\mathcal{G}}\mathbf{x}_1^1$$

$$\mathcal{P}^T\mathbf{x}_1^1 + \mathcal{R}\mathbf{x}_1^2 = \lambda_1^{\mathcal{G}}\mathbf{x}_1^2$$

where $\mathbf{x}_1^1 \in \mathbb{R}^{n_1}$ is the upper part and $\mathbf{x}_1^2 \in \mathbb{R}^{n_2}$ is the lower part of PEV ($\mathbf{x}_1 \in \mathbb{R}^n$) of \mathbf{A} . Moreover $\mathcal{W} \in \mathbb{R}^{n_1 \times n_1}$ and $\mathcal{R} \in \mathbb{R}^{n_2 \times n_2}$ are real symmetric matrices. Hence, eigenvectors of \mathcal{W} , $\{\mathbf{v}_1^{\mathcal{W}}, \mathbf{v}_2^{\mathcal{W}}, \dots, \mathbf{v}_{n_1}^{\mathcal{W}}\}$ are orthonormal and form a basis for the n_1 dimensional real vector space. Similarly, eigenvectors of \mathcal{R} , $\{\mathbf{v}_1^{\mathcal{R}}, \mathbf{v}_2^{\mathcal{R}}, \dots, \mathbf{v}_{n_2}^{\mathcal{R}}\}$ are orthonormal and form a basis for the n_2 dimensional real vector space. Therefore, we can represent \mathbf{x}_1^1 and \mathbf{x}_1^2 as a linear combinations of the eigenvectors of \mathcal{W} and \mathcal{R} as follows,

$$\mathbf{x}_1^1 = \sum_{i=1}^{n_1} c_i \mathbf{v}_i^{\mathcal{W}} \quad \text{and} \quad \mathbf{x}_1^2 = \sum_{i=1}^{n_2} d_i \mathbf{v}_i^{\mathcal{R}} \quad (4.8)$$

where $c_i \in \mathbb{R}$ and $d_i \in \mathbb{R}$ are the scalar quantity respectively. In Eq. (4.8), multiplying both sides by $\mathbf{v}_1^{\mathcal{W}T}$ and $\mathbf{v}_1^{\mathcal{R}T}$ we get,

$$c_1 = \mathbf{v}_1^{\mathcal{W}T} \mathbf{x}_1^1 \quad \text{and} \quad d_1 = \mathbf{v}_1^{\mathcal{R}T} \mathbf{x}_1^2 \quad (4.9)$$

Now, substitute Eq. (4.8) in Eq. (4.7) and we get

$$\mathcal{W} \sum_{i=1}^{n_1} c_i \mathbf{v}_i^{\mathcal{W}} + \mathcal{P} \mathbf{x}_1^2 = \lambda_1^{\mathcal{G}} \sum_{i=1}^{n_1} c_i \mathbf{v}_i^{\mathcal{W}}$$

[replace $\mathcal{W} \mathbf{v}_i^{\mathcal{W}}$ with $\lambda_i^{\mathcal{W}} \mathbf{v}_i^{\mathcal{W}}$ and multiply both sides by $\mathbf{v}_1^{\mathcal{W}T}$ we get]

$$\lambda_1^{\mathcal{W}} + \frac{1}{c_1} \mathbf{v}_1^{\mathcal{W}T} \mathcal{P} \mathbf{x}_1^2 = \lambda_1^{\mathcal{G}}$$

[as $\|\mathbf{v}_i^{\mathcal{W}}\|_2^2 = 1$ and $\mathbf{v}_i^{\mathcal{W}} \perp \mathbf{v}_j^{\mathcal{W}}, \forall i \neq j$]

$$(4.10)$$

Similarly, from the second equation in (4.7) we get,

$$\lambda_1^{\mathcal{R}} + \frac{1}{d_1} \mathbf{v}_1^{\mathcal{R}T} \mathcal{P}^T \mathbf{x}_1^1 = \lambda_1^{\mathcal{G}} \quad (4.11)$$

Hence, from Eqs. (4.10) and (4.11) we get,

$$\begin{aligned} \lambda_1^{\mathcal{W}} + \frac{1}{c_1} \mathbf{v}_1^{\mathcal{W}T} \mathcal{P} \mathbf{x}_1^2 &= \lambda_1^{\mathcal{R}} + \frac{1}{d_1} \mathbf{v}_1^{\mathcal{R}T} \mathcal{P}^T \mathbf{x}_1^1 \\ \lambda_1^{\mathcal{W}} - \lambda_1^{\mathcal{R}} &= \frac{1}{d_1} \mathbf{v}_1^{\mathcal{R}T} \mathcal{P}^T \mathbf{x}_1^1 - \frac{1}{c_1} \mathbf{v}_1^{\mathcal{W}T} \mathcal{P} \mathbf{x}_1^2 \end{aligned} \quad (4.12)$$

Further, we know

$$\lambda_1^{\mathcal{W}} > \lambda_1^{\mathcal{R}} \quad (4.13)$$

We substitute Eq. (4.9) in Eq. (4.12) and get,

$$\begin{aligned} \frac{1}{d_1} \mathbf{v}_1^{\mathcal{R}T} \mathcal{P}^T \mathbf{x}_1^1 &> \frac{1}{c_1} \mathbf{v}_1^{\mathcal{W}T} \mathcal{P} \mathbf{x}_1^2 \\ \frac{c_1}{d_1} &> \frac{\mathbf{v}_1^{\mathcal{W}T} \mathcal{P} \mathbf{x}_1^2}{\mathbf{v}_1^{\mathcal{R}T} \mathcal{P}^T \mathbf{x}_1^1} \\ \frac{\mathbf{v}_1^{\mathcal{W}T} \mathbf{x}_1^1}{\mathbf{v}_1^{\mathcal{R}T} \mathbf{x}_1^2} &> \frac{\mathbf{v}_1^{\mathcal{W}T} \mathcal{P} \mathbf{x}_1^2}{\mathbf{v}_1^{\mathcal{R}T} \mathcal{P}^T \mathbf{x}_1^1} \\ \frac{\frac{1}{\beta} (x_1^1)_1 + \frac{\alpha}{\beta} \sum_{i=2}^{n_1} (x_1^1)_i}{\frac{1}{\sqrt{n_2}} \sum_{i=1}^{n_2} (x_1^2)_i} &> \frac{\frac{\alpha}{\beta} (x_1^2)_1}{\frac{1}{\sqrt{n_2}} (x_1^1)_{n_1}} \\ \frac{(n_1 - 1)(x_1^1)_1 (x_1^1)_{n_1} + (\sqrt{n_1} + 1)(x_1^1)_{n_1} \sum_{i=2}^{n_1} (x_1^1)_i}{(\sqrt{n_1} + 1)(x_1^2)_1 \sum_{i=1}^{n_2} (x_1^2)_i} &> 1 \end{aligned} \quad (4.14)$$

where $\mathbf{v}_1^{\mathcal{W}} = \left(\frac{1}{\beta}, \frac{\alpha}{\beta}, \dots, \frac{\alpha}{\beta} \right)$ such that $\alpha = \frac{\sqrt{n_1+1}}{n_1-1}$, $\beta = \sqrt{1 + \frac{(\sqrt{n_1+1})^2}{n_1-1}}$ [78] and $\mathbf{v}_1^{\mathcal{R}} = \left(\frac{1}{\sqrt{n_2}}, \frac{1}{\sqrt{n_2}}, \dots, \frac{1}{\sqrt{n_2}} \right)$, respectively.

From Eq. (4.14), one can say that holding the relation $\lambda_1^{\mathcal{W}} > \lambda_1^{\mathcal{R}}$, PEV of the combined network for which maximum contribution comes from the wheel graph

part. Even if we vary $n_2 \rightarrow \infty$, the above relation holds true due to the Perron-Frobenius theorem that all the PEV entries should receive positive quantity.

Chapter 5

Extension to the multilayer networks

5.1 Introduction

The traditional monolayer network framework offers only a limited representation of complex systems having different layers of interactions. Recent years have witnessed emergence of the multilayer network (MN) framework, which provides more accurate insights into the behaviors of complex systems possessing multiple types of relations among the same units [32–41]. For example, the collective behavior of a society, which is modeled by individuals interacting through the Facebook and Twitter social networks, can be better understood by considering a MN consisting of layers representing the network of people in each social media. The interactions within a layer (intra-layer connection) encode friendship relationships between the pairs of two people within each social media. Whereas the interactions between the layers (inter-layer connection) represent the impact of interactions in one layer on the other; for example, two people actively interacting by Facebook may lead to an increase in their Twitter activities as well [33]. Another example of a real-world system which inherently has multiple types of relations is the brain. In the brain

MN, one layer corresponds to a physical network, and another to a functional relationship among neurons [124]. Furthermore, the physical layer can also itself a MN in the synaptic level. Neurons can be connected by chemical or electric synapses forming a brain MN [125, 126].

Furthermore, interactions among the constituents of a system provide a backbone for the sustenance of the dynamical behavior or functionality of the entire system. For instance, in the Facebook-Twitter MN, information propagates through the links in the individual layer and spread of information propagation depends on the architecture of the underlying network. Neurons in the brain interact to perform specific functions. Reconfiguration or rewiring of functional brain networks is required during the learning phases [127, 128]. Therefore scrutiny of network architecture is thus important as ‘structure affects function’ and vice-versa [2].

The last 20 years have witnessed the development of methods and techniques to characterize various structural properties and functional activities of networks representing complex systems. Particularly, it has been reported that the eigenvector corresponding to the largest eigenvalue, the so-called PEV of the network’s adjacency matrices, provides information about both the structural and dynamical properties of the underlying systems [4, 5, 9, 25, 92, 129]. For various dynamical processes on networks, for instance, disease-spreading, the steady-state vector has been approximated using PEV of the adjacency matrix [4, 129]. To understand how an individual entity is infected or how information spreads in a network in the steady-state, it is sometimes enough to analyze the PEV of the corresponding adjacency matrices. The behavior of the disease spreading in the SIS model has been investigated with the help of PEV localization revealing its connection with various structural properties of the underlying monolayer networks [4, 23, 92, 123]. The localization of an eigenvector refers to a state where few components of the vector take very high values, and the rest of the components take very small values. We quantify the localization of an eigenvector using the inverse participation ratio (IPR) [4] (see also Eq. (5.1)). Moretti et al. used PEV localization of the corresponding adjacency matrix to analyze the brain network dynamics [11]. Recently,

Arruda et al. extended the PEV localization concepts for MNs [73] and identified that the PEV localization behaviors for MNs could be different from the monolayer networks. Specifically, in the monolayer networks, localization can happen on a few nodes [4] whereas in MNs, a layer can be localized [73]. These investigations shed light on the properties of the networks and their relations with eigenvectors, particularly PEV. However, it remains unclear what specific structural properties the MNs should have so that they make the corresponding PEV localized. Additionally, how the network structure of an individual layer affects or regulates the PEV localization of the entire MN? What role other layers of a MN play in restricting the impact on the regulating layers. Specifically, the question which we address here using the optimization technique is that what structural properties an individual layer should possess so that they correspond to a highly localized PEV of the entire MN.

We organize the chapter as follows: Section 5.2 describes the notations and definitions used in the following discussion. Besides, section 5.3 contains a brief explanation of the optimization procedure used in multilayer networks. Section 5.4 illustrates different numerical results for single-layer and both-layer rewiring protocols and exhibits the emergence of network properties during the optimization process. Additionally, it contains results of the localization behavior of large scale real-world multilayer networks. Finally, in section 5.5, we summarize the current study.

5.2 Background

First, we represent a MN, $\mathcal{M} = (\mathcal{G}, \mathcal{C})$ [34], where $\mathcal{G} = \{\mathcal{L}_\alpha; \alpha \in \{1, 2, \dots, l\}\}$ is the family of connected monolayer network $\mathcal{L}_\alpha = \{V_\alpha, E_\alpha\}$, where $V_\alpha = \{v_1^\alpha, v_2^\alpha, \dots, v_n^\alpha\}$ is the set of vertices and $E_\alpha = \{e_1^\alpha, e_2^\alpha, \dots, e_{r(\alpha)}^\alpha : e_{r(\alpha)}^\alpha = (v_i^\alpha, v_j^\alpha)\} \subseteq U_\alpha$ is the set of edges in the α layer of the MN. We define the universal set $U_\alpha = V_\alpha \times V_\alpha = \{(v_i^\alpha, v_j^\alpha) : v_i^\alpha, v_j^\alpha \in V_\alpha \text{ and } i \neq j\}$ which contains all possible unordered pairs of vertices excluding the self-loops and the complementary set can be defined as $E_\alpha^c = U_\alpha - E_\alpha = \{(v_i^\alpha, v_j^\alpha) : (v_i^\alpha, v_j^\alpha) \in U_\alpha \text{ and } (v_i^\alpha, v_j^\alpha) \notin E_\alpha\}$ i.e., $E_\alpha \cap E_\alpha^c = \emptyset$ and $E_\alpha \cup E_\alpha^c = U_\alpha$. In addition, $\mathcal{C} = \{E_{\alpha\beta} \subseteq V_\alpha \times V_\beta : \alpha, \beta \in \{1, 2, \dots, l\}, \alpha \neq \beta\}$ is

the set of edges between \mathcal{L}_α and \mathcal{L}_β layers. We refer E_α as the set of all intra-layer edges and $E_{\alpha\beta} = \{e_1^{\alpha\beta}, e_2^{\alpha\beta}, \dots, e_n^{\alpha\beta}\}$ as the set of all inter-layer edges of \mathcal{M} . Here, we consider each node in one layer connected to its mirror node in the other layers of the MN, and all the layers consist of exactly the same number of nodes.

Second, we denote the adjacency matrices corresponding to \mathcal{L}_α as $\mathbf{A}^\alpha \in \mathbb{R}^{n \times n}$ which can be defined as $(a^\alpha)_{ij} = 1$, if $v_i^\alpha \sim v_j^\alpha$ and 0 otherwise. We represent degree of a node v_i^α as $k_{v_i^\alpha} = \sum_{j=1}^{n_\alpha} (a^\alpha)_{ij}$ and the average degree of α layer as $\langle k_\alpha \rangle = \frac{1}{n_\alpha} \sum_{i=1}^{n_\alpha} k_{v_i^\alpha}$. The average degree of the MN is denoted as $\langle k \rangle = 1 + \frac{\sum_{\alpha=1}^l \langle k_\alpha \rangle}{l}$. For all the model MNs, each layer has the same average degree and the same number of nodes. However, there is no such restriction on the average degree and nodes for the real-world multilayer networks. Here, we consider two layers MN with $\mathcal{L}_1 = \{V_1, E_1\}$ and $\mathcal{L}_2 = \{V_2, E_2\}$, where $|V_1| = |V_2| = n$, $|E_1| = m_1$, $|E_2| = m_2$, $|E_1^c| = \frac{n(n-1)}{2} - m_1$, $|E_2^c| = \frac{n(n-1)}{2} - m_2$ and $|E_{12}| = n$. Hence, the total number of nodes in \mathcal{M} is $|V| = 2n = N$ and edges $|E| = m_1 + m_2 + n = M$. The supra-adjacency matrix [34] of the MN is a block matrix and can be defined as:

$$\mathbf{A} = \begin{bmatrix} \mathbf{A}^1 & \mathbf{I} \\ \mathbf{I} & \mathbf{A}^2 \end{bmatrix}$$

where \mathbf{I} is an $n \times n$ identity matrix. As \mathbf{A}^1 , \mathbf{A}^2 and \mathbf{A} are real symmetric matrices, each has real eigenvalues. In addition, the networks are connected. Hence, we know from the Perron-Frobenius theorem [26] that all the entries in the PEV of \mathbf{A} are positive. We calculate the IPR of the MN [4] as follows:

$$Y_{\mathbf{x}_k^{\mathcal{M}}} = \sum_{i=1}^N (x_k)_i^4 \quad (5.1)$$

where $(x_k)_i$ is the i th component of the orthonormal eigenvector, \mathbf{x}_k , with $1 \leq k \leq N$, of the MN. A delocalized eigenvector with component $[1/\sqrt{N}, 1/\sqrt{N}, \dots, 1/\sqrt{N}]$ has the IPR value $1/N$, whereas the most localized eigenvector with components $[1, 0, \dots, 0]$ yields an IPR value equal to 1. For a connected MN, IPR value of the PEV lies between $1/N \leq Y_{\mathbf{x}_1^{\mathcal{M}}} < 1$.

In addition, to assess the contribution of an individual layer to the IPR value of PEV of the MN, we define,

$$Y_{\mathbf{x}_1^{\mathcal{M}}} = C_{\mathbf{x}_1^{\mathcal{L}_1}} + C_{\mathbf{x}_1^{\mathcal{L}_2}} \quad (5.2)$$

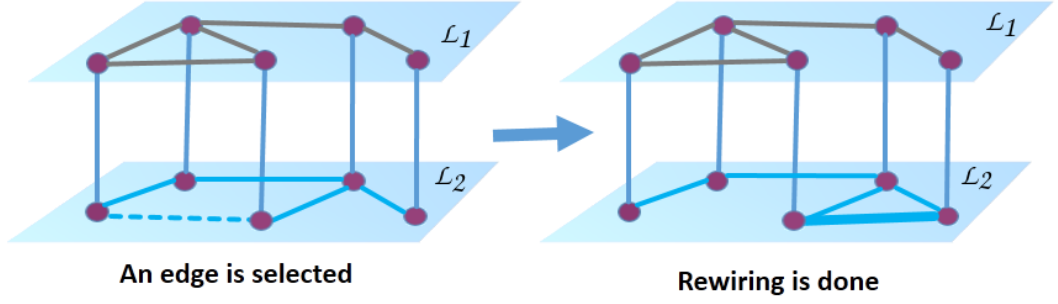


Figure 5.1: Schematic representation of the evolution of a multilayer network using the single-layer optimized edge rewiring scheme. A rewiring is accepted if it increases the IPR value of PEV of the multilayer networks.

$$Y_{x_1^M} = \underbrace{(x_1^1)^4 + (x_1^2)^4 + \dots + (x_1^n)^4}_{\mathcal{L}_1} + \underbrace{(x_1^{n+1})^4 + (x_1^{n+2})^4 + \dots + (x_1^{2n})^4}_{\mathcal{L}_2}$$

where $(x_1^1)_i$ and $(x_1^2)_j$ are the i th and j th entry in the PEV of MN from the \mathcal{L}_1 and \mathcal{L}_2 layers respectively. Note that contribution from the individual layers in the IPR value of the PEV of the entire MN (represented by $C_{x_1^{\mathcal{L}_1}}$ & $C_{x_1^{\mathcal{L}_2}}$) and the IPR value of the PEV of layers as monolayer networks (represented by $Y_{x_1^{\mathcal{L}_1}}$ & $Y_{x_1^{\mathcal{L}_2}}$) are different.

5.3 Methods

Starting from a connected two layers MN with each layer constructed from an Erdős-Rényi (ER) random network, we rewire the edges uniformly at random with an optimization-based method. Only those edge rewirings are approved, which lead to an increase in the IPR value (Fig. 5.1). We are interested in assessing various properties of the MNs during the network evolution and of those networks which have highly localized PEV, i.e., the optimized MNs.

We first examine the impact of the optimized rewiring for the two layers MN, with both-layers and single-layer rewiring protocols, and then apply the rewiring scheme to the MNs consisting of three and four layers. For a two layers MN, the optimization process can be implemented considering two different edge rewiring protocols; (1) by rewiring edges in both-layers or (2) by rewiring edges in only one (accessible) layer. For the single-layer rewiring protocol, we choose an edge $e_i^1 \in E_1$ uniformly at random from \mathcal{L}_1 and remove it (Fig. 5.1). At the same time,

we introduce an edge in the \mathcal{L}_1 layer from E_1^c , which preserves the total number of edges during the network evolution in \mathcal{L}_1 and also in \mathcal{M} . Similarly, for the both-layers rewiring protocol, we choose a layer uniformly at random from \mathcal{M} and follow the same approach as adopted for the single-layer rewiring protocol for the selected layer. Note that for both the rewiring protocols, we do not rewire any edges in E_{12} . We remark that during the network evolution there is a possibility that an edge rewiring disconnects the corresponding layer, i.e., leads to the layer having isolated nodes which are connected only through inter-layer connections without having any intra-layer connection. To avoid this situation, we only approve those rewirings which yield the nodes in a layer connected. Further, evolution takes place in a manner that keeps the network size fixed.

The optimization problem can be defined as: Given an input MN \mathcal{M} with N vertices, M edges and a function $\zeta : \mathbb{R}^N \rightarrow \mathbb{R}$, we want to compute the maximum possible value of an objective function $\zeta(\mathbf{x}_1^{\mathcal{M}})$ over all the simple, connected, and undirected MN \mathcal{M} . Thus, we maximize the objective function, $\zeta(\mathbf{x}_1^{\mathcal{M}}) = Y_{\mathbf{x}_1^{\mathcal{M}}}$ subject to the constraints that $\sum_{i=1}^N (x_1)_i^2 = 1$ and $0 < (x_1)_i < 1$. The first constraint simply says that the PEV of \mathbf{A} is normalized to the Euclidean norm. The second constraint implicitly stipulates that the network must be connected in the optimization method. In our numerical simulation, we keep the layers, as well as the MN, connected using Depth-first search method [83]. We perform the optimization process by applying simulated annealing method [130]. We refer the initial network as \mathcal{M}_{init} and the optimized network as \mathcal{M}_{opt} .

5.4 Results and Discussion

We begin the investigation by analyzing the impact of changes in the architecture of the individual layers on the PEV localization of the entire MNs. For the layers in an MN, we consider various combinations of ER random network, Barabási-Albert scale-free (SF) network, star network (STAR), and regular lattice (or regular network) network and denoted as 1D [28]. The ER random network is generated with an edge probability $\langle k_\alpha \rangle / n_\alpha$, where $\langle k_\alpha \rangle$ is the average degree of the \mathcal{L}_α layer.

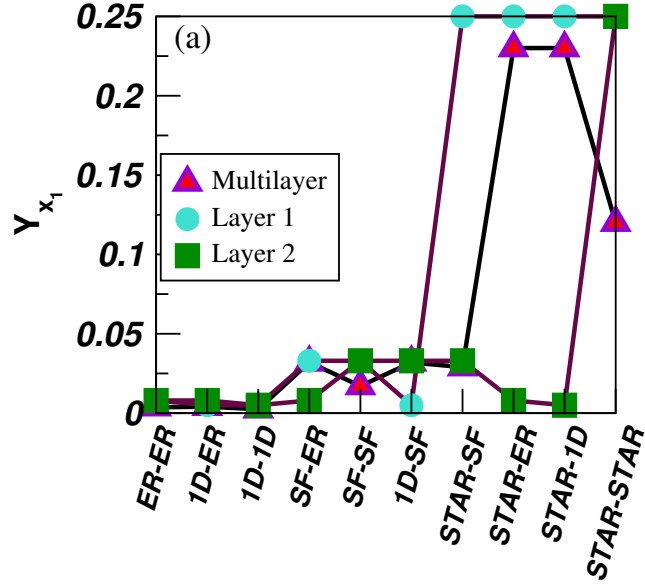


Figure 5.2: IPR value of monolayer and multilayer model networks for different combinations. The size of the monolayer networks; $n_1 = n_2 = 200$ and $\langle k_1 \rangle = \langle k_2 \rangle = 10$. Thus, size and the average degree of the MN is $N = 400$ and $\langle k \rangle = 11$ respectively.

The SF network is constructed using Barabási-Albert preferential attachment model [28].

5.4.1 Localization of model multilayer network

After multilayering of two monolayer networks, we conjecture that the IPR value of the entire MN is smaller than the maximum IPR value of the individual layers for the same number of nodes.

$$Y_{\mathbf{x}_1^{\mathcal{M}}} < \max_{1 \leq \alpha \leq l} \{Y_{\mathbf{x}_1^{\mathcal{L}\alpha}}\} \quad (5.3)$$

For the few combinations, multilayering may yield a high $Y_{\mathbf{x}_1^{\mathcal{M}}}$ value and for the few combinations, the multilayering can lead to a low $Y_{\mathbf{x}_1^{\mathcal{M}}}$ value (Fig. 5.2) however, the Eq. (5.3) always holds. For example, the STAR-ER and STAR-1D MNs have higher IPR values as compared to other multilayer configurations investigated here (Fig. 5.2). For the regular monolayer network (Theorem 6 [26]), we have

$$\mathbf{x}_1^{\mathcal{L}\alpha} = \left(\frac{1}{\sqrt{n}}, \frac{1}{\sqrt{n}}, \dots, \frac{1}{\sqrt{n}} \right)$$

Therefore, from Eq. (5.1) we get $Y_{\mathbf{x}_1^{\mathcal{L}\alpha}} = \frac{1}{n}$ which corresponds to the most delocalized PEV for a network size n . Next, for a star monolayer network consisting of n

nodes with the hub node being labeled as 1, we get the PEV as

$$\mathbf{x}_1^{\mathcal{L}\alpha} = \left(\frac{1}{\sqrt{2}}, \frac{1}{\sqrt{2(n-1)}}, \dots, \frac{1}{\sqrt{2(n-1)}} \right)$$

which yields,

$$Y_{\mathbf{x}_1^{\mathcal{L}\alpha}} = \frac{1}{4} + \frac{1}{4(n-1)}$$

For $n \rightarrow \infty$, $Y_{\mathbf{x}_1^{\mathcal{L}\alpha}} \rightarrow \frac{1}{4} \approx 0.25$. Upon multilayering two 1D monolayer networks of size n and node degree $\langle k_1 \rangle = \langle k_2 \rangle = r$, the degree of each node of MN gets increased by one yielding the same degree to each node of the MN as $(r+1)$. Thus, 1D-1D MN network becomes regular network of $\langle k \rangle = r+1$ and $2n$ number of nodes. Therefore, PEV of the 1D-1D MN will be

$$\mathbf{x}_1^{\mathcal{M}} = \left(\frac{1}{\sqrt{2n}}, \frac{1}{\sqrt{2n}}, \dots, \frac{1}{\sqrt{2n}} \right) \text{ and } Y_{\mathbf{x}_1^{\mathcal{M}}} = \frac{1}{2n} \quad (5.4)$$

resulting in the same contribution of each layer which is calculated from Eq. (5.2)

as $C_{\mathbf{x}_1^{\mathcal{L}1}} = C_{\mathbf{x}_1^{\mathcal{L}2}} = \frac{1}{4n}$, and $Y_{\mathbf{x}_1^{\mathcal{L}1}} = Y_{\mathbf{x}_1^{\mathcal{L}2}} = \frac{1}{n}$ from Eq. (5.1), respectively. Therefore, both the layers contribute equally to the IPR value of the MN and the IPR value of the overall MN decreases by a factor of $1/2$ for 1D-1D MN configurations. The ER random network has a delocalized PEV for large n [79], therefore, again multilayering of two ER random networks brings upon the same contribution from both the layers in $Y_{\mathbf{x}_1^{\mathcal{M}}}$.

Next, if we consider STAR-1D or STAR-ER MN, the contribution $C_{\mathbf{x}_1^{\mathcal{L}2}}$ becomes very small as compared to $C_{\mathbf{x}_1^{\mathcal{L}1}}$. In these cases, 99.99% of the contribution comes from the layer which has the STAR network for $n \rightarrow \infty$. For STAR-ER case, the PEV entry corresponding to the hub node of the STAR network has a significantly high value. On the contrary, ER random network has a delocalized PEV. After multilayering, PEV of the STAR-ER MN contains one very large entry which in combination with other tiny entries lead to a significantly high IPR value. However, for the case of STAR-STAR MN, the presence of two hub nodes leads to a decrease in the IPR value of \mathcal{M} (Fig. 5.2). Similarly, for SF-ER and SF-SF networks, the presence of several hub nodes reduces the IPR value of \mathcal{M} . Following Eqs. (5.3) and (5.4) we get a bound for the IPR value of MNs having the same number of nodes in all the layer,

$$\frac{1}{2n} \leq Y_{\mathbf{x}_1^{\mathcal{M}}} < \max\{Y_{\mathbf{x}_1^{\mathcal{L}1}}, Y_{\mathbf{x}_1^{\mathcal{L}2}}\}$$

In general, for l layers MNs, we get

$$\frac{1}{nl} \leq Y_{\mathbf{x}_1^{\mathcal{M}}} < \max_{1 \leq \alpha \leq l} \{Y_{\mathbf{x}_1^{\mathcal{L}_\alpha}}\}$$

It is not surprising that multilayering of a delocalized monolayer network with a localized monolayer network structure leads to a higher IPR value of the MN as compared to multilayering with a delocalized monolayer network ($Y_{\mathbf{x}_1^{ER-STAR}} > Y_{\mathbf{x}_1^{ER-ER}}$). Additionally, it is also possible that multilayering of a localized monolayer network with another localized monolayer network (e.g., STAR-STAR) yields an IPR value which is lower than that of the localized & delocalized (e.g., STAR-ER) multilayer network combinations (Fig. 5.2). These experiments demonstrate that PEV localization of a multilayer network can be regulated by changing topological properties of one or both of its layers.

5.4.2 Layer rewiring based on simulated annealing

From the above experiments, we already have obtained an idea of the structural properties of an individual layer corresponding to a localized PEV state as well as how by choosing an appropriate multilayering one can make the PEV of the entire MN more localized. These investigations have been carried out for a few specific network structures representing each layer of the MNs. In the following, we aim to address the issue of the PEV localization for MN, having a general network architecture representing each layer. Particularly, we investigate that starting with an initial random MN, how an optimized rewiring of one or more than one layer, can build a MN having a highly localized PEV. Additionally, we investigate various structural and spectral properties of the rewired layers and those of the entire MN during the optimized evolution process at various rewiring stages.

It can be noticed that from an initial ER-ER random MN, the optimized rewiring for both-layers, as well as for the single-layer significantly increase the IPR value (Fig. 5.3(a)) of \mathcal{M} . The choice of an ER-ER MN at the beginning of the evolution provides a delocalized PEV to start with [79]. During the network evolution, there are several changes in the structural and spectral properties of the network architecture of the rewired layer. For both the optimization protocols as evolution

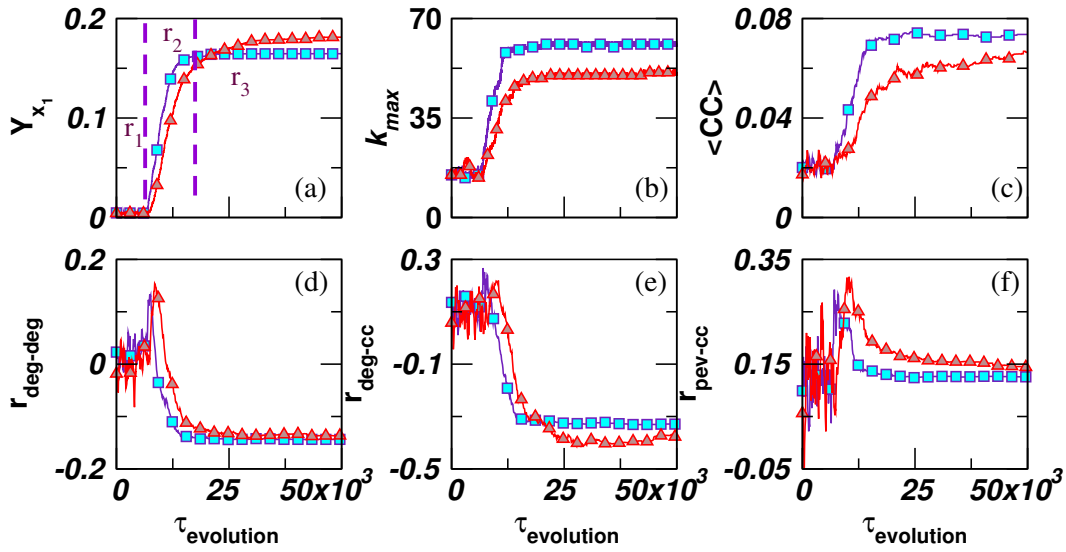


Figure 5.3: Optimized evolution of an initial ER-ER multilayer network for 50,000 edge rewirings for single-layer (■) and both-layers (▲). Size of the MN is $N = 400$, $\langle k \rangle = 7$, and $\langle k_1 \rangle = \langle k_2 \rangle$.

progress, IPR value of the PEV shows an increase and finally becomes saturated. Based on the nature of the increment in the IPR value, we can divide the evolution into three different regions, the slow (r_1), the fast (r_2), and the saturation (r_3) regions respectively (Fig. 5.3(a)).

5.4.3 Network properties during network evolution

As evolution progresses, there is a formation of the hub node (Fig. 5.3(b)) and IPR value of the PEV shows an increase which finally becomes saturated in \mathcal{M}_{opt} . This evolution process leads to a drastic change in the degree distribution of the final MN (Fig. 5.4). There exists one node in the MN coming from the smaller part of the network (Fig. 5.5) which has a very high degree as it is connected with all the nodes in that part of the network. Rest of the nodes in this part of the network has very small degrees. The other part of the layer, which does not consist the hub node, has all the nodes having degree again very small but different than those lying in the smaller part. This leads to two distinguishable peaks in the degree distribution of the optimized MN (Fig. 5.4). Note that instead of random initial MN, if we start with a MN having both the layers having SF topology, the final optimized

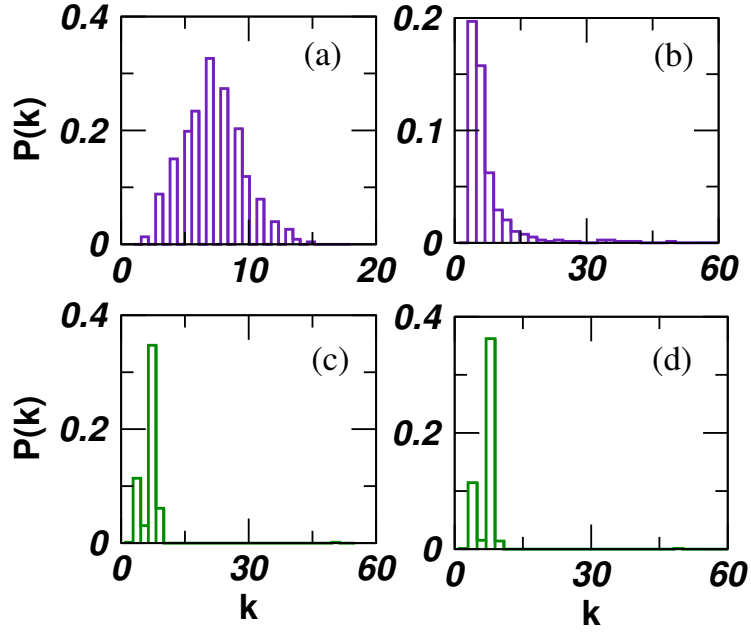


Figure 5.4: Degree distribution of the initial multilayer network of (a) ER-ER ($N = 400$, $\langle k_1 \rangle = \langle k_2 \rangle = 6$) and (b) SF-SF ($N = 400$, $\langle k_1 \rangle = \langle k_2 \rangle = 6$). (c) and (d) depict the degree distribution of the optimized MN achieved through the both-layers rewiring protocol.

network will be same as achieved for the initial MN having a random structure. We have plotted degree distribution of the final optimized MNs as well as those of the initial networks (Fig. 5.4). It is interesting to note that, despite the scalefree (SF) networks being more localized than the corresponding ER random networks, if we evolve a SF-SF MN using the optimization technique, the degree sequence of the final optimized structure will be the same to that achieved for optimizing the ER-ER MNs.

Additionally, \mathcal{M}_{opt} has a higher average clustering coefficient ($\langle CC \rangle$) value (Fig. 5.3(c)) and low degree-degree correlation ($r_{deg-deg}$) value (Fig. 5.3(d)) as compared to those of \mathcal{M}_{init} [28]. It indicates that localization of the PEV leads to the triangle formation in the MN structure. Similarly, the existence of a lower degree-degree correlation suggests that hub nodes are connected with lower degree nodes in individual layer leading to the MN with highly localized PEV being disassortative.

Furthermore, to check the relation between the degree and local clustering co-

efficient of each node as PEV gets localized, we calculate the Pearson product-moment correlation coefficient [28] measure of degree vector and local clustering coefficient vector (r_{deg-cc}) during the optimization process. It unveils that as evolution progresses the r_{deg-cc} value decreases (Fig. 5.3(e)) which indicates that as the PEV gets localized, the participation of lower degree nodes is more to the cluster formation than the higher degree nodes. We measure the Pearson product-moment correlation coefficient between pairs of various other structural properties to accomplish a better understanding of the network structures. It is surprising to see that r_{pev-cc} value increases (Fig. 5.3(f)) as compared to \mathcal{M}_{init} as PEV gets localized. From the r_{deg-cc} and r_{pev-cc} values, we can also infer the correlation between degree vector and PEV ($r_{deg-pev}$) which decreases as PEV gets more localized. From these correlation measures, it is evident that lower degree nodes contribute more to the triangle formation and also contributing more to the PEV entry of the \mathcal{M}_{opt} . These correlation measures provide insight for possible architectures of the \mathcal{M}_{opt} structure corresponding to highly localized PEV. Note that $\langle CC \rangle$ and all the correlation measures are evaluated for the entire MN.

5.4.4 Revealing optimized multilayer structure and sensitivity in PEV

Network visualization software reveals that the optimized layer consists of two components which are connected with each other via a single node (Fig. 5.5). One of the components in this structure contains a hub node. For both-layers rewiring protocol, we get a network structure in which one layer is similar to that obtained for the monolayer network rewiring [92]. However, another layer has a network structure consisting of two components of different sizes devoiding of the hub node (Fig. 5.5(a)). Various structural properties of \mathcal{M}_{opt} obtained through the single-layer rewiring protocol (Fig. 5.5(b)) is qualitatively the same as that observed for the rewiring of the monolayer networks. However, for the both-layers and single-layer rewiring protocols, there is a striking (Fig. 5.6(a-b)) difference in the spectral properties in the saturation region, r_3 . In this region, there exist several edges, rewiring which do not lead to an increase in the IPR value. If we consider rewiring

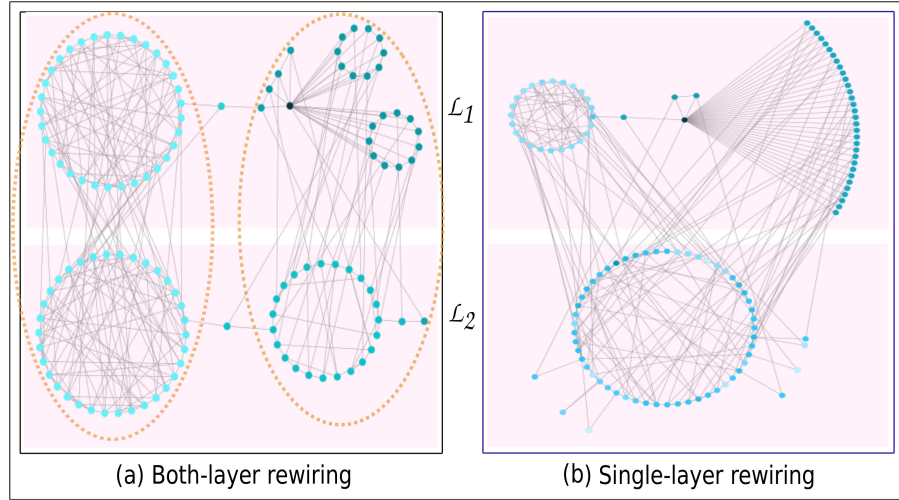


Figure 5.5: Cytoscape diagram of optimized MN obtained for (a) both-layers and (b) single-layer rewirings. For both the protocols, $N = 120$ and $\langle k \rangle = 3$, where $\langle k_1 \rangle = \langle k_2 \rangle$. A smaller size MN is considered here for a clear illustration of the optimized network structure.

of all the edges during each step of the evolution, we can notice a substantial difference between both vs. single layer rewiring protocols of the MNs. In the r_3 region (Fig. 5.6), the IPR value gets almost saturated, and there may exist only a subtle increment in the IPR value with a further evolution of the network. Although the MN in this region has the maximum IPR value, in the \mathcal{M}_{opt} achieved through the both-layers rewiring protocol there exist only a few edges, for which rewiring leads to a sudden drop in the IPR value. It leads to a complete delocalization of the PEV from a highly localized state (Fig. 5.6(b)). Thus, for both-layers rewiring, the PEV in the r_3 region is sensitive to a single edge rewiring as also observed for the monolayer network rewiring [92]. However, for the \mathcal{M}_{opt} in the r_3 region achieved through the single-layer rewiring protocol, there are no such sudden drops (Fig. 5.6(a)) and PEV is robust to a single edge rewiring. For the single-layer rewiring, the component consisting of the hub node (in the rewired layer) has a major contribution to the IPR value of the PEV of the MN, followed by the contribution from the fixed layer and the second component of the rewired layer connected to the hub-component (Fig. 5.5(b)). Similarly, for the case of both-layers rewiring, the hub-component contributes the most, followed by the contribution from the other parts of \mathcal{M}_{opt}

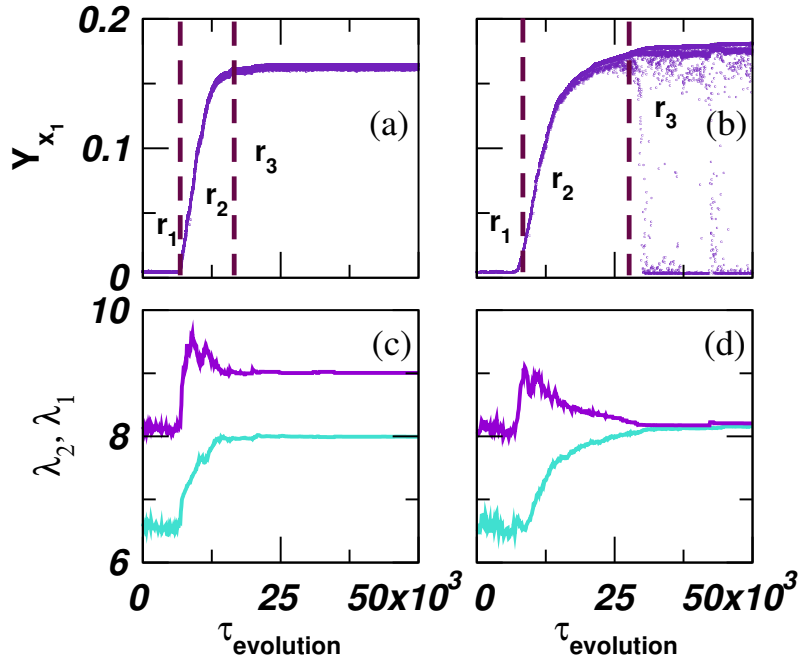


Figure 5.6: Changes in the IPR values (Y_{x_1}) with the evolution. (a) Single-layer rewiring protocol (PI) does not show IPR drops in the saturation region. (b) Both-layers rewiring protocol (PII) shows drops in the IPR value in the saturation region. (c) The behavior of the largest two eigenvalues of the single-layer and (d) both-layer rewiring protocols. Here, $N = 400$, $\langle k \rangle = 7$, and $\langle k_1 \rangle = \langle k_2 \rangle$.

(Fig. 5.5(a)). The component containing the hub node has an overwhelming contribution in the corresponding PEV entries accompanied by an equally negligible contribution from the rest of the nodes leading to a high IPR value in the optimized structure.

Next, we attempt to understand the sensitivity of the PEV in the critical region (r_3) for the both-layers rewiring protocol and in the absence of the same in the single-layer protocol. We can witness that for the case of single-layer rewiring, during the evolution of λ_1 and λ_2 , both show an increase and remain separated to each other (Fig. 5.6(c)). However, for the both-layers rewiring protocol, as evolution progresses, λ_2 starts shifting towards λ_1 , (Fig. 5.6(d)) as a consequence of λ_2 drifting away from the bulk region [55, 56]. This drift in λ_2 is not surprising as we know that the final optimized structure obtained from the both-layers rewiring consists of two parts in both-layers of \mathcal{M}_{opt} . We can observe from Fig. 5.5(a) that there exist two communities (surrounded by a dotted ellipse) such that for each community one

part resides in \mathcal{L}_1 layer and another part of the community belongs to \mathcal{L}_2 layer of the MN. Hence, there should be two eigenvalues which lie outside the bulk. However, the interesting observation is that for the \mathcal{M}_{opt} obtained from the both-layers rewiring, λ_2 not only drifts away from the bulk but becomes very close to λ_1 , in fact, $\lambda_1 \sim \lambda_2$. Almost the same value for both the eigenvalues might be a reason behind the sensitivity of the PEV [92] for the both-layers rewiring. Note that, for the single-layer rewiring protocol (Fig. 5.5(b)) it is hard to get two communities as one layer is fixed which prohibits λ_2 being separated from the bulk. Hence, there is no possibility of λ_2 being close to λ_1 , which is always well separated from the bulk of the sparse networks.

5.4.5 Impact of layer rewiring

For various combinations of the layer forming the MN (Fig. 5.7)(a)), for the single-layer rewiring protocol, the fixed layer restricts the IPR value of the entire MN. In Fig. 5.7(b), we depict the values of $C_{x_1^{\mathcal{L}_1}}$ and $C_{x_1^{\mathcal{L}_2}}$ of $Y_{x_1^{\mathcal{M}}}$ during the network evolution for the initial MN having ER-ER and ER-SF configurations. For the ER-ER MNs, the layer which undergoes rewiring associates more weight to the PEV entries on the expense of that of the contributions from the fixed layer (Fig. 5.7(b)). Both of these factors lead to a high value of $Y_{x_1^{\mathcal{M}}}$. For ER-SF MNs considered as initial networks, we observe that rewiring of the ER random layer through the optimized evolution is not sufficient to change the IPR value of PEV which is reflected by almost a constant value of $C_{x_1^{\mathcal{L}_1}}$ and $C_{x_1^{\mathcal{L}_2}}$ (Fig. 5.7(b)). This constant value of IPR is a consequence of the existence of the hub nodes in the fixed SF layer which imposes a restriction on the increase in $Y_{x_1^{\mathcal{M}}}$. However, for the combination of SF-ER MN, rewiring of the SF layer leads to an enhancement in the $Y_{x_1^{\mathcal{M}}}$ value (Fig. 5.7)(a)).

We can see that during the evolution (Fig. 5.7(b)), though one layer is fixed and rewiring is performed on the other layer, changes happen in both $C_{x_1^{\mathcal{L}_1}}$ and $C_{x_1^{\mathcal{L}_2}}$ leading to an increase in the $Y_{x_1^{\mathcal{M}}}$ value. This is a direct consequence of the multilayering of the layers indicating that by rewiring ('dynamics of the networks') one can change the value of the PEV entries, i.e. 'dynamics on networks' [124]. In

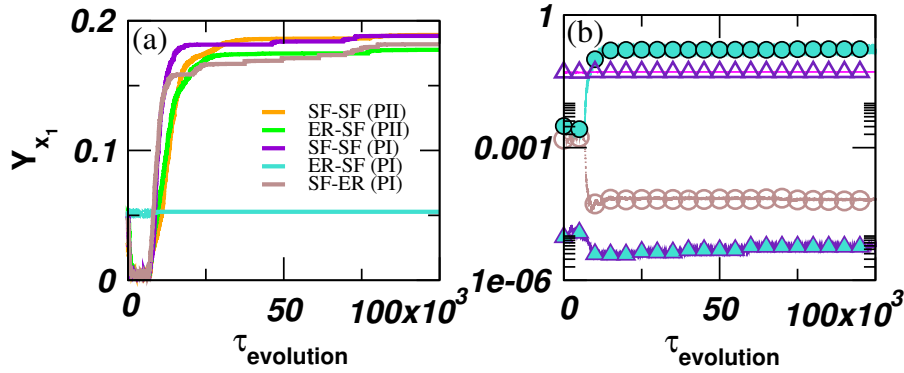


Figure 5.7: (a) Change in the IPR value during the evolution of MNs with various combinations of the initial networks for single-layer rewiring protocol (PI) and both-layer rewiring protocol (PII). (b) Value of $C_{x_1^{\mathcal{L}_1}}$ and $C_{x_1^{\mathcal{L}_2}}$ as two layers are multilayered and evolved. The initial multilayer network takes two different combinations; ER-ER and ER-SF with $N = 400$, $\langle k \rangle = 7$, and $\langle k_1 \rangle = \langle k_2 \rangle$. The rewiring has been done in the first layer (i.e., ER layer). The contribution of the rewired ER layer is represented by $C_{x_1^{\mathcal{L}_1}}$. (●) and (▲) represents this contribution for ER-ER, and ER-SF multiplex networks, respectively. Similarly, the fixed layer contribution ($C_{x_1^{\mathcal{L}_2}}$) for ER-ER and ER-SF multiplex network is depicted by (○) and (△), respectively.

other words, our framework is useful in connecting ‘dynamics on’ and ‘dynamics of’ networks for MNs in terms of the PEV localization.

Furthermore, we present the results for three layers and four layers MNs (Fig. 5.8). Starting with the three and four layers initial random MNs, we evolve them using the optimization technique as described above. Again, the optimized rewiring leads to an increase in the IPR value of the MN during the evolution (Fig. 5.8) with the existence of r_1 , r_2 and r_3 regions. For the three layer MNs, we can adopt the rewiring protocol in various manners, (i) rewiring only one layer by fixing other layers, (ii) rewire two layers and fix one layer, (iii) rewire all the layers independently. All the three ways of the rewiring yield the network properties similar to those obtained for the two layers MN in the optimized state.

5.4.6 Localization in real-world multilayer networks

Furthermore, we examine the PEV localization of many real-world MNs. We find that the real-world MNs have the PEV which is much more localized than the corresponding random MNs, however, much less localized than the optimized multilayer

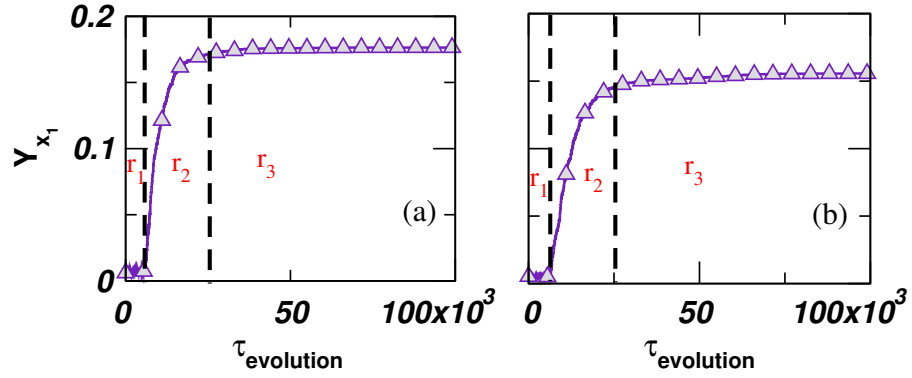


Figure 5.8: The IPR value ($Y_{x_1}^{\mathcal{M}}$) of (a) three layers and (b) four layers MN. The simulation is performed for (a) three and (b) four layers rewiring protocols. Each layer of \mathcal{M} contains 100 nodes and $\langle k_\alpha \rangle = 5$.

structure. We present results for MN of the Twitter data collected during the occurrence of different exceptional events like the discovery of Higgs boson in 2012, Cannes Film Festival, the 14th IAAF World Championships in Athletics held in Moscow 2013, Martin Luther King’s famous public speech celebrating 50 years “I have a dream” in 2013, official visit of US President Barak Obama in Israel in 2013 [132], a large-scale event on global climate change in New York in 2014. The choice of the Twitter network data provides a good proxy for the large population of the social behaviors [132]. The individual layers of the Twitter MN follow the power-law degree distribution and reflect scale-free topology. In addition to these social networks, we consider biological MNs as well. The multilayer gene-interaction networks, *Drosophila* and *Homo-genetic* [134–136] consist of layers denoting the physical association, direct interaction, colocalization, and association respectively. We make crude approximations that all the networks are undirected and unweighted. Table 5.1 presents PEV localization and structural properties of these MNs. All the networks have IPR value much larger than the corresponding random networks.

We can estimate the IPR value of a random MN consisting of layers of size N/l represented by ER random network as $Y_{x_1}^{\mathcal{M}} \approx 3/N$ [52]. Other structural properties of such random MN can be calculated as $\langle CC \rangle \approx \frac{\langle k \rangle}{N}$, and $r_{deg-deg} \approx 0$ for large N [28]. The real-world multilayer networks considered here comprise of structural properties which differ considerably from the corresponding random MNs. From

Network	l	N	$\langle k \rangle$	$Y_{\mathbf{x}_1}$	k_{max}	$\langle CC \rangle$	$r_{deg-deg}$	λ_1	λ_2	$r_{pev-deg}$	r_{pev-cc}
Moscow Athl.	3	124423	4.01	0.03	4840	0.11	-0.13	75.22	71.5	0.66	0.05
NYClimate	3	148936	5.39	0.07	9742	0.11	-0.1	118.5	99.2	0.65	0.08
MLKing2013	3	318962	2.51	0.08	8689	0.07	-0.11	93.2	85.5	0.25	0.01
Cannes2013	3	573353	3.98	0.2	8676	0.1	-0.1	94.26	86.9	0.38	0.004
Higgs mux	2	886744	31.09	0.003	51387	0.09	-0.1	653.5	436.7	0.71	-0.15
Obamaisrael	3	2258678	3.55	0.15	21650	0.1	0.0	151.77	139.9	0.43	0.02
CKM	3	329	5.95	0.02	25	0.16	0.1	7.84	5.75	0.78	-0.17
<i>Drosophila</i>	4	10255	7.62	0.008	175	0.11	0.1	46.96	31.0	0.6	-0.27
<i>Homo</i>	4	34363	10.22	0.09	9570	0.19	-0.05	118.76	67.2	0.7	0.09
<i>Arabidopsis</i>	4	8163	4.45	0.24	1296	0.1	-0.1	36.28	23.03	0.6	-0.02
<i>HumanHIV1</i>	2	1138	2.48	0.24	250	0.01	-0.45	15.87	14.93	0.5	-0.05
<i>Celegans-conn</i>	3	791	9.74	0.025	82	0.18	0.11	21.18	13.53	0.8	0.1
<i>Mus</i>	4	9657	4.22	0.03	368	0.09	-0.16	34.56	24.57	0.46	0.05
<i>Plasmodium</i>	3	1161	4.15	0.03	83	0.03	0.0	13.12	8.75	0.8	0.13
<i>Rattus</i>	4	2906	2.98	0.23	814	0.14	-0.14	29.16	14.14	0.74	-0.17
<i>SacchCere</i>	4	20482	17.37	0.02	3187	0.22	-0.1	110.81	70.51	0.65	0.1
<i>SacchPomb</i>	4	6401	8.62	0.06	1021	0.17	-0.14	47.95	36.62	0.57	0.12

Table 5.1: Various properties of real-world social (first seven) and biological (last ten) multilayer networks. Inverse participation ratio ($Y_{\mathbf{x}_1}$), maximum degree (k_{max}), average clustering coefficient ($\langle CC \rangle$), degree-degree correlation ($r_{deg-deg}$), PEV-degree correlation ($r_{pev-deg}$), PEV-cc correlation (r_{pev-cc}), the largest eigenvalue (λ_1), and the second-largest eigenvalue (λ_2) of few real-world MNs. Ref. [131] is used to calculate IPR and eigenvalues of MNs having large network size. The IPR values of the corresponding random networks are very close to $3/N$, which is predicted by the random matrix theory [52]. First, six networks with l layers are constructed based on the Twitter data with different exceptional events ranging from sports, politics to scientific discovery of Higgs boson. The layers represent retweet, reply, and mention on twitter [132] network. The CKM is a multilayer social network of a sample of physicians in US [133]. The *Drosophila* and *Homo* are the multilayer genetic and protein interaction networks where layers are the physical association, direct interaction, colocalization, association respectively [134–136]. The rest of the networks are also multilayer genetic and protein interaction networks, where we consider only the first four layers when the number of layers is more. We consider the largest connected component to calculate various properties and treat all the edges undirected and unweighted. Moreover, we measure the clustering coefficient value for all the nodes of the multiplex network having degree 2 or more, as nodes with degree 1 have zero clustering coefficient.

Table 5.1, it is clear that all the real-world multilayer networks considered here contain a hub node having a very large degree. Additionally, they have higher average clustering coefficient value ($\langle CC \rangle$) and smaller degree-degree correlation than the corresponding random networks. Additionally, PEV of these MNs is more localized than the corresponding random MN. From the Table 5.1, it is evident that the less localized networks possess high $r_{pev-deg}$ value, and for most of the real-world MN the r_{pev-cc} value is positive. Although these are not very surprising observations, by combining the comparison of measures of various structural properties and IPR values of the real MNs with those of the model MNs achieved during the optimized

evolution process, it is evident that real-world MNs lie well above the r_1 region. Furthermore, Table 5.1 depicts that the largest and the second largest eigenvalue of the real-world MNs are well separated from each other, indicating that these real-world MN lie below the r_3 region. Note that in the r_3 region, the largest and the second-largest eigenvalues lie very close to each other, leading to the sensitivity of the IPR value of the PEV to single edge rewiring. Based on these two sets of observations, we can fairly conclude that the real-world multilayer networks lie in the r_2 region of the evolution process of the model multilayer networks.

5.5 Conclusion

In this chapter, we explore the impact of the optimized rewiring for the PEV localization in MNs. We construct MN structures through an optimization process that yields highly localized PEV quantified by the IPR value. Our approach provides a comprehensive way to investigate not only the properties of the optimized multilayer structure but also the intermediate multilayer networks before the most optimized structure is found. In other words, we develop a learning framework to explore the evolution of the eigenvector from a delocalized to a highly localized state. We analyze several structural and spectral properties during the network evolution process for the single-layer as well as all the layers of the MNs. For both the protocols, we find that there is an emergence of various structural features as PEV gets localized. Moreover, for both the protocols, there is a noticeable difference present in the spectral properties in the saturation region. For both-layers rewiring protocol, in the saturation region, PEV is sensitive to a single edge rewiring as also observed for the optimized evolution of the monolayer networks. However, interestingly, we get rid of the sensitivity in the PEV in the saturation region by implementing a single-layer rewiring of the MN. Additionally, we have investigated the PEV localization behavior of several large empirical MNs constructed using the data ranging from social to biological systems. Our analysis reveals that these real-world MNs are much more localized than the corresponding random MNs, and also have structural properties close to those obtained in the r_2 region of the optimized

evolution process of the model MNs. Further, we show that by rewiring a single-layer, one can tune the contribution of the node weights of the other layer to the PEV of the entire MN. Rearrangement of the node weights used in semi-supervised based learning and has great practical importance in machine learning [137]. The study is relevant to confine or facilitate the propagation of perturbation in a network by an appropriate multilayering with other networks.

Chapter 6

Conclusion and future scope

6.1 Conclusion

In this dissertation, we focus on understanding the structural as well as spectral properties of the networks through localizing PEV associated with the adjacency matrices. We study monolayer and multilayer network properties which enhance the localization behavior of PEV. In particular, we have developed a novel framework based on optimization techniques to find out PEV localized network structure. In other words, we develop a learning framework to explore the localization of PEV through a sampling-based optimization method. We reveal that optimized structure possesses a distinctive architecture. It consists of two subgraph components of different sizes. Further, scrutinizing the structural and spectral properties of the optimized network structure demonstrates that highly localized PEV is closely related to the closeness of the largest two eigenvalues and the presence of a hub node. Finally, we develop an analytical formulation based on the eigenvalue relation of the subgraphs component, which assists in constructing the PEVs localized network and avoid the optimization techniques. In the following, chapter wise, we

summarize our works.

- Chapter 2 mainly concentrates on the numerical investigation to find network properties leading to high localization of PEV through the optimized network evolution process. Starting from an initial random network, we achieve a network structure through a Monte Carlo based optimization method. The optimized network possesses a highly localized PEV quantified by the IPR value. We analyze various structural and spectral properties of the optimized network as well as the networks at the intermediate state before the optimized structure is reached. We demonstrate that PEV localization is not a consequence of a single network property and rather requires the collective impact of several structural features. The final optimized network possesses a special structure and which we have shown to be robust against changes in the initial network structure. We demonstrate the robustness of the results by considering various popular models as well as real-world networks as an initial network structure. Our analysis identifies a particular set of edges which are essential for the localization of PEV in the optimized network structure. Rewiring any one edge of this set leads to a complete delocalization of PEV in the optimized network structure, and we referred to as sensitivity in PEV. We observe that this emergence of sensitivity in the PEV and shifting of λ_2 close to λ_1 happens simultaneously suggesting a relation between the particular structure of the optimized network and the second largest eigenvalue.
- Chapter 3, reveals that the eigenvalue crossing along with the presence of a hub node is the prime reason behind the sensitivity of the PEV in the optimized network. We found that a single edge rewiring in the optimized network structure leads to an eigenvalue crossing, which is detected through the dot product of the two largest eigenvectors. We show that the eigenvalue crossing leads to a change in the eigenvalue relation of the individual components and which in turn, governs the sensitivity of the PEV localization. From the observation of the eigenvalue crossing phenomenon, we derive an analyt-

ical formulation for the direct construction of a PEV localized network structure through a wheel and random regular network. Importantly, this structure is obtained without performing an optimization scheme. In other words, we use the information of spectral properties of the optimized network to perform reverse engineering to construct a network structure having a highly localized PEV. Finally, we observe that the eigenvalue crossing phenomenon on the RNA neutral network population dynamical model due to a single edge rewiring on the wheel-random regular (WRR) network structure.

- In chapter 4, by using the wheel-random-regular model network, we have demonstrated that not only the localization transition of PEV can cause difficulties for EC in assigning weights to the nodes, but also the delocalization transition of PEV can also cause a problem to the EC measure. Based on numerical simulations for large size networks, we demonstrate that for PEV being localized, the size of the network imparts minor effects to the PEV entry weights corresponding to the hub and its neighboring nodes. Therefore, for a localized PEV, it is predetermined that the hub node and its neighboring nodes will receive significant weights with the rest of the nodes receiving negligible weights, causing the failure of EC. Similarly, in the delocalized PEV, EC is unable to assign centrality weight to the higher degree node. As a result, EC becomes inefficient and uninformative for measuring of the centrality of the nodes when PEV is delocalized.
- Finally, in chapter 5, we extend the optimized edge rewiring method for the multilayer networks (MNs). We explore the impact of the optimized rewiring for the PEV localization in MNs. For two-layer multilayer networks, we proposed two edge rewiring protocols (i) both-layer rewiring and (ii) single-layer rewiring protocols. For both the protocols, we find that there is an emergence of various structural features as PEV gets localized. However, for both the protocols, there is a noticeable difference present in the spectral properties in the saturation region. For both-layers rewiring protocol, in the saturation

region, PEV is sensitive to a single edge rewiring as also observed for the optimized evolution of the monolayer networks. However, interestingly, we get rid of the sensitivity in the PEV in the saturation region by implementing a single-layer rewiring of the MN. Additionally, we have investigated the PEV localization behavior of several large empirical MNs constructed using the data ranging from social to biological systems. Our analysis reveals that these real-world MNs are much more localized than the corresponding random MNs. The study is relevant to confine or facilitate the propagation of perturbation in a network by an appropriate multilayering with other networks.

The prime concern of our analysis to have insights into the network structure and PEV localization, using disease spread model, we verify that network structure in the optimal and the intermediate stages spreading of disease is much slower than the initial random structure. It may not always be feasible to rewire a real-world network to such an extent to get a desired PEV localization behavior. However, the results and approach used here will be more useful in constructing an artificial network with the desired localization behavior.

On the other hand, the WRR network structure is quite special and depicts a very typical behavior of PEV in the localized-delocalized state, and which may be difficult to observe for real-world systems. However, it provides us an understanding of the localization behavior observed for the networks evolved through the optimized evolution process. Indeed, we know that many real-world networks follow power-law degree distributions and thus contain several large degree nodes, naturally forming imperfect wheel graph (i.e., star, friendship networks). Our study offers a platform to understand PEV localization behaviors of real-world systems, as well as to relate them with the network's structural properties by providing fundamental insight to localization and delocalization behavior of eigenvectors of networks [122, 123].

To conclude, our study provides a more in-depth insight into the PEV localization on synthetic as well as on empirical networks. Additionally, earlier work has

related spectral properties with a change in the matrix elements [77]; here we show that how a function of PEV relates with the change in the matrix elements.

6.2 Future scope

- The optimized edge rewiring method developed here may be useful for optimizing other structural and spectral properties of the network (e.g., eigenvalues, IPR of other eigenvectors). The algorithm can be easily extended to the different functions and on a broader class of matrices.

The present work mainly focuses on connected, unweighted, and undirected networks (i.e., irreducible binary symmetric matrices). However, our framework can easily be extended to obtain a comprehensive picture of PEV localization on directed networks (non-negative asymmetric matrices). Furthermore, this thesis is restricted to PEV of adjacency matrices or steady-state behavior of linear-dynamical processes associated with adjacency matrices. However, how did the systems attain the steady-state? i.e., the transient behavior of the systems can be analyzed through the non-principal eigenvectors and eigenvalues of the adjacency matrix [58]. Hence, it is also important to understand the emergence of network properties and their relation with the localization behavior of other eigenvectors.

Furthermore, as eigenvectors and eigenvalues provide information for energy controllability and synchronization of complex networks [10, 32], the investigation carried out here for PEV of adjacency matrix can be extended for finding localization of eigenvector for other matrix representations of networks. For instance, Laplacian [138–140], and Jacobian [141] matrices which are closely related with coupled nonlinear dynamical evolution on networks. Another important matrix which is associated with the dynamical processes is the Hessian matrix [142, 143]. However, the connection between the Hessian matrix and the network is not clear [144]. It might be useful to understand the connection between the adjacency matrix associated with a network and the Hessian matrix to analyze the localization behavior of the eigenvectors of the

Hessian matrix from the perspective of networks.

- For directed networks associated with Markov chains, maximal entropy random walk or Google matrix the corresponding matrix becomes non-negative and asymmetric [90, 145, 146]. Hence, the matrix may have left and right eigenvector as well as eigenvalues becomes complex. The PEV for the above models are probability vectors (i.e. in l_1 norm) and needs some normalization to the IPR values. We calculate the IPR of the PEV [4, 92] as follows:

$$Y_{\mathbf{x}_1} = \frac{\sum_{i=1}^n (x_1)_i^4}{\left[\sum_{i=1}^n (x_1)_i^2 \right]^2} \quad (6.1)$$

where $(x_i)_j$ is the j th component of \mathbf{x}_i and $\|\mathbf{x}_1\|_1 = 1$, with $1 \leq i \leq n$. A delocalized PEV with component $(\frac{1}{n}, \frac{1}{n}, \dots, \frac{1}{n})$ has $Y_{\mathbf{x}_1} = \frac{1}{n}$, whereas the most localized PEV with components $(1, 0, \dots, 0)$ yields an IPR value equal to $Y_{\mathbf{x}_1} = 1$. Network should be strongly connected (i.e. there exists a directed path between every pair of nodes) to get positive PEV entries.

- It will be interesting to analyze motifs and nodal domains in PEV localized networks [147].
- Searching for an orthonormal basis that is “as localized as possible” is an important problem in certain physics applications [148–150]. Hence, an important question can be asked that how can we localize all the eigenvectors of a network simultaneously and learn the network properties?
- It will be interesting to optimize the structure when tuning the zeros, or negative entries of eigenvectors instead of localization of PEV. We know that for a non-negative symmetric matrices PEV entries are all positive but for other eigenvectors entries may be negative, zeros, positive or mixed of them. Here, eigenvector behavior has been regulated based on a particular function, which is IPR. It is good to define other functions which can tune the negative or zeros entries of the eigenvectors or some part of the eigenvector, and based on that; one can construct network structure. However, we have first to define a particular measure.

- We have seen that localizing PEV provides a structure which is far from the scalefree networks. However, many real-world networks follow a scalefree nature. In other words, is it possible to generate power-law degree distribution through localizing eigenvectors? Now, how can we create functions on the eigenvectors and eigenvalues such that the evolved network should follow power-law degree distribution? It will provide a new way to look into the network structure and dynamics.
- We have used edge rewiring process to achieve localized PEV without providing any restriction on the structural and spectral properties. Now, keeping degree distribution fixed how can we rewire edges of a network such that we can achieve PEV localized networks. It will be interesting to apply different rewiring protocols like 1-k, 2-k, d-k on the monolayer as well as on the multilayer networks and explore PEV localization [151].
- This framework can be extended for regulating the eigenspace of a network or even might be useful to tune the singular vector entries of a matrix [152–154].

Appendix A

6.3 Basic definitions

Positive vector and non-negative matrix: A vector $v \in \mathbb{R}^n$ is a positive vector if $v_i > 0$ for all i . A matrix A is said to be non-negative matrix if $a_{ij} \geq 0$ for all i and j [93]. Here, \mathbb{R}^n represents n dimensional real vector space.

Norms: A norm is a function $\|\cdot\| : \mathbb{C}^n \rightarrow \mathbb{R}$ that assigns a real-valued length to each vector. The most two important vector norms are 1-norm (l_1) and 2-norm (l_2) defined in the following.

$$\begin{aligned} \|\mathbf{x}\|_1 &= \sum_{i=1}^n |x_i| \\ \|\mathbf{x}\|_2 &= \left(\sum_{i=1}^n |x_i|^2 \right)^{1/2} \end{aligned} \tag{6.2}$$

The l_2 norm is the Euclidean length of a vector and l_1 norm is use in case of probability vector [93]. Here, \mathbb{C}^n stands for n dimensional vector space of complex numbers and \mathbb{R} is the one dimensional real vector space.

6.4 Results related to eigenvalues

We restate the proposition and theorem related to spectral properties from [119] as follows,

Proposition 1.3.10 If $\mathcal{G} - uv$ is the graph obtained from a connected graph \mathcal{G} by deleting the edge uv , then $\lambda_1^{\mathcal{G}-uv} < \lambda_1^{\mathcal{G}}$.

Theorem: Real symmetric matrix has real eigenvalues and all the eigenvectors are orthogonal.

Theorem: A graph is connected if and only if its largest eigenvalue is simple with a positive eigenvector.

Theorem: The number of components of a (labelled) graph \mathcal{G} is equal to the maximal number of linearly independent non-negative eigenvectors of \mathcal{G} .

6.5 Non-degenerate test of close eigenvalues

Our investigations always consider connected networks, and from the Perron-Frobenius theorem largest two eigenvalues are distinct. However, to find the gap between the largest two eigenvalues, we use Sylvester's law of inertia theorem (chapter 3, section 3.3 [155]). For a given adjacency matrix \mathbf{A} , we first calculate λ_1 and λ_2 . Now, for $(\mathbf{A} - \lambda_1\mathbf{I})$ and $(\mathbf{A} - \lambda_2\mathbf{I})$ perform the triangular factorization (\mathbf{LDL}^T) using Gauss elimination method (for single and double precision) without row exchange where \mathbf{D} contains the pivots. We count the negative pivots, and the difference is one which ensures that λ_1 and λ_2 has healthy separation (chapter 3, section 3.3 [155]). Furthermore, we use spectral slicing (bisection method) to find the bound between the two largest eigenvalues and which is 0.012 in single and double precision arithmetic which ensures that λ_1 and λ_2 are distinct (non-degenerate).

Further, to measure the working accuracy, we have found the Rayleigh quotient after calculating the eigenvector from the numerical software. The eigenvalues obtained from the numerical software and Rayleigh quotient are the same up to 12 digits after the decimal point. Further, after calculating λ_1 and λ_2 we form the system of linear homogeneous equations $[(\mathbf{A} - \lambda_1\mathbf{I})\mathbf{x}_1 = 0$ and $(\mathbf{A} - \lambda_2\mathbf{I})\mathbf{x}_2 = 0]$ and find the nullspace (through singular value decomposition) and check that dimension of the null space is one and is same as the eigenvectors obtain through the numerical software. Additionally, we checked the re-orthogonality of two largest eigenvectors. LAPACK routine in C++, with single (*ssyev*, *ssyevd*, *ssyevr*, *ssyevx*) as well as double precision (*dsyev*, *dsyevd*, *dsyevr*, *dsyevx*) arithmetic is used to calculate the results. Moreover, we have run the numerical simulation on different platforms (C++, Python, and Matlab), and all of them yields exactly the same results.

6.6 Details of optimization process

Given an undirected, unweighted connected network \mathcal{G} with n vertices, m edges and a function $\zeta : \mathbb{R}^n \rightarrow \mathbb{R}$, we compute the maximum possible value of an objective function $\zeta(\mathbf{x}_1) = \sum_{i=1}^n (x_1)_i^4$ over all the simple, connected, unweighted and undirected network \mathcal{G} . The optimization problem can be written as finding an irreducible binary symmetric matrix \mathbf{A} , for which $\sum_{i=1}^n (x_1)_i^4$ will be maximum subject to the constraint that $\sum_{i=1}^n (x_1)_i^2 = 1$ and $(x_1)_i > 0 \quad \forall i \in \{1, 2, \dots, n\}$. The first constraint simply says that \mathbf{x}_1 is in l_2 norm. The second constraint implicitly stipulates that the network must be connected (from the Perron-Frobenius theorem). The following theorem says that the optimization problem belongs to non-convex class.

Lemma 1: $\zeta(\mathbf{x}_1) = \sum_{i=1}^n (x_1)_i^4$ is a convex function when $(x_1)_i \in (0, 1)$, $i \in \{1, 2, \dots, n\}$.

Proof: Convexity of the objective function $\zeta(\mathbf{x}_1)$ can be examined by employing Hessian test [156]. One can construct the Hessian matrix from $\zeta(\mathbf{x}_1)$ and show that it is positive semidefinite. The partial derivative of $\zeta(\mathbf{x}_1)$ are given by

$$\frac{\partial \zeta(\mathbf{x}_1)}{\partial (x_1)_i} = 4(x_1)_i^3, \quad i = \{1, 2, \dots, n\} \quad (6.3)$$

and hence,

$$\frac{\partial^2 \zeta(\mathbf{x}_1)}{\partial (x_1)_i \partial (x_1)_j} = \begin{cases} 12(x_1)_i^2 & i = j \\ 0 & i \neq j \end{cases} \quad (6.4)$$

Now we can write the Hessian matrix as

$$\nabla^2 \zeta(\mathbf{x}_1) = \begin{bmatrix} 12(x_1)_1^2 & & \mathbf{0} \\ & \ddots & \\ \mathbf{0} & & 12(x_1)_n^2 \end{bmatrix}$$

Hessian matrix is positive semidefinite if all the eigenvalues of $\nabla^2 \zeta(\mathbf{x}_1)$ are non-negative. Here it is clear that eigen values of $\nabla^2 \zeta(\mathbf{x}_1)$ are $\{12(x_1)_i^2 : i = 1, 2, \dots, n\}$ as $\nabla^2 \zeta(\mathbf{x}_1)$ is a diagonal matrix. Since $(x_1)_i \in (0, 1)$, therefore all the eigenvalues of $\nabla^2 \zeta(\mathbf{x}_1)$ are nonnegative, and hence the Hessian matrix is a positive semidefinite matrix. Therefore, the objective function $\sum_{i=1}^n (x_1)_i^4$ is a convex function.

Lemma 2: $\mathcal{C} = \{\mathbf{x}_1 \in (0, 1)^n \mid \|\mathbf{x}_1\|_2^2 = 1\}$ is a non-convex set.

Proof: A set $\mathcal{C} \subseteq \mathbb{R}^n$ is called convex if for any $\mathbf{x}, \mathbf{y} \in \mathcal{C}$, $\mathbf{x} \neq \mathbf{y}$ and any $\theta \in [0, 1]$,

the point $\theta\mathbf{x} + (1 - \theta)\mathbf{y}$ belongs to \mathcal{C} [156]. To validate \mathcal{C} as a non-convex set, any arbitrary point $\mathbf{z} \in \mathbb{R}^n$ has been considered and it can be written as a convex combinations of \mathbf{x} and \mathbf{y} i.e., $\mathbf{z} = \theta\mathbf{x} + (1 - \theta)\mathbf{y}$ by choosing an arbitrary value of θ . Thus, we have

$$(z_1, z_2, \dots, z_n) = (\theta x_1 + (1 - \theta)y_1, \theta x_2 + (1 - \theta)y_2, \dots, \theta x_n + (1 - \theta)y_n) \quad (6.5)$$

From the above equation, we get,

$$\sum_{i=1}^n z_i^2 = \theta^2 + (1 - \theta)^2 + 2\theta(1 - \theta) \sum_{i=1}^n x_i y_i \quad (6.6)$$

Now, to check the convexity, one has to show that $\mathbf{z} \in \mathcal{C}$, i.e., $\sum_{i=1}^n z_i^2 = 1$. Since $\mathbf{x} \neq \mathbf{y}$, it gives $\sum_{i=1}^n x_i y_i \neq 1$. Now, for specific $\theta = 1/2$, $\sum_{i=1}^n z_i^2 \neq 1$, this implies that the relation $\sum_{i=1}^n z_i^2 = 1$ does not satisfy for any arbitrary value of θ . Hence, $\mathbf{z} \notin \mathcal{C}$ and therefore, \mathcal{C} is a non-convex set.

Theorem: Considering $\sum_{i=1}^n (x_i)^4$ as an objective function, principal eigenvector localization over undirected unweighted connected network is a non-convex optimization problem.

Proof: It is notable from Lemma 1 that the objective function $\sum_{i=1}^n (x_i)^4$ is a convex function but on the other hand, Lemma 2, says that the constraint, $\mathcal{C} = \{\mathbf{x}_1 \in (0, 1)^n \mid \|\mathbf{x}_1\|_2^2 = 1\}$ is a non-convex set. By definition, a convex optimization problems consist of minimizing of a convex functions over convex sets, or maximizing a concave functions over convex sets [156]. Jointly, conflicting characteristic of constraint and objective function shows that the principal eigenvector localization over simple undirected unweighted and connected network is a non-convex optimization problem.

The above theorem indicates that we can not find a simple undirected and unweighted connected network with most localized PEV by using a convex optimization method. To get an adjacency matrix corresponds to highly localized PEV, we have borrowed the evolution of networks with edge rewiring and used optimization on top of that. We use Monte Carlo (MC) and simulated annealing (SA) based randomized optimized edge rewiring method.

Before going to discuss about the network evolution method we start with a star

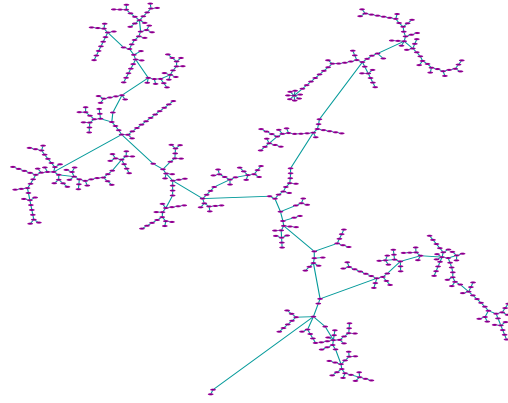


Figure 6.1: An initial star network structure having $Y_{\mathbf{x}_1}^s \approx 0.25$. However, optimized edge rewiring process leads to a network structure having $Y_{\mathbf{x}_1} \approx 0.267$ and network structure is substantially different than star network structure. Here, $n = 500$ nodes and $m = 499$ edges.

network. If we consider a star network with n nodes labelled as $\{1, 2, \dots, n\}$ with the hub node being labelled with 1, then using eigenvalue equation corresponding to λ_1 , we get $\mathbf{x}_1 = \left(\frac{1}{\sqrt{2}}, \frac{1}{\sqrt{2(n-1)}}, \dots, \frac{1}{\sqrt{2(n-1)}} \right)$ and hence, $Y_{\mathbf{x}_1}^s = \frac{1}{4} + \frac{1}{4(n-1)}$. Therefore, when $n \rightarrow \infty$, we get $Y_{\mathbf{x}_1}^s \rightarrow \frac{1}{4} \approx 0.25$. By looking the IPR of PEV, we can think that star network has the most localized PEV. However, we show that optimized network evolution method provides larger IPR value than the star networks and architecture is also significantly different (Fig. 6.1). In the following, we discuss both of the methods used in our thesis.

6.6.1 Monte Carlo based algorithm

The Monte-Carlo (MC) based optimization (in algorithm 1) can be summarized as follows. We find \mathbf{x}_1 of an initial ER random graph \mathcal{G} and calculate the IPR value of \mathbf{x}_1 . We rewire one edge uniformly at random in \mathcal{G} to obtain another graph \mathcal{G}' . We check whether \mathcal{G}' is connected, if not the edge rewiring step is repeated till we get another \mathcal{G}' which is a connected network. We find the PEV of \mathbf{A}' matrix and calculate the IPR value of \mathbf{x}'_1 . We replace \mathbf{A} with \mathbf{A}' , if $Y_{\mathbf{x}'_1} > Y_{\mathbf{x}_1}$. Steps from third to twelve are repeated until IPR value gets saturated which corresponds to the optimized network. The recorded value of $Y_{\mathbf{x}_1}$ variable during the optimization process

Algorithm 1: MC-based-IPR-Optimization($n, \langle k \rangle$)

```

1   $\mathbf{A} \leftarrow \mathcal{G}(n, p)$ 
2   $Y_{x_1} \leftarrow \sum_{i=1}^n (x_1)_i^4$ 
3  while  $Y_{x_1}$  not saturated do
4      rewire an edge uniformly at random in  $\mathcal{G}$  and denotes it as  $\mathcal{G}'$ 
5      if  $\mathcal{G}'$  is not connected then goto step 4
6       $Y_{x'_1} \leftarrow \sum_{i=1}^n (x'_1)_i^4$ 
7      if  $Y_{x'_1} > Y_{x_1}$  then
8           $\mathbf{A} \leftarrow \mathbf{A}'$ 
9           $Y_{x_1} \leftarrow Y_{x'_1}$ 
10     end
11     store  $Y_{x_1}$  and  $\mathbf{A}'$ 
12 end

```

gives an increment in the IPR value which is depicted in Fig. 2.1(a). Instead of ER random network as initial, one can choose SF network and observe the same results. However, we observe that for a given star network structure there is a chance of failure to the MC method. Interestingly, simulated annealing based method overcome the failure and provide optimized network structure.

6.6.2 Simulated annealing based algorithm

The simulated annealing (SA) is a randomized algorithm widely used in solving optimization problem motivated from the principles of statistical mechanics [130]. It also provides global optimal value for several optimization problems. The important part of the SA-based algorithm is accepting solutions which satisfy the Gibbs-Boltzmann function $e^{-\mathcal{E}/\delta * temp}$. In our problem, we consider the objective function to be maximize instead of minimize, so we have made the changes accordingly in the algorithm. We set the initial temperature, $temp = 0.9$ and after each iteration decreases it by the cooling schedule $tem = tem * 0.98$ and also fix the Boltzmann constant δ to 100. We have seen that these parameters are precise and works well.

The simulated-annealing (SA) based optimization (in algorithm 1) can be summarized as follows. If $Y_{x'_1} > Y_{x_1}$, \mathbf{A} is replaced with \mathbf{A}' for the next evolution step. On the otherhand, if $Y_{x'_1} < Y_{x_1}$, we choose a random number from the uniform

Algorithm 2: SA-based-IPR-Optimization($n, \langle k \rangle, temp, \delta$)

```

1   $\mathbf{A} \leftarrow \mathcal{G}(n, p)$ 
2   $Y_{x_1} \leftarrow \sum_{i=1}^n (x_1)_i^4$ 
3   $temp = 0.9$ 
4  while  $Y_{x_1}$  not saturated do
5      rewire an edge uniformly at random in  $\mathcal{G}$  and denotes it as  $\mathcal{G}'$ 
6      if  $\mathcal{G}'$  is not connected then goto step 5
7       $Y_{x'_1} \leftarrow \sum_{i=1}^n (x'_1)_i^4$ 
8      if  $Y_{x'_1} > Y_{x_1}$  then
9           $\mathbf{A} \leftarrow \mathbf{A}'$ 
10          $Y_{x_1} \leftarrow Y_{x'_1}$ 
11     end
12     else
13         pick a random number  $r$  from uniform distribution in  $(0,1)$ 
14         if  $r < e^{-\frac{(Y_{x'_1} - Y_{x_1})}{(\delta * temp)}}$  then
15              $\mathbf{A} \leftarrow \mathbf{A}'$ 
16              $Y_{x_1} \leftarrow Y_{x'_1}$ 
17         end
18     end
19     store  $Y_{x_1}$  and  $\mathbf{A}'$ 
20      $temp \leftarrow temp * 0.998$ 
21 end

```

distribution and if it is less than $e^{-\mathcal{E}/\delta * temp}$, we accept the bad solution otherwise we reject the solution and perform another edge rewiring on \mathbf{A} and repeat the process. This step is important to get rid of from the local maxima. The recorded value of Y_{x_1} variable during the optimization process gives an increment in the IPR value. One interesting part of the algorithms is in line 19, to store the value $Y_{x'_1}$. It stores the increment as well as the decrement in the IPR value during the network evolution. Here, we consider a star network as an initial, and the optimized structure again contains two-component graph structure (Fig. 6.1). In general, both methods provide an optimized network structure, but the SA method sometimes takes more edge rewiring steps than the MC based method. From the extensive numerical simulation, it is precise that to overcome local maxima; it is better to use SA based methods.

6.7 Structural properties during network evolution

We summarize the ensemble average results for the initial network taken as an ER random network (\mathcal{G}_{init}) and the optimized network (\mathcal{G}_{opt}) in the Table 6.1. To check the plausible correlation between the degree sequence of the final optimized network and PEV localization, we construct a network which has the same degree sequence as of the optimized network. For this purpose, we use the configuration model [31], which we denote as \mathcal{G}_{opt}^{conf} . We observe that \mathcal{G}_{opt}^{conf} has an IPR value which is much lesser than that of the \mathcal{G}_{opt} network (Table 6.1). It concludes that having a specific degree sequence is important, but is not the only factor for the PEV localization. Nevertheless, there exist other structural properties which are acquired by the evolved network during the optimization process. In the following, we discuss the impact of other structural properties on the localization of PEV.

Further, we find the clustering coefficient [28] of a node as,

$$C_i = \frac{2\Delta_i}{k_i(k_i - 1)}$$

where k_i denotes the degree of node i , and Δ_i is the number of triangles the node i is participating in. Subsequently, the average clustering coefficient [28] can be defined as,

$$\langle CC \rangle = \frac{1}{n} \sum_{i=1}^n C_i$$

During the optimization process, we keep a record of the average clustering coefficient $\langle CC \rangle$ which indicates an increase in $\langle CC \rangle$. To check a correlation between $\langle CC \rangle$ and IPR, we use an algorithm given in Ref. [84] which takes a degree sequence and average clustering coefficient as an input and creates a random network having the exactly same degree sequence and $\langle CC \rangle$ as of \mathcal{G}_{opt} . We denote the network generated using the algorithm in [84] as \mathcal{G}_{opt}^{cc} . It is interesting to observe that though \mathcal{G}_{opt} and \mathcal{G}_{opt}^{cc} have the same degree sequence and $\langle CC \rangle$, they are having different IPR value (Table 6.1). It asserts that by tuning $\langle CC \rangle$, we cannot achieve a network structure corresponding to \mathcal{G}_{opt} network.

Further, we track the degree-degree correlation coefficient ($r_{deg-deg}$) during the

evolution process. The $r_{deg-deg}$ is measured as follows [29],

$$r_{deg-deg} = \frac{[m^{-1} \sum_{i=1}^m j_i k_i] - [m^{-1} \sum_{i=1}^m \frac{1}{2}(j_i + k_i)^2]}{[m^{-1} \sum_{i=1}^m \frac{1}{2}(j_i^2 + k_i^2)] - [m^{-1} \sum_{i=1}^m \frac{1}{2}(j_i + k_i)^2]}$$

where m is the total number of edges in the network and j_i, k_i are the degrees of nodes with i^{th} connection. As a consequence of the evolution process, the $r_{deg-deg}$ of the optimized network becomes negative indicating the presence of disassortativity in the optimized network. To check how evolution of disassortativity has an impact on the enhancement in the IPR value, we use Sokolov algorithm [87] to construct a network with the same number of n, m and $r_{deg-deg}$ as in the \mathcal{G}_{opt} network and is denoted by $\mathcal{G}_{opt}^{r_{deg-deg}}$. Again IPR value of the network constructed in this manner is far from the \mathcal{G}_{opt} network (Table 6.1).

Further, we measure the correlation between the local clustering coefficient vector and PEV, using Pearson product-moment correlation coefficient [29]. We measure correlation coefficient between the degree vector and clustering coefficient (cc) vector denoted as r_{deg-cc} and the correlation between the PEV entries and the cc vector denoted as r_{pev-cc} .

$$r = \frac{\sum_{i=1}^n (x_i - \bar{x})(y_i - \bar{y})}{\sqrt{\sum_{i=1}^n (x_i - \bar{x})^2} \sqrt{\sum_{i=1}^n (y_i - \bar{y})^2}}$$

To calculate r_{deg-cc} and r_{pev-cc} , we normalize the degree vector in the Euclidean norm as in [157]. These measures provide an insight to the network structure of the most optimized network.

In chapter 2, we have discussed the results of various network properties during the evolution process with an initial network being taken as ER random network. In fact, if we separate the two components of the optimized network, these do not manifest highly localized PEV individually. However, these two components taken as \mathcal{G}_{init} separately, the evolution leads to two optimized networks which have the same structure as in (Fig. 3(right)). However, to achieve a better localized PEV, the network should be sparse. For the dense network, the evolution process does not lead to a significant increase in the IPR value. The IPR value saturates for a dense network without being appreciably different from the initial network.

Index	\mathcal{G}_{init}	\mathcal{G}_{opt}	\mathcal{G}_{opt}^{conf}	\mathcal{G}_{opt}^{cc}	$\mathcal{G}_{opt}^{r_{deg-deg}}$
n	500	500	500	500	500
$\langle k \rangle$	10	10	10	10	10
m	2499 ± 55	2499 ± 55	2499 ± 55	2499	2499
k_{max}	21 ± 2	90 ± 7	90 ± 7	100	100
λ_1	11.04 ± 0.20	11.13 ± 0.29	12.67 ± 0.46	11.36	11.60
$r_{deg-deg}$	-0.002 ± 0.02	-0.16 ± 0.005	-0.02 ± 0.005	-0.17	-0.16
Y_{x_1}	0.003 ± 0.0002	0.18 ± 0.0095	0.05 ± 0.006	0.02	0.03
$\langle CC \rangle$	0.02 ± 0.002	0.11 ± 0.01	0.02 ± 0.003	0.14	0.01

Table 6.1: Results are shown for the average over 31 realizations with 6,00,000 edge rewiring steps. \mathcal{G}_{opt} denotes the optimized network achieved through the network evolution from the initial base network being \mathcal{G}_{init} network. \mathcal{G}_{opt}^{conf} refers to the network constructed from the configuration model having the same degree sequence as of the \mathcal{G}_{opt} network. \mathcal{G}_{opt}^{cc} refers to the network constructed with the same $\langle CC \rangle$ and degree sequence as in the \mathcal{G}_{opt} network. Finally, $\mathcal{G}_{opt}^{r_{deg-deg}}$ refers to the network having the degree-degree correlation as in the \mathcal{G}_{opt} network.

6.8 Behavior of all IPR values

The appendix revolves around explaining the behavior of all the IPR and eigenvalues during the optimization process. During the evolution, by considering only those edge rewirings which perform increments in the IPR value of PEV, we observe that the localization of PEV leads to a complete delocalization of the second largest eigenvector as well as localization of the lowest eigenvector. Whereas, IPR values of rest of the eigenvectors fluctuate around almost a constant value without noticeable changes (Fig. 6.2). Further, one can observe from the eigenvalue behavior, in the r_2 region, the second largest (λ_2) and the lowest eigenvalues (λ_n) start drifting away from the bulk part of the eigenvalues, whereas rest of the eigenvalues does not show significant changes (Fig. 6.3). It is known that localization of PEV leads to a localization of the lowest eigenvector [24]; however, the behavior of the second largest eigenvector, and moreover, its relation with the PEV localization have so far not been explored. Our analysis reveals that the localization behavior of the second largest eigenvector is related to the sensitive behavior of PEV in the r_3 region. To check the robustness of our results, we have considered power-law degree distributed networks as the initial networks (Figs. 6.4, and 6.5) and find that the be-

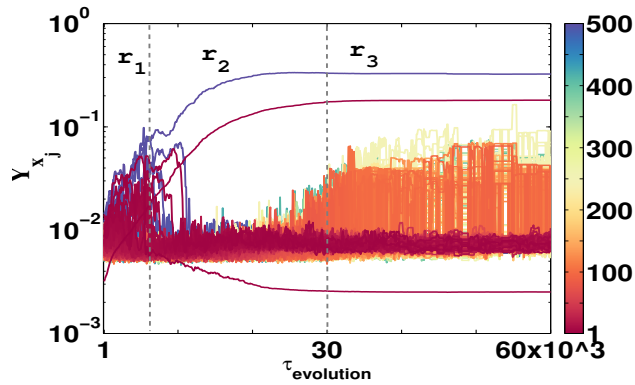


Figure 6.2: Changes in IPR values of all eigenvectors (Y_{x_j}) of ER as initial network is rewired using the scheme depicted in section 2.3. Here, only those edge rewirings in the r_3 region are allowed which lead to an increase in Y_{x_1} value. Network size $n = 500$ and $\langle k \rangle = 10$. The color scheme is generated through the code in Ref. [158].

havior of the network evolution remains the same irrespective of the type of initial network chosen.

6.9 Eigenvalues behavior of real-world networks

Next, we turn our attention to understand the localization properties of real-world networks which provides more insight into the relationship between the PEV localization and the closeness of the largest two eigenvalues. We analyze various real-world networks ranging from the social, biological to synthetic systems [134, 159, 160]. Table 6.2 presents various different properties of real-world networks, and one can see that two largest eigenvalues are close to each other, however, the PEV of such networks are delocalized (Table 6.2).

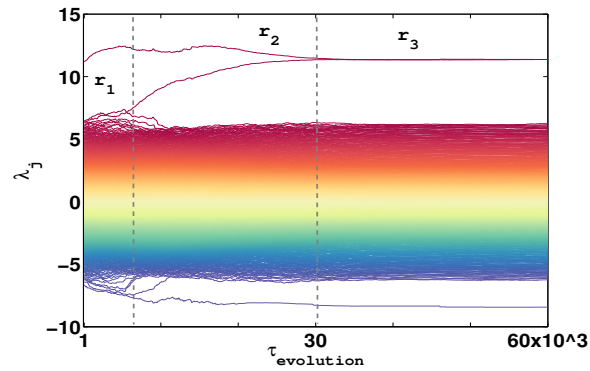


Figure 6.3: Overall behavior of all the eigenvalues during the network evolution process started from ER network. Network parameters are same as in Fig. (6.2).

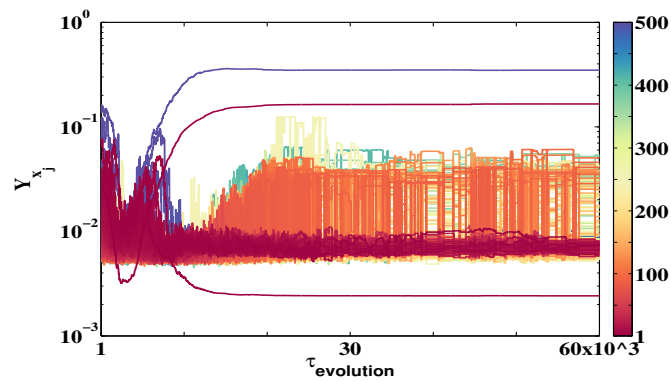


Figure 6.4: Changes in IPR values of all eigenvectors (Y_{x_j}) of SF as initial network is rewired using the scheme depicted in section 2.3. Network size $n = 500$ and $\langle k \rangle = 10$.

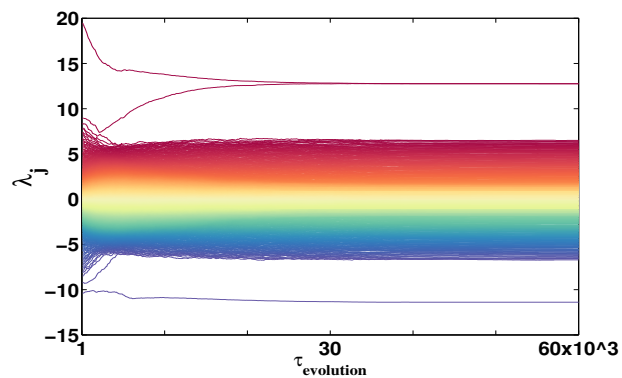


Figure 6.5: Overall behavior of all the eigenvalues during the network evolution process started from SF network. Network parameters are same as in Fig. (6.4).

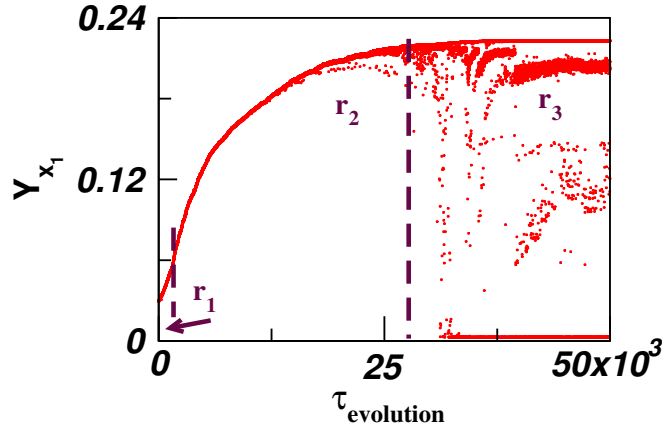


Figure 6.6: IPR as a function of edge-rewiring. The networks with large IPR value in r_3 region consists of few edge-rewiring, which leads to a sudden drop in the IPR value. Rewiring of the first 50,000 edges is depicted for SF as initial network. Here, $n = 500$ and $\langle k \rangle = 10$.

No.	Networks	n	k_{max}	$\langle k \rangle$	Y_{x_1}	λ_3	λ_2	λ_1
1.	<i>3elt</i>	4720	9	5.81	0.0033	6.01	6.02	6.03
2.	<i>3elt_dual</i>	9000	3	2.95	0.0004	2.992	2.993	2.996
3.	<i>G48</i>	3000	4	4.00	0.0003	3.989	3.989	4.000
4.	<i>airfoill</i>	4253	9	5.78	0.0040	5.992	6.006	6.029
5.	<i>airfoill_dual</i>	8034	3	2.94	0.0009	2.989	2.991	2.992
6.	<i>delaunay_n10</i>	1024	12	5.97	0.0038	6.226	6.256	6.293
7.	<i>delaunay_n11</i>	2048	13	5.98	0.0088	6.335	6.370	6.412
8.	<i>grid1_dual</i>	224	4	3.75	0.0076	3.815	3.832	3.897
9.	<i>grid2_dual</i>	3136	4	3.90	0.0012	3.980	3.983	3.988
10.	<i>netz4504_dual</i>	615	4	3.81	0.0038	3.916	3.943	3.966
11.	<i>ukerbe1_dual</i>	1866	4	3.79	0.0031	3.926	3.942	3.968
12.	<i>whitaker3</i>	9800	8	5.92	0.0007	6.013	6.015	6.024
13.	<i>grid2</i>	3296	5	3.90	0.0011	3.980	3.984	3.988
14.	<i>stufe</i>	1036	4	3.61	0.0031	3.690	3.699	3.713
15.	<i>uk</i>	4824	3	2.83	0.0011	2.985	2.988	2.993
16.	<i>grid1</i>	252	4	3.78	0.0064	3.838	3.852	3.917
17.	<i>diag</i>	2559	4	3.20	0.0006	3.2655	3.2658	3.2659

Table 6.2: Various spectral properties of different synthetic and real-world networks [134, 159, 160]. We consider symmetric adjacency matrices corresponding to the connected networks having binary entries. For the networks largest two eigenvalues are close to each other however having a delocalized PEV.

n	m	κ_1	n_1	n_2	$Y_{x_1}^d$	κ_2	n_1	n_2	$Y_{x_1}^d$
500	2512	18	290	209	0.005	13	145	354	0.003
520	2630	19	325	194	0.005	13	145	374	0.003
2448	14806	46	2027	420	0.002	13	145	2302	0.0004
4720	13712	69	4627	92	0.01	6	26	4693	0.0002
10498	52490	101	10005	492	0.002	11	101	10396	0.0001
20422	163376	138	18775	1646	0.0006	17	257	20164	0.00001

Table 6.3: Various network parameters and IPR values of PEV for a given n and m . From the analytical derivations in Eq. (3.11), we decide κ , n_1 and n_2 . Thereupon, we construct a wheel graph of size n_1 and a random regular graph of size n_2 , and join them with a node. We rewire an edge connected to the hub node and connect in random regular network. This leads to a delocalized PEV denoted as $Y_{x_1}^d$. We consider here $\epsilon = 0.02$.

Bibliography

- [1] Kim J. Z. *et al.* (2017), Role of graph architecture in controlling dynamical networks with applications to neural systems, *Nat. Phys.* **14**, 91-98 (DOI: 10.1038/nphys4268).
- [2] Strogatz S. H. (2001), Exploring complex networks, *Nature* **410**, 268-276 (DOI: 10.1038/35065725).
- [3] Vespignani A. (2012), Modelling dynamical processes in complex socio-technical systems, *Nat. Phys.* **8**, 32 (DOI: 10.1038/nphys2160).
- [4] Goltsev A. V. *et al.* (2012), Localization and Spreading of Diseases in Complex Networks, *Phys. Rev. Lett.* **109**, 128702 (DOI: 10.1103/PhysRevLett.109.128702).
- [5] Chaudhuri R., Bernacchia A., and Wang X. J. (2014), A diversity of localized timescales in network activity, *eLife* **3**, e01239 (DOI: 10.7554/eLife.01239.001).
- [6] Barzel B., and Barabási A-L (2013), Universality in network dynamics, *Nat. Phys.* **9**, 673-681 (DOI: 10.1038/nphys2741).
- [7] Suweis S. *et al.* (2015), Effect of localization on the stability of mutualistic ecological networks, *Nat. Commun.*, **6**, 10179 (DOI: 10.1038/ncomms10179).
- [8] Aguiar M. A. M. and Bar-Yam Y. (2000), Spectral analysis and the dynamic response of complex networks, *Phys. Rev. E* **71**, 016106 (DOI: 0.1103/PhysRevE.71.016106).
- [9] Aguirre J., Papo D., and Buldú J. M. (2013), Successful strategies for competing networks, *Nat. Phys.* **9**, 230-234 (DOI: 10.1038/nphys2556).

- [10] Yan G., Tsekenis G., Barzel B., Slotine J. J., Liu Y. Y., Barabási A. L. (2015), Spectrum of controlling and observing complex networks, *Nat. Phys.* **11**, 779-786 (DOI: 10.1038/nphys3422).
- [11] Moretti P., and Muñoz M. A. (2013), Griffiths phases and the stretching of criticality in brain networks, *Nat. Commun.*, **4**, 2521 (DOI: 10.1038/ncomms3521).
- [12] Safari A., Moretti P., and Muñoz M. A. (2017), Topological dimension tunes activity patterns in hierarchical modular networks, *New. J. Phys.* **19**, 113011 (DOI: 10.1088/1367-2630/aa823e).
- [13] Pastor-Satorras R., and Castellano C. (2018), Eigenvector localization in real networks and its implications for epidemic spreading, *Journal of Statistical Physics*, **173**(3-4), 1110-1123 (DOI: 10.1007/s10955-018-1970-8).
- [14] Schaub M. T., Billeh Y. N., Anastassiou C. A., Koch C., and Barahona M. (2015), Emergence of slow-switching assemblies in structured neuronal networks, *PLoS Comput. Biol.* **11**, e1004196 (DOI: 10.1371/journal.pcbi.1004196).
- [15] Hernandez-Hernandez G., Myers J., Alvarez-Lacalle E., and Shiferaw Y. (2017), Nonlinear signaling on biological networks: The role of stochasticity and spectral clustering, *Phys. Rev. E* **95**, 032313 (DOI: 10.1103/PhysRevE.95.032313).
- [16] Sade M., Kalisky T., Havlin S., and Berkovits R. (2005), Localization transition on complex networks via spectral statistics, *Phys. Rev. E* **72**, 066123 (DOI: 10.1103/PhysRevE.72.066123).
- [17] Slanina F., and Konopásek Z. (2010), Eigenvector localization as a tool to study small communities in online social networks, *Advances in Complex Systems*, **13**(06), 699-723 (DOI: 10.1142/S0219525910002840).
- [18] Jeub L. G., Balachandran P., Porter M. A., Mucha P. J., and Mahoney M. W. (2015), Think locally, act locally: Detection of small, medium-sized, and large communities in large networks. *Phys. Rev. E* **91**(1), 012821 (DOI: 10.1103/PhysRevE.91.012821).
- [19] Ermann L., Frahm K. M. and Shepelyansky D. L. (2015), Google matrix analysis of directed networks, *Rev. Mod. Phys.* **87**, 1261 (DOI: 10.1103/RevModPhys.87.1261).

- [20] Benzi M. (2016), Localization in Matrix Computations: Theory and Applications, Exploiting Hidden Structure in Matrix Computations: Algorithms and Applications, Springer, 211-317 (DOI: 10.1007/978-3-319-49887-4_4).
- [21] Chen C., Tong H., Prakesh B. A., Rad T., Faloutsos M., Faloutsos C. (2016), Eigen-Optimization on large graphs by edge manipulation, *ACM Tran. on Knowledge Discovery from Data* **10**(4), 49 (DOI: 10.1145/2903148).
- [22] Nishikawa T., Sun J., and Motter A. E. (2017), Sensitive Dependence of Optimal Network Dynamics on Network Structure, *Phys. Rev. X* **7**, 041044 (DOI: 10.1103/PhysRevX.7.041044).
- [23] Pastor-Satorras R., and Castellano C. (2016), Distinct types of eigenvector localization in networks, *Sci. Rep.* **6**, 18847 (DOI: 10.1038/srep18847).
- [24] Martin T., Zhang X. and Newman M. E. J. (2014), Localization and centrality in networks, *Phys. Rev. E* **90**, 052808 (DOI: 10.1103/PhysRevE.90.052808).
- [25] Castellano C. and Pastor-Satorras R. (2017), Relating Topological Determinants of Complex Networks to Their Spectral Properties: Structural and Dynamical Effects, *Phys. Rev. X* **7**, 041024 (DOI: 10.1103/PhysRevX.7.041024).
- [26] Miegheem P. V. (2011), *Graph Spectra for Complex Networks*, Cambridge University Press, (ISBN: 9780521194587).
- [27] Newman M. E. J. (2010), *Networks: An Introduction*, Oxford University Press (ISBN: 9780199206650).
- [28] Barabási A-L (2016), *Network Science*, Cambridge University Press, New York (ISBN: 1107076269).
- [29] Newman M. E. J. (2002), Assortative Mixing in Networks, *Phys. Rev. Lett.* **89**, 208701 (DOI: 10.1103/PhysRevLett.89.208701).
- [30] Cvetković D., Rowlinson P., and Simić S. (1997), *Eigenspaces of Graphs*, Cambridge University Press, New York (ISBN: 0521573521).
- [31] Genio C. I. D. *et al.* (2010), Efficient and Exact Sampling of Simple Graphs with Given Arbitrary Degree Sequence, *PLoS One*, **5**, e10012 (DOI: 10.1371/journal.pone.0010012).
- [32] Genio C. I. del, Gardeñes J. G., Bonamassa I., and Boccaletti S. (2016), Synchronization in networks with multiple interaction layers, *Science Advances* **2**(11), e1601679 (DOI: 10.1126/sciadv.1601679).

- [33] Domenico M. D., Granell C., Porter M. A., and Arenas A. (2016), The physics of spreading processes in multilayer networks, *Nat. Phys.* **12**, 901-906 (DOI: 10.1038/nphys3865).
- [34] Boccaletti S., Bianconi G., Criado R., del Genio C. I., Gómez-Gardeñes J., Romance M., Sendiña-Nadal I., Wang Z., and Zanin M. (2014), The structure and dynamics of multilayer networks, *Physics Reports* **544**, 1-122 (DOI: 10.1016/j.physrep.2014.07.001).
- [35] Sarkar C., Yadav A., and Jalan S. (2016), Multilayer network decoding versatility and trust, *EPL* **113**, 18007 (DOI: 10.1209/0295-5075/113/18007).
- [36] Jalan S., and Singh A. (2016), Cluster synchronization in multiplex networks, *EPL* **113**(3), 30002 (DOI: 10.1209/0295-5075/113/30002).
- [37] Dwivedi S. K., Sarkar C., and Jalan S. (2015), Optimization of synchronizability in multiplex networks, *EPL* **111**(1), 10005 (DOI: 10.1209/0295-5075/111/10005).
- [38] Dwivedi S. K., Baptista M. S., and Jalan S. (2017), Optimization of synchronizability in multiplex networks by rewiring one layer, *Phys. Rev. E* **95**, 040301 (DOI: 10.1103/PhysRevE.95.040301).
- [39] Shinde P. and Jalan S. (2015), A multilayer protein-protein interaction network analysis of different life stages in *Caenorhabditis elegans*, *EPL* **112**(5), 58001 (DOI: 10.1209/0295-5075/112/58001).
- [40] Osat S., Fageeh A., and Radicchi F. (2017), Optimal percolation on multiplex networks, *Nat. Commun.* **8**, 1540 (DOI: 10.1038/s41467-017-01442-2).
- [41] Timóteo S., Correia M., Echeberría S. R., Freitas H., and Heleno R. (2018), Multilayer networks reveal the spatial structure of seed-dispersal interactions across the Great Rift landscapes, *Nat. Commun.* **9**, 140 (DOI: 10.1038/s41467-017-02658-y).
- [42] Batkovich D., Kirilenko Y., Kompaniets M., and Novikov S. (2014), Graph-State: a tool for graph identification and labeling, arXiv:1409.8227v1.
- [43] Kisku D. R., Gupta P., and Sing J. K. (2010), Feature Level Fusion of Face and Palmprint Biometrics by Isomorphic Graph-Based Improved K-Medoids Partitioning, *Advances in computer science and information technology*. Springer, Berlin, 70-81 (DOI: 10.1007/978-3-642-13577-4_7).

- [44] Randić M. (1977), On Canonical Numbering of Atoms in a Molecule and Graph Isomorphism, *J. Chem. Inf. Comput. Sci.* **17**(3), 171-180 (DOI: 10.1021/ci60011a013).
- [45] Lestringant P., Guihéry F., and Fouque P. A. (2015), Automated Identification of Cryptographic Primitives in Binary Code with Data Flow Graph Isomorphism, *Proceedings of the 10th ACM Symposium on Information, Computer and Communications Security*, Singapore, 203-214 (DOI: 10.1145/2714576.2714639).
- [46] Harary F. and Palmer E. (1973), *Graphical enumeration*, Academic Press (ISBN: 9781483273785).
- [47] Gleich D. F. (2015), PageRank Beyond the Web, *SIAM Rev.* **57**(3), 321-363 (DOI: 10.1137/140976649).
- [48] Froyland G. and Dellnitz M. (2003), Detecting and locating near-optimal almost-invariant sets and cycles, *SIAM J. Sci. Comput.* **24**(6), 1839-1863 (DOI: 10.1137/S106482750238911X).
- [49] Newman M. E. J. (2006), Finding community structure in networks using the eigenvectors of matrices, *Phys. Rev. E* **74**, 036104 (DOI: 10.1103/PhysRevE.74.036104).
- [50] Sarkar S., Chawla S., Robinson P. A., and Fortunato S. (2016), Eigenvector dynamics under the perturbation of modular matrix, *Phys. Rev.* **93**, 062312 (DOI: 10.1103/PhysRevE.93.062312).
- [51] Tang J. and Wang K. W. (2004), Vibration Confinement via Optimal Eigenvector Assignment and Piezoelectric Networks, *J. Vib. Acoust.* **126**(1), 27-36 (DOI: 10.1115/1.1597213).
- [52] Jalan S. *et al.* (2010), Random matrix analysis of localization properties of gene coexpression network, *Phys. Rev. E* **81**, 046118 (DOI: 10.1103/PhysRevE.81.046118) and references therein.
- [53] Ide T. and Kashima H. (2004), Eigenspace-based Anomaly Detection in Computer Systems, *KDD04, Proceedings of the tenth ACM SIGKDD international conference on Knowledge discovery and data mining (KDD)*, Seattle, Washington, USA, 440-449 (DOI: 10.1145/1014052.1014102).

- [54] Sarkar C. and Jalan S. (2018), Spectral properties of complex networks, *Chaos* **28**, 102101 (DOI: 10.1063/1.5040897).
- [55] Jalan S. and Dwivedi S. K. (2014), Extreme-value statistics of brain networks: Importance of balanced condition, *Phys. Rev. E* **89**, 062718 (DOI: 10.1103/PhysRevE.89.062718).
- [56] Ghosh S. *et al.* (2016), Interplay of inhibition and multiplexing: Largest eigenvalue statistics, *EPL* **115**, 10001 (DOI: 10.1209/0295-5075/115/10001).
- [57] Chauhan S., Girvan M., Ott E. (2009), Spectral properties of networks with community structure, *Phys. Rev. E* **80**, 056114 (DOI: 10.1103/PhysRevE.80.056114).
- [58] Nimwegen E. V., Crutchfield J. P., and Huynen M. (1999), Neutral evolution of mutational robustness, *PNAS* **96**, 9716-9720 (DOI: 10.1073/pnas.96.17.9716).
- [59] Pomerance A., Ott E., Girvan M., and Losert W. (2009), The effect of network topology on the stability of discrete state models of genetic control, *PNAS* **106**(20), 8209-8214 (DOI: 10.1073/pnas.0900142106).
- [60] Edwards J. T. and Thouless D. J. (1972), Numerical studies of localization in disordered systems, *J. Phys. C* **5**, 807 (DOI: 10.1088/0022-3719/5/8/007).
- [61] Lee P. A., and Ramakrishnan T. V. (1985), Disordered electronic systems, *Rev. Mod. Phys.* **57**, 287 (DOI: 10.1103/RevModPhys.57.287).
- [62] Kahnke L. *et al.* (2008), Wave Localization in Complex Networks with High Clustering, *Phys. Rev. Lett.* **101**, 175702 (DOI: 10.1103/PhysRevLett.101.175702).
- [63] Hu H., Strybulevych A., Page J. H., Skipetrov S. E., and Tiggelen B. A. V. (2008), Localization of ultrasound in a three-dimensional elastic network, *Nat. Phys.* **4**, 945-948 (DOI: 10.1038/nphys1101).
- [64] Filoche M. and Mayboroda S. (2012), Universal mechanism for Anderson and weak localization, *PNAS* **109**(37), 14761-14766 (DOI: 10.1073/pnas.1120432109).
- [65] Zhang B. J., Chamanzar M. and Alam M. R. (2017), Suppression of epileptic seizures via Anderson localization, *J. R. Soc. Interface* **14**, 20160872 (DOI: 10.1098/rsif.2016.0872).

- [66] Elsner U., Mehrmann V., Milde F., Römer R. A., and Schreiber M. (1999), The Anderson model of localization: A Challenge for modern eigenvalue methods, *SIAM J. Sci. Comput.* **20**(6), 2089-2102 (DOI: 10.1137/S1064827598332217).
- [67] Wiersma D. S. (2010), Random Quantum Networks, *Science* **327**(5971), 1333-1334 (DOI: 10.1126/science.1187084).
- [68] Kimble H. J. (2008), The quantum internet, *Nature* **453**, 1023-1030 (DOI: 10.1038/nature07127).
- [69] Prigodin V. N. and Efetov K. B. (1993), Localization transition in a random network of metallic wires: A model for highly conducting polymers, *Phys. Rev. Lett.* **70**, 2932 (DOI: 10.1103/PhysRevLett.70.2932).
- [70] Ortuño M., Somoza A. M. and Chalker J. T. (2009), Random Walks and Anderson Localization in a Three-Dimensional Class C Network Model, *Phys. Rev. Lett.* **102**, 070603 (DOI: 10.1103/PhysRevLett.102.070603).
- [71] Ferreira R. S., Costa R. A., Dorogovtsev S. N., and Mendes J. F. F. (2016), Metastable localization of diseases in complex networks, *Phys. Rev. E* **94**, 062305 (DOI: 10.1103/PhysRevE.94.062305).
- [72] Zanette D. H. (2002), Dynamics of rumor propagation on small-world networks, *Phys. Rev. E* **65**, 041908 (DOI: 10.1103/PhysRevE.65.041908).
- [73] Arruda G. F. de, Cozzo E., Peixoto T. P., Rodrigues F. A., and Moreno Y. (2017), Disease Localization in Multilayer Networks, *Phys. Rev. X* **7**, 011014 (DOI: 10.1103/PhysRevX.7.011014).
- [74] Wegner F. (1980), Inverse Participation Ratio in $2 + \varepsilon$ Dimensions, *Z. Physik B* **36**, 209-214 (DOI: 10.1007/BF01325284).
- [75] Bell R. J., Dean P. (1970), Atomic Vibrations in Vitreous Silica, *Discuss. Faraday Soc.* **50**, 55-61 (DOI: 10.1039/DF9705000055).
- [76] Wang Y., Chakrabarti D., Wang C. and Faloutsos C. (2003), Epidemic spreading in real networks: An eigenvalue viewpoint, *Proceedings of the 22nd International Symposium on Reliable Distributed Systems*, IEEE, 25-34 (DOI: 10.1109/RELDIS.2003.1238052).
- [77] Mieghem P. V. *et al.* (2011), Decreasing the spectral radius of a graph by link removals, *Phys. Rev. E* **84**, 016101 (DOI: 10.1103/PhysRevE.84.016101).

- [78] Abu-Jeb I. T. (2006), The Determinant of the Wheel graph and conjectures by Yong, *Missouri J. Math. Sci.* **18**(2), 142 (DOI: 10.1.1.555.3385).
- [79] Tran L. V., Vu V. H., and Wang K. (2013), Sparse random graphs: Eigenvalues and eigenvectors, *Random Structures & Algorithms* **42**, 110-134 (DOI: 10.1002/rsa.20406).
- [80] Boccaletti S. et al. (2006), Complex networks: Structure and dynamics, *Phys. Rep.*, **424**, 175-308 (DOI: 10.1016/j.physrep.2005.10.009)
- [81] Dwivedi S. K., Sarkar C. and Jalan S. (2015), Optimization of synchronizability in multiplex networks, *EPL* **111**, 10005 (DOI: 10.1209/0295-5075/111/10005).
- [82] Dwivedi S. K. and Jalan S. (2014), Emergence of clustering: Role of inhibition, *Phys. Rev. E* **90**, 032803 (DOI: 10.1103/PhysRevE.90.032803).
- [83] Cormen T. H., Leiserson C. E., Rivest R. L., and Stein C. (2009), *Introduction to Algorithms*, 3rd ed., MIT Press Cambridge, (ISBN: 8120340078).
- [84] Heath L. S. and Parikh N. (2011), Generating random graphs with tunable clustering coefficients, *Physica A* **390**, 4577-4587 (DOI: 10.1016/j.physa.2011.06.052).
- [85] Jalan S. and Yadav A. (2015), Assortative and disassortative mixing investigated using the spectra of graphs, *Phys. Rev. E* **91**, 012813 (DOI: 10.1103/PhysRevE.91.012813).
- [86] Jalan S. et al. (2016), Interplay of degree correlations and cluster synchronization, *Phys. Rev. E* **94**, 062202 (DOI: 10.1103/PhysRevE.94.062202).
- [87] Brunet R. X. and Sokolov I. M. (2004), Reshuffling scale-free networks: From random to assortative, *Phys. Rev. E* **70**, 066102 (DOI: 10.1103/PhysRevE.70.066102).
- [88] Kaiser M. and Hilgetag C. C. (2006), Nonoptimal Component Placement, but Short Processing Paths, due to Long-Distance Projections in Neural Systems, *PLoS Computat. Biol.* **2**, 0805 (DOI: 10.1371/journal.pcbi.0020095).
- [89] Watts D. J., and Strogatz S. H. (1998), Collective dynamics of small-world networks, *Nature* **393**, 440-442 (DOI: 10.1038/30918).

- [90] Meyer C. D. (1994), Sensitivity of the Stationary Distribution of a Markov Chain, *SIAM J. Matrix Anal. Appl.* 15(3), 715-728 (DOI: 10.1137/S0895479892228900).
- [91] Hartfiel D. J., and Meyer C. D. (1998), On the structure of stochastic matrices with a subdominant eigenvalue near 1, *Linear Algebra and its Applications* **272**, 193-203 (DOI: 10.1016/S0024-3795(97)00333-9).
- [92] Pradhan P., Yadav A., Dwivedi S. K., and Jalan S. (2017), Optimized evolution of networks for principal eigenvector localization, *Phys. Rev. E* **96**, 022312 (DOI: 10.1103/PhysRevE.96.022312).
- [93] Meyer C. D. (2000), *Matrix Analysis and Applied Linear Algebra*, Society for Industrial and Applied Mathematics (SIAM), Philadelphia, (ISBN: 0898714540).
- [94] Liu Q. and Mieghem P. V. (2018), Network localization unalterable by infections in bursts, *IEEE Trans. Network Science and Engineering*, early access, (DOI: 10.1109/TNSE.2018.2889539).
- [95] Militello B. D. and Vitanov N. V. (2015), Dynamics of a two-state system through a real level crossing, *Phys. Rev. A* **91**, 053402 (DOI: 10.1103/PhysRevA.91.053402).
- [96] Shapiro B. and Zarembo K. (2017), Level crossing in random matrices: I random perturbation of a fixed matrix, *J. Phys. A: Math. Theor.* **50**, 26 (DOI: 10.1088/1751-8121/aa5186).
- [97] Bhattacharya M. and Raman C. (2006), Detecting level crossings without looking at the spectrum, *Phys. Rev. Lett.* **97**, 140405 (DOI: 10.1103/PhysRevLett.97.140405).
- [98] Kim J. H. and Vu V. H. (2003), Generating random regular graphs, *Proceedings of the thirty-fifth ACM symposium on Theory of computing (STOC)*, San Diego, CA, USA, 213-222, (DOI: 10.1145/780542.780576).
- [99] Yan-Bin Jia (2018), Roots of Polynomials, *Com S 477/577 Notes*, pp. 1-2.
- [100] Abramowitz M. and Stegun I. A. (1972), *Handbook of Mathematical Functions: with Formulas, Graphs, and Mathematical Tables*, New York: Dover, pp. 17-18 (ISBN: 0486612724).
- [101] Grove L. C. (2004), *Algebra*, Dover, pp. 278-279 (ISBN: 048643947X).

- [102] Aguirre J., Buldú J. M., and Manrubia S. C. (2009), Evolutionary dynamics on networks of selectively neutral genotypes: effects of topology and sequence stability, *Phys. Rev. E* **80**, 066112 (DOI: 10.1103/PhysRevE.80.066112).
- [103] Bauer E. B. and Chan H. S. (1999), Modeling evolutionary landscapes: mutational stability, topology, and superfunnels in sequence space, *PNAS* **96**, 10689-10694 (DOI: 10.1073/pnas.96.19.10689).
- [104] Aguirre J., Catalán P., Cuesta J. A., and Manrubia S. C. (2018), On the networked architecture of genotype spaces and its critical effects on molecular evolution, *Open Biol.* **8**, 180069 (DOI: 10.1098/rsob.180069).
- [105] Brown J. W. and Churchill R. V. (2009), *Complex Variables and Applications*, 8th ed., McGraw-Hill New York, (ISBN: 0073383171).
- [106] Jalan S., Sarkar C. (2017), Complex networks: an emerging branch of science, *Physics news* **47**, 3-4 (ISSN: 0253-7583).
- [107] Bonacich P. (2007), Some unique properties of eigenvector centrality, *Social Networks* **29**(4), 555-564 (DOI: 10.1016/j.socnet.2007.04.002).
- [108] Reino L. *et al.* (2017), Networks of global bird invasion altered by regional trade ban, *Sci. Adv.* **3**(11), e1700783 (DOI: 10.1126/sciadv.1700783).
- [109] Lohmann G. *et al.* (2010), Eigenvector Centrality Mapping for Analyzing Connectivity Patterns in fMRI Data of the Human Brain, *PloSOne* **5**(4), e1023 (DOI: 10.1371/journal.pone.0010232).
- [110] Karim H. T. *et al.* (2017), Intrinsic functional connectivity in late-life depression: trajectories over the course of pharmacotherapy in remitters and non-remitters, *Molecular Psychiatry* **22**, 450-457 (DOI: 10.1038/mp.2016.55).
- [111] Parand F. A., Rahimi H., Gorzin M. (2016), Combining fuzzy logic and eigenvector centrality measure in social network analysis, *Physica A* **459**, 24-31 (DOI: 10.1016/j.physa.2016.03.079).
- [112] Yin R. R., Guo Q., Yang J. N., Liu J. G. (2018), Inter-layer similarity-based eigenvector centrality measures for temporal networks, *Physica A* **512**, 165-173 (DOI: 10.1016/j.physa.2018.08.018).
- [113] Bof N., Baggio G., Zampieri S. (2017), On the Role of Network Centrality in the Controllability of Complex Networks, *IEEE Trans. on Control of Network Science* **4**(3), 643-653 (DOI: 10.1109/TCNS.2016.2550862).

- [114] Lotfi N., Darooneh A. H., Rodrigues F. A. (2018), Centrality in earthquake multiplex networks, *Chaos* **28**, 063113 (DOI: 10.1063/1.5001469).
- [115] Benson A. R. (2019), Three hypergraph eigenvector centrality, *SIAM J. MATH. DATA SCI.* 1(2), 293-312 (DOI: 10.1137/18M1203031).
- [116] Nadakuditi R. R., Newman M. E. J. (2013), Spectra of random graphs with arbitrary expected degrees, *Phys. Rev. E* **87**, 012803 (DOI: 10.1103/PhysRevE.87.012803).
- [117] Our codes and data are available at the following link https://github.com/priodyuti/pev_loc_in_evec_centrality.
- [118] Batagelj V., Brandes U. (2005), Efficient generation of large random networks, *Phys. Rev. E* **71**, 036113 (DOI: 10.1103/PhysRevE.71.036113).
- [119] Cvetković D., Rowlinson P., Simić S. (2009), *An introduction to the theory of graph spectra*, Cambridge University Press; 1st ed., (ASIN: B01CEKK9N6).
- [120] Abdollahi A., Janbaz S. and Oboudi M. R. (2013), Graphs cospectral with a friendship graph or its complement, *Transactions on Combinatorics* **2**(4), 37-52 (ISSN: 2251-8665).
- [121] Barucca P., Tantari D., Lillo F. (2016), Centrality metrics and localization in core-periphery networks, *J. Stat. Mech.* 2016, 023401 (DOI: 10.1088/1742-5468/2016/02/023401).
- [122] Sharkey K. J. (2019), Localization of eigenvector centrality on networks with a cut-vertex, *Phys. Rev. E* **99**, 012315 (DOI: 10.1103/PhysRevE.99.012315).
- [123] Slanina F. (2017), Localization in random bipartite graphs: Numerical and empirical study, *Phys. Rev. E* **95**, 052149 (DOI: 10.1103/PhysRevE.95.052149).
- [124] Bassett D. S. and Sporns O. (2017), Network neuroscience, *Nat. Neurosci.* **20**, 353-364 (DOI: 10.1038/nn.4502).
- [125] Baptista M. S., Moukam Kakmeni F. M., and Grebogi C. (2010), Combined effect of chemical and electrical synapses in Hindmarsh-Rose neural networks on synchronization and the rate of information, *Phys. Rev. E* **82**, 036203 (DOI: 10.1103/PhysRevE.82.036203).

- [126] Jalan S., Ghosh S., and Patra B. (2017), Is repulsion good for the health of chimeras?, *Chaos* **27**, 101104 (DOI: 10.1063/1.5005576).
- [127] Bassett D. S., Wymbs N. F., Porter M. A., Mucha P. J., Carlson J. M. and Grafton S. T. (2011), Dynamic reconfiguration of human brain networks during learning, *PNAS* **108**, 7641-7646 (DOI: 10.1073/pnas.1018985108).
- [128] Chen B. L., Hall D. H., and Chklovskil D. B. (2006), Wiring optimization can relate neuronal structure and function, *PNAS* **103**, 4723-4728 (DOI: 10.1073/pnas.0506806103).
- [129] Miegheem P. V. (2012), Epidemic phase transition of the SIS type in networks, *EPL* **97**, 48004 (DOI: 10.1209/0295-5075/97/48004).
- [130] Kirkpatrick S., Gelatt C. D., and Vecchi M. P. (1983), Optimization by Simulated Annealing, *Science* **220**(4598), 671-680 (DOI: 10.1126/science.220.4598.671).
- [131] Pedregosa F. *et al.* (2011), Scikit-learn: Machine Learning in Python, *Journal of Machine Learning Research* **12**, 2825-2830 (DOI: <http://www.jmlr.org/papers/v12/>).
- [132] Omodei E., Domenico M. D., and Arenas A. (2015), Characterizing interactions in online social networks during exceptional events, *Frontiers in Physics* **3**, 59 (DOI: 10.3389/fphy.2015.00059).
- [133] Coleman J., Katz E., and Menzel H. (1957), The Diffusion of an Innovation Among Physicians, *Sociometry* **20**, 253-270 (DOI: 10.2307/2785979).
- [134] Stark C., Breitkreutz B. J., Reguly T., Boucher L., Breitkreutz A., and Tyers M. (2006), BioGRID: a general repository for interaction datasets, *Nucleic Acids Research* **34**, D535-D539 (DOI: 10.1093/nar/gkj109).
- [135] Domenico M. D., Nicosia V., Arenas A., and Latora V. (2015), Structural reducibility of multilayer networks, *Nat. Commun.* **6**, 6864-6872 (DOI: 10.1038/ncomms7864).
- [136] Domenico M. D., Porter M. A., and Arenas A. (2014), MuxViz: a tool for multilayer analysis and visualization of networks, *Journal of Complex Networks* **3**, 159-176 (DOI: 10.1093/comnet/cnu038).

- [137] Peel L. (2017), Graph-based semi-supervised learning for relational networks, in *Proceedings of the 2017 SIAM International Conference on Data Mining* (SIAM, Texas, 2017), 435-443 (DOI: 10.1137/1.9781611974973.49).
- [138] Hata S. and Nakao H. (2017), Localization of Laplacian eigenvectors on random networks, *Sec. Rep.* **7**, 1121 (DOI: 10.1038/s41598-017-01010-0).
- [139] Forrow A., Woodhouse F. G., and Dunkel J. (2018), Functional control of network dynamics using designed laplacian, *Phys. Rev. X* **8**, 041043 (DOI: 10.1103/PhysRevX.8.041043).
- [140] Jalan S. and Bandyopadhyay J. N. (2008), Random matrix analysis of network Laplacians, *Physica A* **387**, 667-674 (DOI: 10.1016/j.physa.2007.09.026).
- [141] Aufderheide H. E. (2014), Implications of eigenvector localization for dynamics on complex networks, PhD Dissertation.
- [142] Huang B. J. and Wu T.-M. (2009), Localization-delocalization transition in Hessian matrices of topologically disordered systems, *Phys. Rev. E* **79**, 041105 (DOI: 10.1103/PhysRevE.79.041105).
- [143] Pettinato L., Calistri E., Patti F. D., Livi R., and Luccioli S. (2014), Genome-wide analysis of promoters: clustering by alignment and analysis of regular pattern, *Plos One* **9**, e85260 (DOI: 10.1371/journal.pone.0085260).
- [144] Yazawa A. (2018), The Hessians of the complete and complete bipartite graphs and its application to the strong lefschetz property, (arXiv: 1812.07199v1).
- [145] Nassar H., Kloster K., Gleich D. F. (2015), Strong localization in personalized PageRank vector, *Algorithms and models for the web graph*, 190 (DOI: 10.1007/978-3-319-26784-5_15).
- [146] Burda Z., Duda J., Luck J. M., and Waclaw B. (2009), Localization of the Maximal Entropy Random Walk, *Phys. Rev. Lett.* **102**, 160602 (DOI: 10.1103/PhysRevLett.102.160602).
- [147] Dekel Y., Lee J. R., Linial N. (2011), Eigenvectors of Random Graphs: Nodal Domains, *Random Structures & Algorithms* **39**, 436-448 (DOI: 10.1007/978-3-540-74208-1_32).

- [148] Damle A., Lin L., Ying L. (2015), Compressed representations of Kohn-Sham orbitals via selected columns of the density matrix, *J. Chem. Theory Comput.* **11**, 1463-1469 (DOI: 10.1021/ct500985f).
- [149] Damle A., Lin L., Ying L. (2017), Computing Localized Representations of the Kohn-Sham Subspace Via Randomization and Refinement, *SIAM J. Sci. Comput.*, **39**(6), B1178-B1198 (DOI: 10.1137/16M1098589).
- [150] Goedecker S., Ivanov O. V. (1999), Frequency localization properties of the density matrix and its resulting hypersparsity in a wavelet representation, *Phys. Rev. B* **59**, 7270-7273 (DOI: 10.1103/PhysRevB.59.7270).
- [151] Mahadevan P., Krioukov D., Fall K., and Vahdat A. (2006), Systematic topology analysis and generation using degree correlations, *ACM SIGCOMM*, 135-146 (DOI: 10.1145/1159913.1159930).
- [152] Cucuringu M. and Mahoney M. W. (2011), Localization on low-order eigenvectors of data matrices, arxiv:1109.1355v1.
- [153] Drineas P., Mahoney M. W., Muthukrishnan S., Sarlós T. (2011), Faster least squares approximation, *Numer. Math.* 117:219-24 (DOI: 10.1007/s00211-010-0331-6).
- [154] Drineas P., Magdon-Ismail M., Mahoney M. W., Woodruff D. P. (2012), Fast Approximation of Matrix Coherence and Statistical Leverage, *Journal of Machine Learning Research* **13**, 3475-3506 (DOI is not available).
- [155] Parlett N. B. (1987), *The Symmetric Eigenvalue Problem*, Society for Industrial and Applied Mathematics, (DOI: 10.1137/1.9781611971163).
- [156] Beck A. (2014), *Introduction to nonlinear optimization Theory, Algorithms, and Applications with MATLAB*, Society for Industrial and Applied Mathematics (DOI: 10.1137/1.9781611973655).
- [157] Li C., Wang H. and Miegheem P. V. (2012), Degree and Principal Eigenvectors in Complex, Networks, Networking, *Lecture Notes in Computer Science*, vol 7289, 149 (DOI: 10.1007/978-3-642-30045-5_12).
- [158] Jonathan C. Lansley (2015), Beautiful and distinguishable line colors + colormap, version 1.4.0.0 <https://in.mathworks.com>

- [159] Davis T. A. and Hu Y. (2011), The University of Florida Sparse Matrix Collection, *ACM Transactions on Mathematical Software* **38**(1), 1 (DOI: 10.1145/2049662.2049663).
- [160] Shinde P., Yadav A., Rai A., and Jalan S. (2015), Dissortativity and duplications in oral cancer, *Eur. Phys. J. B* **88**, 197 (DOI: 10.1140/epjb/e2015-60426-5).
- [161] Our codes and data are available at the following link https://github.com/priodyuti/pev_loc_eigval_crossing.
- [162] Our codes on multilayer network rewiring are available at the following link https://github.com/priodyuti/multiplex_localization.